

# Assessment of flood early warning and response in an urbanized catchment

A case study of the Tub Ma basin in Thailand

S.D.G. van Haaren



*Plenty of beautiful photos of Tub Ma's striking scenery were available for the front page of this thesis. However, my largest motivation for this thesis was not the nice fieldwork environment, but the fact that this research addressed an actual case study. The urban floods assessed in this thesis were real. The picture on the front page was taken in the very first stage of the research, when the floods and proposed solutions were discussed at the office of local water authority (RID) in Rayong, Thailand. I believe this cover photo illustrates the true meaning of this thesis: contributing to disaster risk reduction while operating in the local context.*

FLTR: Seksun Supcharoen (Head of Engineering, RID Rayong), me, Punpim Puttaraksa Mapiam (supervisor Kasetsart University), Thom Bogaard (supervisor TU Delft).

# Assessment of flood early warning and response in an urbanized catchment

A case study of the Tub Ma basin in Thailand

By

S.D.G. van Haaren

to obtain the degree of Master of Science

at the faculty of Civil Engineering and Geosciences at Delft University of Technology,

to be defended publicly on Wednesday September 9, 2020 at 10:00 AM.

Supervisor:

Thesis committee:

Dr. T. A. Bogaard (chair)

Dr. P.P. Mapiam

Dr. H. C. Winsemius

Dr. J. D. Bricker

Delft University of Technology

Kasetsart University

Delft University of Technology

Delft University of Technology

An electronic version of this thesis is available at <http://repository.tudelft.nl/>.



**TU**Delft

## Summary

Rapid urbanization has altered the natural hydrological cycle of the Tub Ma catchment, inducing major floods after heavy rainfall events. For that reason, structural mitigation measures were built, including floodwalls along the channel and a pumping station at the outlet. However, no operational rules were available for operating the river outlet structures and inundation was still common. To prevent or reduce flooding by improving the operational management of the outlet pumping system, an early warning system was required.

The objective of this research was to assess whether informed decision-making resulted in an operational pumping strategy that prevents or reduces fluvial flooding. First, the question was asked whether water level monitoring could result in a timely and reliable warning service for an early warning system. The second question was whether timely operation of the outlet pumping station prevented fluvial flooding.

For the fulfillment of the data requirements in this thesis, a fieldwork trip was organized first. During a short period of dedicated data survey, water level time series and river geometries were obtained. Water levels from three gauging stations were statistically tested as precursors for fluvial flooding in Tub Ma. Consequently, a hydraulic model was built to assess the flood mitigation capabilities of the outlet pumping station. Lastly, synthetic flood design hydrographs were run through the model for different pumping station operation strategies, with and without notification from a flood early warning system.

The results from this thesis demonstrated that monitoring water levels in the upstream tributaries of Tub Ma was a useful information source for an early warning system that forecasts flood waves. This water level based early warning enabled a maximum potential lead time of 13-15 hours for flood mitigation. Nevertheless, connecting flood early warning to the operation of the pumping station did not reduce or prevent flooding. The Tub Ma river had a flow regime of limited baseflow and rapidly rising discharge, and as a result, the discharge capacity of the pumping station ahead of flood waves was physically limited by water level and inflow. Therefore, improved operation of the pumping station was not the solution for preventing or reducing fluvial flooding.

On the basis of the results from this research, structural measures were suggested for flood mitigation, like temporary storage, a bypass channel, and measures that slow down the run-off processes. Also, it was recommended to examine the value of a flood early warning system by using 13-15 hours of lead time within a broader scope of disaster risk reduction in Tub Ma.

## Acknowledgments

In front of you lies the finished product of my thesis, the last step for completing the Civil Engineering master program at Delft University of Technology. I followed the Water Management track and took urban water management and hydrology as specialization. This research project introduced me to the application of flood early warning systems for flood mitigation in urban areas. Accordingly, I have been able to broaden my hydrological knowledge and received hands-on experience in setting up a cross-cultural project. By a short period of dedicated data survey in an area with variable data availability and quality, it was possible to answer the research questions in this thesis. I learned that data or computer models should not only be appreciated by such a thing as 'root mean squared error' but by their usability for a specific use-case as well.

There are many people to whom I am grateful. Firstly, my daily supervisors: Thom from Delft University of Technology and Punpim from Kasetsart University. Thank you, Thom, for your in-depth and overall guidance. It was an absolute pleasure working with you. Without your constant enthusiasm and positive energy, I would not have gotten this far. Thank you, Punpim, for teaching me about urban hydrological systems in Thailand. Your guidance through the Asian culture was of great value to my fieldwork trip. Hessel, my second supervisor in Delft, thank you for your time and effort in providing me valuable insights. The way you emphasize on end-users and the usefulness of findings has been a source of inspiration to me. I also would like to thank Jeremy for joining my graduation committee to provide an independent opinion on the research. Furthermore, I had the privilege of being assisted during all fieldwork practices by two students from Kasetsart University. Prew and Nine, thank you for your efforts and time.

Lastly, friends have always been accompanying me. I am deeply grateful to all friends who have been providing support in my thesis work, career, and life. Dankjulliewel.

Bas van Haaren

Delft, August 2020

# Contents

Summary .....	4
Acknowledgments .....	5
Contents .....	6
1 Introduction.....	7
1.1 Research motivation.....	7
1.2 Problem statement.....	8
1.3 Report outline .....	9
2 Theoretical background .....	10
2.1 Early warning systems.....	10
2.2 Flood wave propagation in rivers.....	11
2.3 Models addressing fluvial flood problems .....	13
3 Study location.....	15
3.1 Thailand (social-) geography and climate .....	15
3.2 Tub Ma catchment.....	16
3.3 Tub Ma river.....	17
4 Methodology.....	19
4.1 Field data overview: collection, processing & quality control .....	19
4.2 Flood early warning assessment.....	25
4.3 Hydraulic model Tub Ma river (tool) .....	26
4.4 Flood mitigation assessment .....	28
5 Results .....	29
5.1 Fieldwork results.....	29
5.2 Flood early warning .....	35
5.3 Hydraulic model Tub Ma catchment.....	38
5.4 Flood mitigation assessment .....	40
6 Discussion .....	46
6.1 Research limitations .....	46
6.2 Usefulness of a flood early warning system in Tub Ma .....	47
7 Conclusion & recommendations.....	49
8 Bibliography.....	50
Appendix A. Summary of differential GNSS set up.....	55
Appendix B. Fieldwork results: time series .....	57
Appendix C. Fieldwork results: bathymetry .....	62
Appendix D. Fieldwork results: structure geometries .....	76
Appendix E. Assessment of information & decision chain .....	77
Appendix F. Model results .....	79
Appendix G. Suggestions for flood mitigation .....	85
Appendix H. Supporting pictures .....	87

# 1 Introduction

## 1.1 Research motivation

Land-use change, including land conversion from one type to another and land cover modification through land-use management, has greatly altered a large proportion of the earth's land surface to satisfy mankind's demands (Vitousek et al., 1997). Southeast Asia has the highest deforestation rate of any major tropical region (Zhao et al., 2006). The consequences of this transformation are manifold, including loss of biodiversity, alteration of climate, and disruption of the balance of an ecosystem (Foley et al., 2005). In fast-developing countries on the Asian continent, mainly forest and agricultural land is changed into urban areas (Zhao et al., 2006). It has been widely acknowledged that urbanization alters the natural hydrological cycle of a catchment (Lee & Heaney, 2003). This process includes a re-organization of surface and subsurface pathways for water (Hirsch, 1977; T. Zhu et al., 2007). The amount of run-off from a precipitation event increases because reduced impervious surfaces suppress infiltration, interception, and depression storage (Hamel, 2013). Also, the catchment's time of concentration decreases because of the hydraulic efficiency of flow provided by rooftops, pavements, storm sewers, and the stream channel itself (Hirsch, 1977). Meanwhile, precipitation events at the Asian continent are characterized by short duration and high intensity (Zhao et al., 2006). Consequently, that water from high-intensity rainfall events is flushed through the catchment resulting in a change of the natural flow regime. While baseflow decreases, high water events increase in frequency and magnitude of both peak discharge and volume (Hamel, 2013). By the increase of high water events, fluvial flood risk increases as well due to the risen chance of overbank flow in the streams (Merz et al., 2010).

Apart from the hydrological perspective, also the contribution of planning and governance to urban flood discharge is of significance in urbanized areas. It is a tendency that adaptation to high stream flows starts when urbanization has already taken place. The reason for this is that river discharge or channel geometry is generally not a design variable for urban planners (Hirsch, 1977; Sieweke, 2013). In densely urbanized areas; dredging, increasing dike crest level, and removal of disturbances are the most common measures to enhance the design-discharge of a stream (Hirsch, 1977). These human-induced measures result in an artificial confined channel without significant irregularities. However, the irregularity of the bed slope, forms of cross-sections, and natural obstructions play a crucial role in dampening out disturbances on the flow (like heavy rainfall events), resulting in steady and nearly uniform flow (Hayami, 1951). Flood mitigation measures increase the design discharge of steady flow through the river but a new problem arises: the stream is not able to dampen out the urbanization-induced flushes from rainfall events, resulting in flood waves propagating through the channel (Hayami, 1951). Compared to steady discharge, flood waves have a much higher peak discharge over the same total discharge volume (Hirsch, 1977).

In the Tub Ma catchment in Thailand, this portrayed process of rapid urbanization and the associated hydrological response took place. In past decades, mainly agricultural land was changed into urban areas (Jiradecha et al., 2011). Both pluvial and fluvial flood events became common in the downstream part of Tub Ma where Rayong is located (Jiradecha et al., 2011). Rayong is now one of Thailand's most hazard-prone areas where citizens suffer from inundation (Mitsubishi Research Institute, 2015). Major fluvial flood events took place in 2009, 2010, 2011, 2015, and 2020. Floods adversely affect the accessibility of infrastructure and harm livelihoods. River flood events are the result of overbank flows, while pluvial floods are mainly caused by sewer system capacity reduction from obstructions by plastic garbage, fat waste, and soil debris (Jiradecha et al., 2011).

According to the local water authority (Royal Irrigation Department, RID), previous research has resulted in implemented measures to mitigate the effects of and adapt to floods in Rayong. To counteract the sewer system capacity reduction, grease traps were installed, trash trapping nets were hanged, and mobile pumps were placed along the roads. To increase bankfull flow, several structures in the river like weirs were removed; concrete floodwalls were built on both sides of the Tub Ma river, and a pumping station and floodgate were built at the outlet.

According to literature, the use of river pumping stations is focused on either decreasing flood volume by increasing river storage and outflow; either on designing a drainage pump capacity that equals the (peak) discharge of on certain return period, or a combination of both (Julien et al., 2010; Komori et al.,

2012). The prior one was the case in Tub Ma: the outlet structure was designed to decrease the flood volume of a 100 years flood by 70% (Jiradecha et al., 2011).

For flood management in Tub Ma, flood mitigation primarily encompassed the operation of the outlet pumping station (Jiradecha et al., 2011). However, a major concern in the reliability of river flood management in Tub Ma was the manual control of the outlet pumping station. Operational forecasting was required based on a flood early warning system to set the pumping station in operation timely. Hence, research was needed to substantiate the decrease in flood risk by increased mitigation time.

The presumption was that early operation of the pumping station generates a negative backwater curve with an increased water level gradient in the downstream part of the river. This idea was fostered by the fact that a concrete confined channel is known for low friction compared to a natural stream. The water level gradient induced by a pumping station increases by decreasing friction losses. According to Manning's equation (Manning, 1891), increased water level gradient results in increased flow velocity and brings down the water level. So, early operation of the pumping station based on flood early warning was believed to mitigate flooding by preventing overbank flow.

### 1.1.1 Research objective

The objective of this research was: *"to define whether flood early warning-based control of the outlet pumping station results in the prevention of river flooding in Tub Ma."*

### 1.1.2 Research scope

For this research, the local water authority (Royal Irrigation Department Rayong) had expressly set attention to the control of the pumping station. Therefore, the Tub Ma river and catchment was taken into consideration in its status quo. The scope was limited to incoming flow from upstream tributaries until water leaves Tub Ma either at the outlet or in the form of overbank flow. In this way, this research addressed the root source of inundation water in Rayong: overbank flow.

### 1.1.3 Research context

The product of this research should be applicable by the Royal Irrigation Department Rayong to enhance river flood management by improved informed decision making. Academic knowledge from both Kasetsart University and Delft University of Technology was brought together. Meanwhile, locally available data, knowledge, and experience were expressly used. Hence, making use of locally surveyed data and dealing with limited data availability was part of the research objective.

Meanwhile, the research objective addressed one of the seven global targets of the Sendai Framework for Disaster Risk Reduction (2015–2030), which is an international document adopted by United Nations member states. The seventh target of the Sendai Framework says: *"Substantially increase the availability of and access to multi-hazard early warning systems and disaster risk information and assessments to people by 2030"* (UNDRR, 2015).

## 1.2 Problem statement

### 1.2.1 Research questions

In line with the research objective, the main research question was:

*Does flood early warning lead to improved control of the catchment outlet structure for preventing fluvial flooding in Tub Ma?*

Which was divided into the following two sub-research questions:

- 1 Do water level fluctuations from upstream tributaries relate to high discharge peaks in the downstream part of the river?
- 2 What is the potential contribution of the outlet pumping station for the prevention of flooding through overbank flow?

These sub-research questions are in line with the implementation checklist for the seventh global target of the Sendai Framework for Disaster Risk Reduction (2015–2030), see Figure 1. For the objective and scope of the thesis, ‘disaster risk knowledge’ (top left in Figure 1) entailed fluvial flooding (note: this is a hazard and not a risk). Research question one aimed to identify the relationship between water level in upstream tributaries and downstream river response. Consequently, the transfer path of information and the corresponding decision chain (bottom left in Figure 1) was researched descriptively and attached to this thesis. The second research question examined the effect of flood early warning on the flood mitigation capability of the pumping station. For answering this question, a hydrological model was set up first.

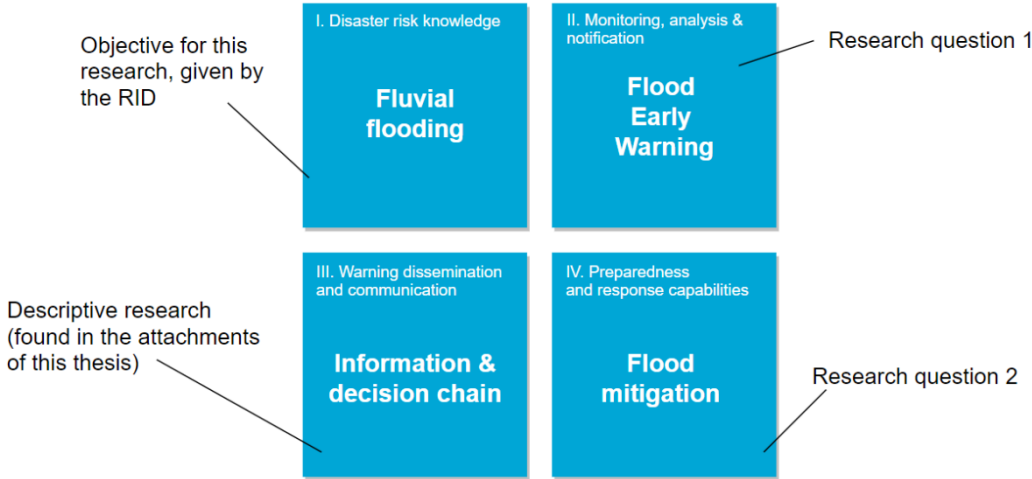


Figure 1: The four elements of the implementation checklist for the seventh global target of the Sendai Framework for Disaster Risk Reduction (2015–2030), more information in chapter 2 ‘Theoretical background’.

### 1.3 Report outline

In the next chapter ‘Theoretical background’, the key-concepts that were relevant for this research are introduced. Chapter 3 ‘Study location’ presents the characteristics of the Tub Ma catchment and river. Chapter 4 ‘Methodology’ describes the analytical framework and was the blueprint for the results presented in the follow-up chapter ‘Results.’ In Chapter 6 ‘Discussion’, the meaning and usefulness of the results are discussed, and recommendations are given for further research. Lastly, Chapter 7 gives answer to the research questions and recommendations are given for this specific case study.

## 2 Theoretical background

This section sheds light on the theoretical background used in the proceedings of the thesis. First, the fundamental requirements for early warning systems are discussed. Secondly, key concepts for the assessment of flood waves are introduced. Furthermore, the fundamentals of models addressing fluvial flood problems are pointed out.

### 2.1 Early warning systems

Early warning is a major element of disaster risk reduction that can decrease vulnerability by preparedness and response (UNDRR, 2015). The objective of an early warning system is to provide reliable and timely information to stakeholders so that they can take (better) informed decisions in response to hazards (Werner et al., 2011).

The United Nations have recently underlined the benefits of early warning systems by making it one of the seven global targets of the Sendai Framework for Disaster Risk Reduction 2015–2030: “Substantially increase the availability of and access to multi-hazard early warning systems and disaster risk information and assessments to people by 2030” (UNDRR, 2015). In order to reach this target and be effective, a checklist is developed for implementation (WMO, 2018). According to the checklist, early warning systems need to involve the following four elements actively:

- I. **Disaster risk knowledge** – Risks arise from the combination of: hazards, exposure of people and assets to the hazards, their vulnerabilities, and coping capacities.
- II. **Monitoring, analysis & notification** – Routinely survey of hazard parameters and their precursors is essential to generate accurate warnings in time. The temporal scale for monitoring must be small enough not to overlook a (short) warning signal. Data must be collected in local context to guarantee that data is correctly understood and used for providing a warning.
- III. **Warning dissemination & communication** – Warnings must reach the end-users: those at risk and the authorities/organizations who are in the position to respond to the warning. Trusted channels are required for the transfer of warning information.
- IV. **Preparedness and response capabilities** – Early warning information is only useful if timely connected to a decision. Decisions to respond compromise both preparedness and mitigation. Preparedness can reduce the loss of properties through simple yet effective measures such as temporary relocating or enacting a flood control strategy (Carpenter et al., 1999). People should be well informed on options for reducing their risks, such as evacuation routes. Mitigation strategies, such as the operation of flood defense structures, need to be well known, practiced, and tested (WMO, 2018).

#### *Flood Forecasting, Warning and Response System*

Flood Forecasting Warning and Response Systems (FFWRS) are a commonly applied disaster management strategy for the implementation of early warning systems addressing flood hazards. FFWRS enables stakeholders to respond in advance of a disaster and create lead time to mitigate the risk (Parker & Fordham, 1996). The implementation of FFWRS emphasizes the transfer of information from observed hazard parameters to decision-makers (Verkade & Werner, 2011).

In response to early warning, some time is needed for mitigation. The forecasting and warning timeline (Figure 2) shows all steps required for an effective FFWRS. From this timeline, it becomes clear that time is required for mitigation as well as for the preceding steps, resulting in lead time requirements for each of the end-users of the early warning system (Werner et al., 2011). Figure 2 suggests that the maximum available lead time equals the time between the start of an event and the threat, which is equivalent to basin response time. Responsive actions, such as temporary relocating or enacting a flood control strategy, need to be completed prior to the threat. So the temporal scale of the responsive actions set the lead time requirements of an effective early warning system. (Werner et al., 2011).

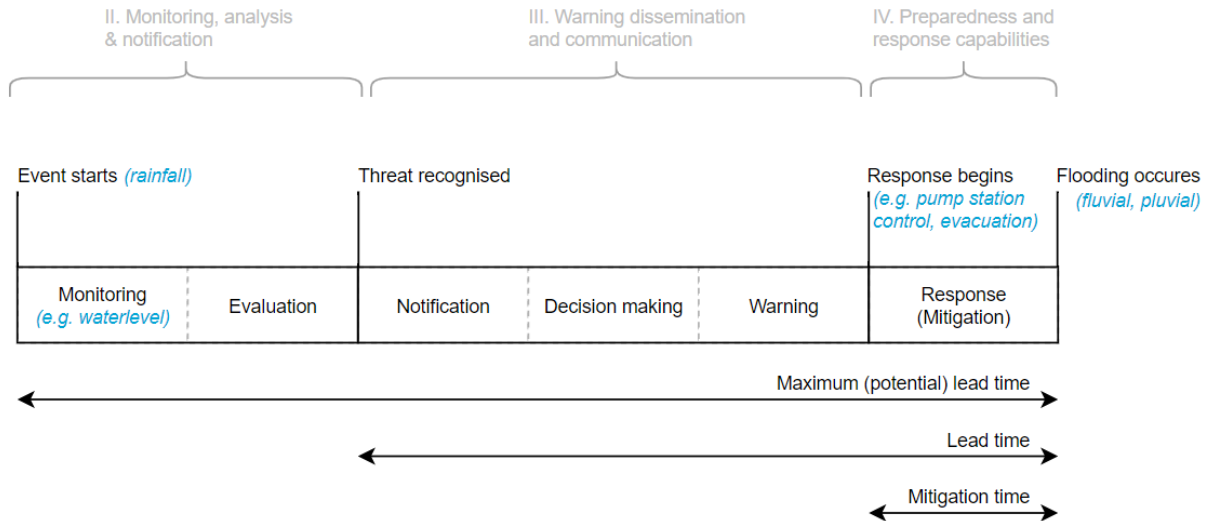


Figure 2: Forecasting and warning timeline (Werner et al., 2011), linked to the early warning implementation checklist (top of figure).

## 2.2 Flood wave propagation in rivers

The term ‘flood wave’ is commonly used to describe the solitary wave that passes down a river channel as a result of a period of heavy rainfall (Sellin, 1969). Flood waves are transient increases and decreases in discharge in a river, observed as a hump in gauged time series (Battjes & Labeur, 2017). Flood wave formation is fostered by catchment characteristics like large run-off ratio and short time of concentration, typically associated with urbanization (see 1.1 Research motivation). Therefore, it is essential to study flood waves for the assessment of fluvial flood problems in urbanized catchments (Merz et al., 2010).

### 2.2.1 Flood wave properties

From a hydrological view, a flood hydrograph follows from the rainfall hydrograph with non-linear processes and threshold processes in between. However, non-linearity and thresholds decrease by the interference of urbanization in hydrological processes. Hence, the flood hydrograph shape from urbanized catchments is closely linked to the shape of the associated rainfall event (Sellin, 1969).

Flood wave amplification is possible in streams with very high friction, but subsiding waves are most common (Battjes & Labeur, 2017). While traveling downstream, the changes in floodwave shape confine a reduction in the elevation of the crest and an increase in overall length. The extent to which these modifications occur depends on the changing cross-sections of the channel and the curvature of the wave (Sellin, 1969). A strong curvature and gradient of the flood wave foster diffusion, resulting in spatial smoothing of the profile (Battjes & Labeur, 2017).

Flood wave speed, generally referred to as flood wave celerity, is an essential parameter for flood alert and forecasting systems (Reszler et al., 2008), optimization of flood management structures (Skublics & Rutschmann, 2014), and a key (calibration) parameter in hydrological and hydraulic modeling (Price, 2009). Flood wave celerity is defined as the speed of propagation of the wave crest (Battjes & Labeur, 2017). Flood wave travel time is most commonly calculated by the reach-scale technique: computing celerity by survey of an upstream and downstream point of the reach (Meyer et al., 2018).

Simplifications of the St. Venant equations are used to numerically describe celerity, for example resulting in Eq. 1 (Battjes & Labeur, 2017). Flood wave celerity is of the order of magnitude of the flow velocity in the channel ( $U$ ). Factor  $\beta$  is dominated by friction and channel geometry. Up to bank full flow:  $\beta > 1$  and celerity is larger than flow velocity. When flood plains are submerged, friction increases and  $\beta < 1$ , which causes the propagation speed of the flood wave to become considerably less than flow velocity in the main channel (Battjes & Labeur, 2017).

$$c_{flood\ wave} \equiv \beta U \quad \text{Eq. 1}$$

Flow velocity ( $U$ ) in open channels typically increases with flow depth, so does flood wave celerity (Sellin, 1969). Hence, larger flood waves (with a larger flow depth) propagate faster than small flood waves. This also implies that flood wave celerity increases by lateral inflow, causing nonlinearity in the downstream propagation of flood waves (Sellin, 1969).

### 2.2.2 Flood wave survey

River discharge is both unsteady and non-uniform during the occurrence of flood waves. The water level slope along the river varies, being larger than the slope of uniform flow in the leading part of a flood wave (rising stage), and less in the tailing part (falling stage). This can be seen in Figure 3. So, at a given stage at a fixed location, water level slope is larger when water level rises than when it falls. The same applies to discharge since discharge is a function of both stage and slope. Hence, at a fixed location i.e. gauging station, discharge is different during the rising stage and falling stage of a flood wave for the same stage.

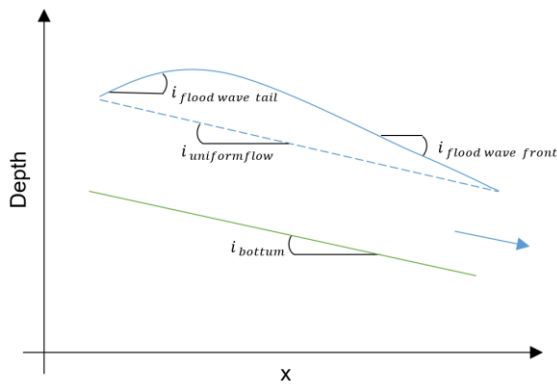


Figure 3: Longitudinal profile flood wave

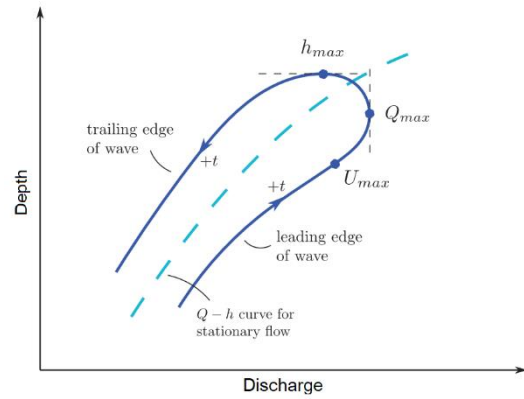


Figure 4: Example of a rating curve and counterclockwise hysteresis of a subsiding flood wave (Battjes & Labeur, 2017)

In Figure 4, the rating curve (for steady, uniform flow conditions) is plotted together with the flood wave hysteresis. The hysteresis is a plot of the discharge with the simultaneous occurring river stage, as a function of time during the passage of a flood wave at a fixed location (Battjes & Labeur, 2017). Figure 4, shows that the use of a rating curve for flood wave survey implies the following errors:

- Maximum discharge occurs ahead of the maximum stage. This is because the enlarged water level slope ahead of maximum stage enhances flow rate, which more than compensates for the larger depth at maximum stage (Battjes & Labeur, 2017).
- Discharge is underestimated during the rising stage and overestimated during the falling stage. When significant flood waves occur, errors in discharge estimation may be greater than 15% (Dottori et al., 2009).

When only stage is gauged, the hysteresis phenomenon can be taken into account using a dynamic rating curve approach, such as Jones' formula (Eq. 2). Jones first applies the rating curve, resulting in  $Q_{rating\ curve}$ , and then corrects this discharge for the non-uniform water level gradient (Jones, 1915). This correction with Jones' formula is made on the basis of water level gradient between two time steps ( $\partial y / \partial t$ ). In Jones' formula,  $U_s$  is the surface velocity divided by 0.85 for smaller streams and  $S_r$  is a "reference" water surface slope used as calibration parameter (Dottori et al., 2009).

$$Q_{hysteresis}(t) = Q_{rating\ curve}(t) \left[ 1 + \frac{1}{U S_r} \frac{\partial y(t)}{\partial t} \right]^{\frac{1}{2}} \quad \text{Eq. 2}$$

## 2.3 Models addressing fluvial flood problems

### 2.3.1 Hydrologic and Hydraulic models

A model is a simplified representation of a real-world system. In water management, models are mainly used for predicting system behavior and understanding various hydrological or hydraulic processes (Devia et al., 2015). Hydrologic and hydraulic flow routing are two mathematical methods (models) that predict the spatial and temporal flow of water between and within the phases of the hydrological cycle. Although both terms are often interchanged, hydrological models mainly address water quantities transferring between phases of the hydrological cycle, while hydraulic models calculate water movement based on its physical properties (Markar et al., 2006).

#### *Models for channel routing*

Channel routing is a mathematical method (model) that can predict the timing of the peak, peak magnitude, and shape of a flood wave as it travels through a river network (Fread, D.L., 1985).

Hydrologic channel routing is based on empirical storage-discharge relationships, of which the Muskingum method (Gill, 1978) is the best-known example. This model can reproduce a flood wave correctly when the assumed storage-discharge relationships are well fitted to the actual flow dynamics characteristic of the river network (Gill, 1978). Since these relationships are empirical-based, river geometries are not considered and the model cannot capture the dynamic flood wave properties caused by channel/floodplain interaction and backwater effects from structures (Chi Choi, 2013). Hydrologic channel routing models are fast and can be set up in simple balance sheet.

Hydraulic channel routing is a different type of model, which attempts to solve the coupled continuity and momentum equations of one-dimensional Saint-Venant equations (Chi Choi, 2013). Therefore, hydraulic models require extensive physical-based data, such as river geometries and topographic information. Dynamic flow characteristics like backwater effects are well handled. Downsides of the hydraulic routing technique are the need for physical information and sometimes long calculation times.

#### *Use-case based modeling*

Rainfall run-off simulations are the most applied models, addressing the non-linear threshold process between rainfall and river discharge by a hand full of free parameters (Savenije, 2009). However, for a design task or problem assessing a specific part of the hydrological cycle, more parameters and data are added for the specific problem. For example, for a case about the effect of trees on run-off generation, parameters are added addressing: canopy interception, throughfall, stem flow, forest floor interception, and transpiration (Marin et al., 2000). Soon, models are over-parameterized with too many degrees of freedom without enough criteria to constrain a model. Over parameterized models generally result in good performance but high uncertainty associated with equifinality (Hrachowitz et al., 2014). The contrasting priorities of increased model complexity and limited uncertainty can be satisfied by narrowing down the scope of the model. By adjusting the scope to the use case, complexity and the degrees of freedom are brought down, and models become less uncertain. In this example about trees, the general scope of 'rainfall- outlet discharge' could be reduced to 'rainfall-groundwater recharge'.

The same applies to models addressing fluvial flooding problems for which river streams are modeled in detail. To bring down the scope, the rainfall run-off part of the model resulting in the (lateral) inflow is often replaced by a synthetic flood design hydrographs (SFDH), regularly referred to as a design storm (Candela et al., 2014).

Lastly, it is generally understood that not the degree of uncertainty or a root mean square error defines whether a model is useful, but that usefulness depends on the required information from the model (Savenije, 2009). More specifically, the research questions or objectives (including the required maximum uncertainty) determine whether a model is useful or not. Among many others, George Box's has emphasized this view on models by his famous quote: "all models are wrong, some are useful" (Box, 1979). So, regarding the example where a design storm replaces a model part, this action does not make the model wrong (since it was already wrong) but can make a model more useful.

### 2.3.2 SOBEK

SOBEK Rural 1DFLOW module (in short: SOBEK) is a hydraulic numerical model designed by Deltares. This module works with the complete Saint Venant equations, including transient flow phenomena and backwater profiles. The program carries out one-dimensional hydraulic calculations of an area that is schematized by a network of open water channels. A network can consist of several branches and structures, cross-sections can vary within a branch. So, for the set-up of a network, physical-based data such as river geometries are required. For a set input flow, e.g. design storm or observed time series, SOBEK calculates the flow routing through the network for a predefined time step. All calculated quantities are cross-section averaged values (Deltares, 2019).

### 3 Study location

In this chapter, the characteristics of the case study location and Tub Ma river are introduced.

#### 3.1.1 Thailand (social-) geography and climate

Thailand, officially the Kingdom of Thailand, is a 510.000 km<sup>2</sup> (Worldbank, 2018) encompassing country and has a population of 70 million people, of which now 51% are urban residents compared to only 21% half a century ago (Worldometer, 2020). According to the Worldbank, Thailand is a fast developing upper-middle income economy. But, Thailand is also facing increasing inequality: the household consumption of the bottom 40% of the population shrank 10% in the last 5 years, and 10% of the population lives in poverty (Worldbank, 2020).

Thailand has a tropical monsoon and tropical savanna climate (Köppen 2020). The country has two distinct monsoons and three seasons (Figure 5).

- *Winter season* corresponds to the north-eastern monsoon. As a result of the prevailing dry offshore wind, winters are characterized by little rain.
- *Summer season*, which is hot, is considered to be a transition period between both monsoons.
- *Rainy season* corresponds to the prevailing southwest monsoon. Onshore wind carries moisture-laden air from the Gulf of Thailand to the mainland.

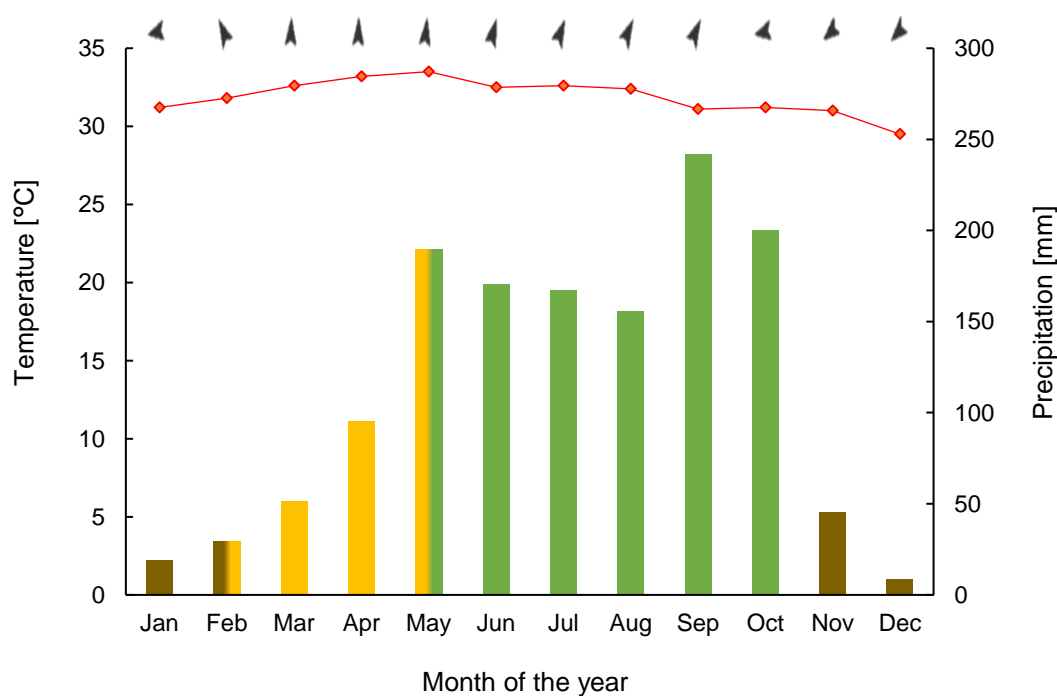


Figure 5: Climate chart of Rayong province (climate-data.org, 2020) with monthly average values of precipitation (bars), temperature (red line), wind direction, and seasonality (brown for winter-, yellow for summer-, and green for rainy season).

Rainfall has an irregular temporal and spatial distribution, associated with the typical convective system of the monsoon rains. Heaviest rainfall peaks mainly occur at the end of the rainy season due to the retreat of the monsoon, generally from August to September (Khedari et al., 2002). On top of that, tropical cyclones and low-pressure cells are other causes of heavy rainfall (Thai Meteorological Department, 2018). Tropical cyclones generally occur from August to October (Mergen & Longshore, 2001).

### 3.2 Tub Ma catchment

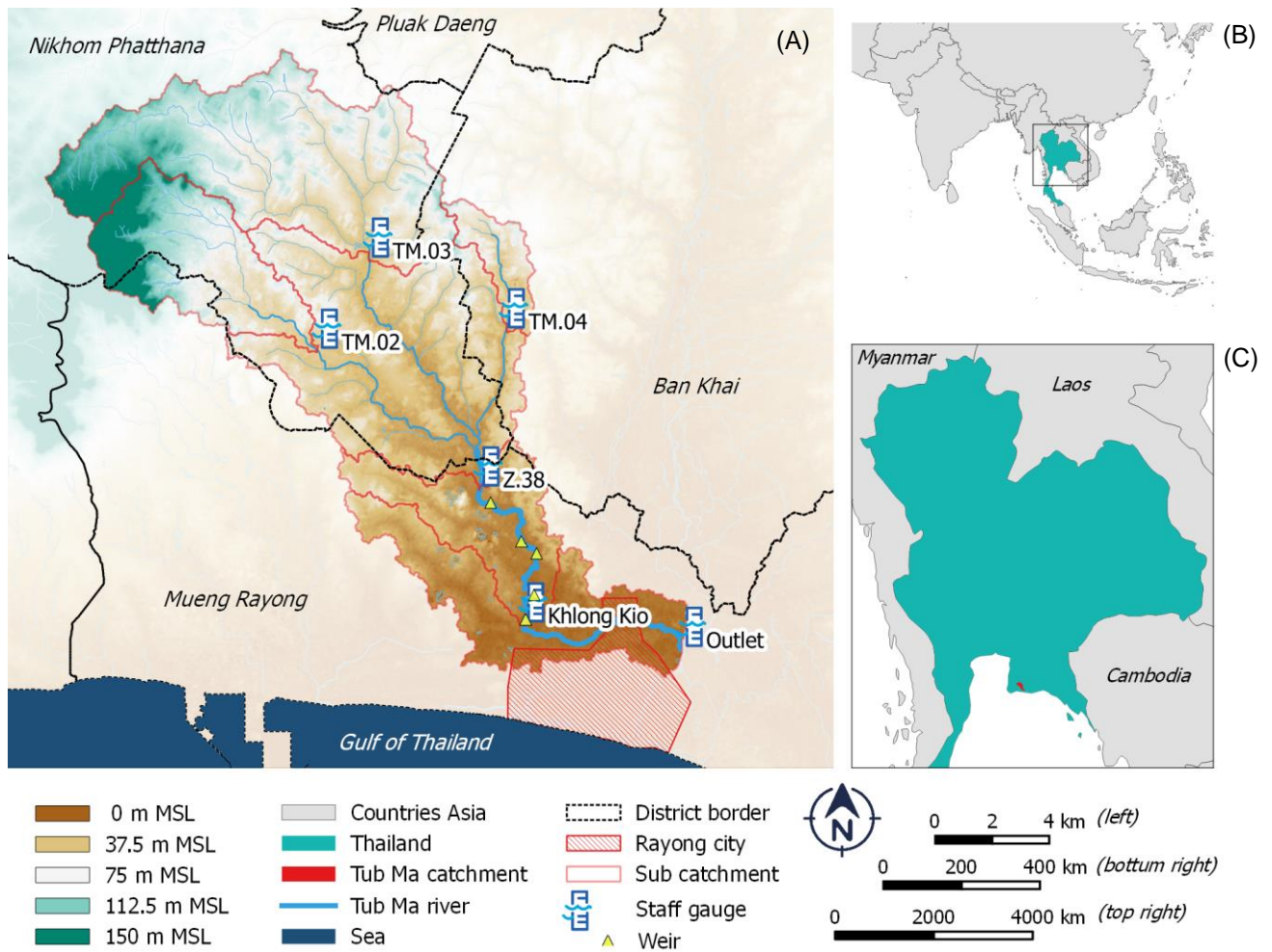


Figure 6: Location overview Tub Ma catchment.

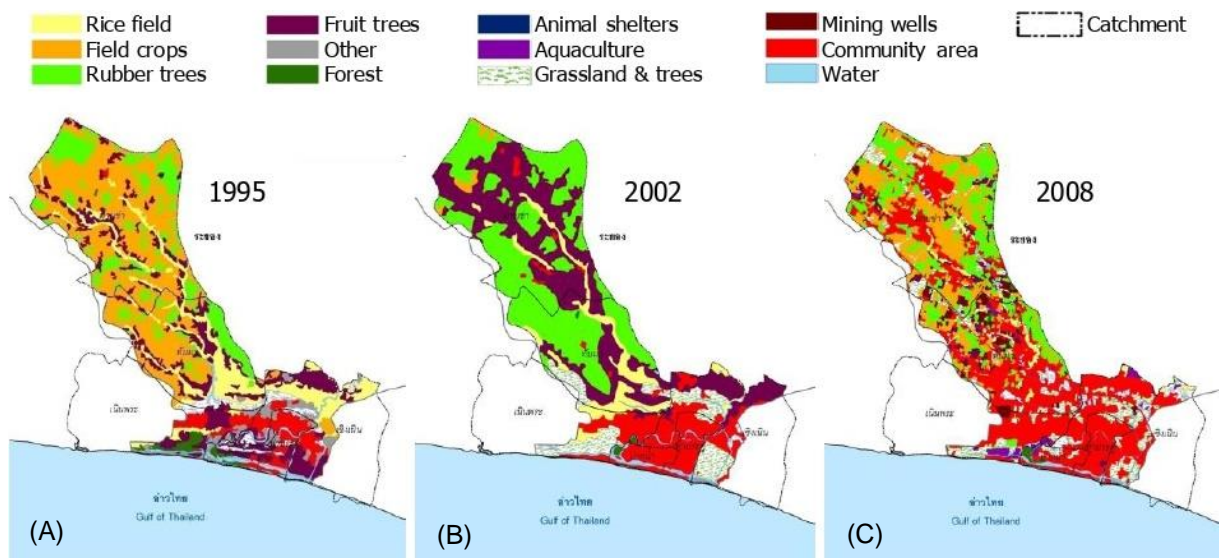


Figure 7: Land cover map of Tub Ma catchment for the year 1995, 2002 and 2008, provided by the Department of Land Development.

Rayong province has seven administrative districts, of which the Tub Ma catchment covers three. Caution is needed when talking about 'Rayong', since one of those three districts is also called "(Mueng) Rayong" and the main city is named "Rayong" as well (see panel A in Figure 6). With a total area of 200 km<sup>2</sup>, the catchment is relatively small compared to the larger Khlong Rayong Basin, where Tub Ma is part of. Dominated by rolling topography, the catchment only has a hillier region in the north-west.

Figure 7 expresses Tub Ma's land cover as a humanized landscape. In the first wave of ongoing humanization (1995-2002), agricultural land was mainly replaced by rubber tree plantations. After 2002, community areas expanded due to the presence of growing industrial sectors in nearby areas.

### 3.3 Tub Ma river

Tub Ma is a rain-fed river. Consequently, the river flow regime is highly variable. Response times are typically in the order of hours. Streamflow consists of rainwater-runoff and water from urban sewer systems that generally have their outlet in the river. Except for the rainy season, no baseflow is present and discharge reaches 0 m<sup>3</sup>/s. In contrast, flood waves with peak discharge up to tens of m<sup>3</sup>/s are recurring after substantial rainfall peaks at the end of the rainy season.

Citizens map water levels by uploading pictures of the staff gauges showed in Figure 8, commonly once a day. Besides, at measuring station Z.38 (Figure 8), a sonar sensor is present that logs water level on a 15-minute interval. Based on this sonar data, Kasetsart University calculated the probability of peak discharges at Z.38 for different return periods, see Table 1 (Jiradecha et al., 2011).

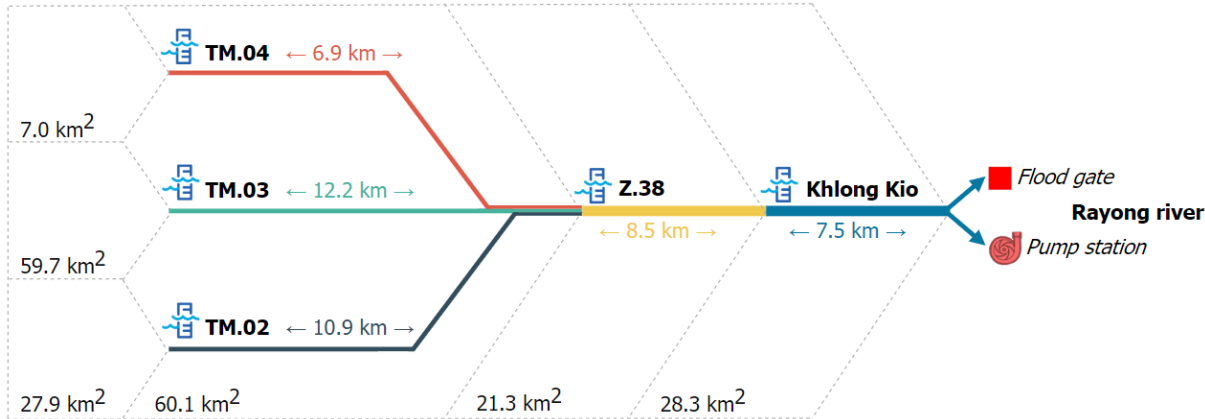


Figure 8: Schematic overview (not on scale) of the Tub Ma river, including the sub-catchment area (from section 5.2.3) and reach length.

Table 1: Return period of peak discharge in Tub Ma channel at gauging station Z.38 (Jiradecha et al., 2011).

Return period [year]	2	5	10	25	50	100
Peak discharge [m <sup>3</sup> /s]	28.2	42.5	52.0	63.9	72.8	81.6

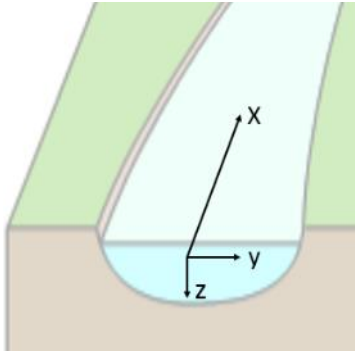


Figure 9: Axis directions for the description of river bathymetry.

Tub Ma is not a natural- or free-flowing river. Between Z.38 and Khlong Kio (Figure 8), five weirs are present for storing irrigation water (Jiradecha et al., 2011). The weirs are effectively small dams and allow water to flow when water level exceeds crest-level. These structures induce friction and threshold values for river flow. Hence, weirs are important to include in a river routing model.

All streams are laterally unconfined: the river is still meandering through the catchment (x-axis, see Figure 9). Meanwhile, the cross-sectional geometry (y- and z-axis) is partly-confined by the construction of concrete floodwalls. Riverbed is still natural and mainly consists of rocks in the upstream parts and fine sediment in the downstream region. Where no floodwalls were constructed, vegetation 0.5 to 1.5 m high is present inside the permanent channel itself and on the riverbanks.

The Tub Ma river discharges through the Rayong river into the Gulf of Thailand. Given the short distance from the Tub Ma's outlet to the coast, tidal fluctuations are present in the most downstream part of the river. The Gulf of Thailand's upper part has a micro-tidal coast (Masselink & Short, 1993) with a diurnal tide and a tidal range of around 0.5 m (Siripong, 2010). Therefore, the diurnal tidal fluctuations in Tub Ma are small.

At the mouth of Tub Ma, all flow has to go through a floodgate to discharge into the Rayong river gravitationally. Occasionally, the floodgate was closed to prevent water from entering the catchment from the downstream direction. Right next to the floodgate, an electrical river pumping station is present for the situations at which the floodgate is closed. This pumping station consists of 5 submersible pumps with free outflow; each turbine has a capacity of 5 m<sup>3</sup>/s and a total head of 4 m. A maximum of 4 pumps are running at the same time, so the total maximum capacity is 20 m<sup>3</sup>/s. Automatically switch-on and switch-off levels are not used. Instead, the pumping station is operated based on a time-to-time expert review from the management op de RID (Royal Irrigation Department).

# 4 Methodology

This chapter describes the applied methodology for data survey, analyses, and applied tools. The first section (4.1) outlines the fieldwork data survey and data processing. The subsequent sections in this chapter follow the elements of the checklist for early warning systems (see Figure 10). Section 4.2 describes the methodology for answering the first research question, assessing flood early warning. Then, the setup of a hydraulic model was described in section 4.3, which was part of the methodology for answering the second research question (section 4.4).

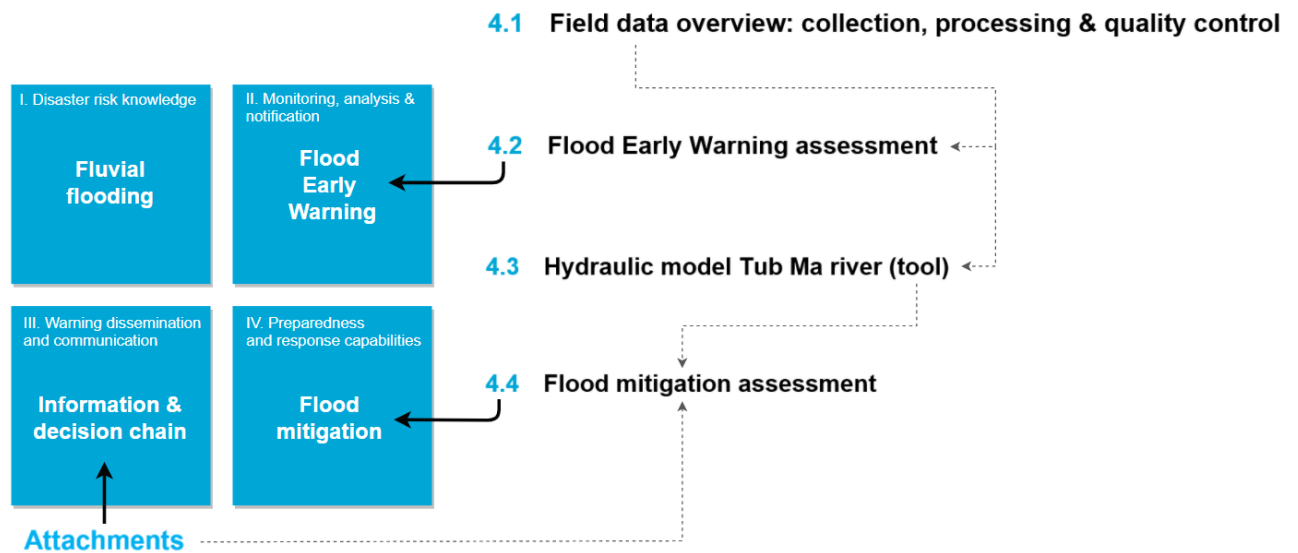


Figure 10: Overview of methodology & checklist for early warning systems (described in chapter 2 'Theoretical background')

## 4.1 Field data overview: collection, processing & quality control

Figure 11 introduces the different types of data(sets) that were surveyed during the fieldwork trip lasting from August until November 2019. This data formed an overarching base for the methodology of all subsequent sections in this chapter.

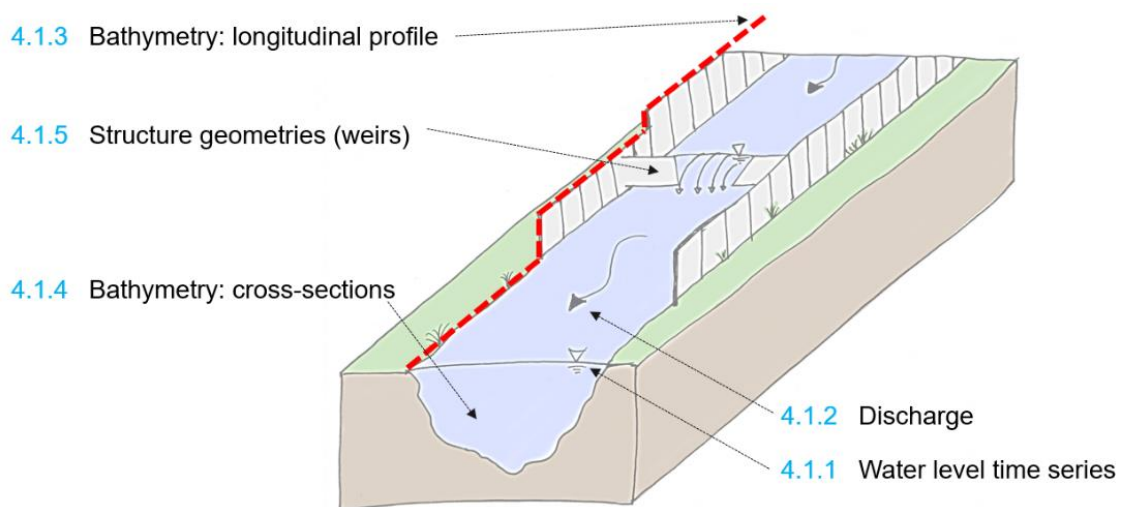


Figure 11: Overview of fieldwork data survey.

#### 4.1.1 Water level time series

Water level time series were collected between August 28 and November 7, 2019. Three different devices were used for stage-monitoring. A schematic overview of the sequence of gauging stations is presented in Figure 12. Table 2 names the different devices that were placed at each gauging station, and Figure 13 illustrates those devices.

Making use of the local devices was a guiding principle in this research. At all gauging stations with local devices, water pressure devices called Divers (Van Essen Instruments B.V. ©) were placed as well. Those Divers had a 5-minute measurement interval and had a 2 cm precision (Van Essen Instruments, 2016). Hence, the time series logged by the Divers were used to understand the flow regime (on a short interval) and used to benchmark the local devices. Consequently, it was assessed whether the local devices were useful for flood early warning.

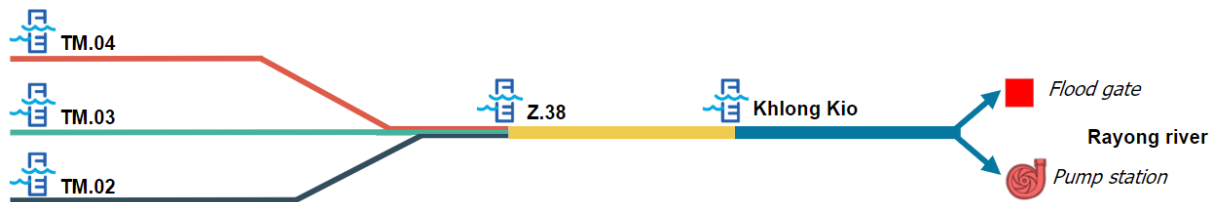


Figure 12: Schematic overview of gauging stations in Tub Ma river.

Table 2: Overview of stage-monitoring devices at gauging stations.

Gauging station:	TM.02	TM.03	TM.04	Z.38	Khlong Kio	Outlet -upstream (Tub Ma river)	Outlet – downstream (Rayong river)
Sonar sensor				x			
Mobile Water Management	x	x	x	x	x		
Diver (Van Essen Instruments B.V. ©)	x	x	x	x	x	x	x

The sonar sensor was hanging next to the bridge at Z.38, owned and controlled by the Royal Irrigation Department (RID). This sonar sensor indirectly monitored stage on a 15-minute interval. The sonar sensor was pre-calibrated, and stage was converted to MSL reference. Stage was automatically logged online and publicly accessible.

Citizen-based water level registration was performed using mobile phones. 'Mobile Water Management' (MWM)-staff gauges were present next to the staff gauges of the RID. Citizens made photographs of the MWM-staff gauges using the 'Peilregistratie' application on their mobile phones. The image recognition module of the application reads water level from the picture right away and stores the information in an online database (Mobile Water Management, 2020). The RID staff gauges were used as a reference to calibrate the image recognition module of the Peilregistratie application. According to the RID, survey by citizens takes place on a daily basis.

The Divers monitored pressure on a 5-minute interval and logged this data to the internal storage of the device. PVC monitoring tubes were installed next to RID's staff gauges in which the pressure sensors were installed. Besides, a barometer (Van Essen Instruments B.V. ©) was hanged for measuring atmospheric pressure on the same 5-minute interval. The height of the water column above each Diver (see Figure 13) was determined by correcting for atmospheric pressure. This barometric compensation for variations in atmospheric pressure was performed using Diver-Office software (Van Essen Instruments B.V. ©). Consequently, water column height was adjusted to water level while using the RID staff gauges as reference for calibration.

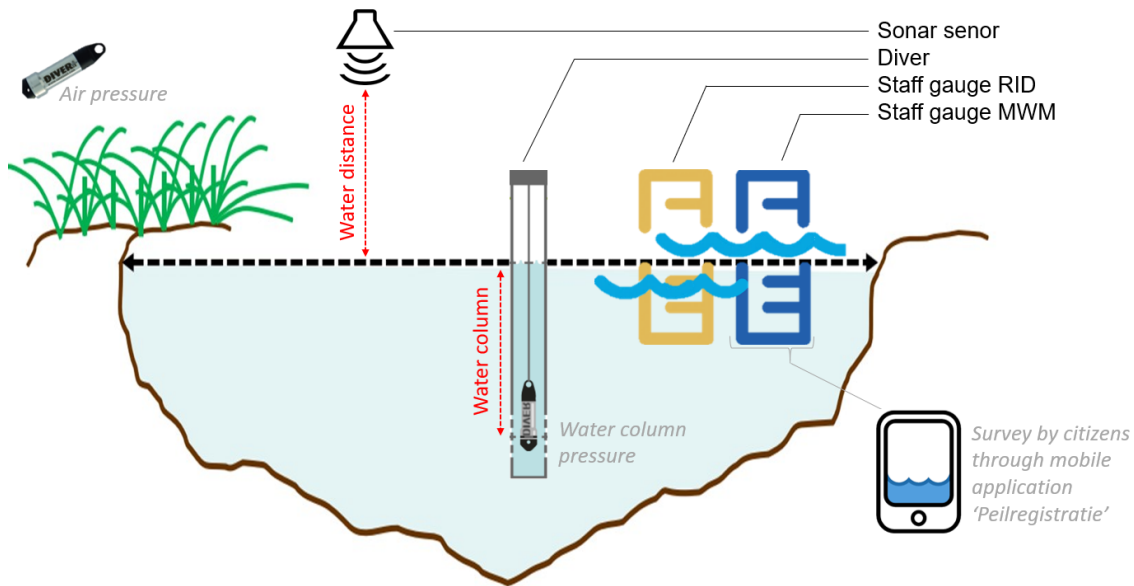


Figure 13: Overview of stage monitoring devices.

#### Quality control

The obtained water level time series from all three devices were plotted together to compare the data visually. Single-timestep outliers (attributed to e.g. debris and temporary failure of the device) were removed from the time series obtained by the sonar sensor and Divers. Outliers in the Mobile Water Management time series were visually checked by searching for the original photos in the online MWM-database. For benchmarking the time series from WMW and the sonar sensor, the double mass analysis and residual mass analysis were applied. These analysis techniques were chosen because they visualized both accuracy and precision over time.

The principle of the double mass analysis is to plot accumulated values of one gauging station ( $\sum X$ , representing the Diver) against accumulated values of a second gauging station ( $\sum Y$ ) over the same period of time (Luxemburg & Coenders, 2017). The principle behind the residual mass analysis (Eq. 3) is to plot  $M_i$  against  $\sum X$ . Hence, inflection points (double mass analysis) and the up-/downward/horizontal direction of the curve (residual mass analysis) indicate any deviation of station  $Y$  from a constant relation between station  $Y$  and  $X$  (Luxemburg & Coenders, 2017).

$$M_i = \sum Y_i - \bar{Y} / \bar{X} \sum X_i \quad \text{Eq. 3}$$

#### 4.1.2 Discharge

Discharge was calculated by converting water stage time series into discharge using rating curves. The water level time series retrieved with the Divers were used for this calculation.

Meanwhile, the high flows in the water level time series required an extra step in the conversion process. Flood waves in streams with a gentle slope ( $>10^{-3}$ ) are associated with a variable energy slope and unsteady flow discharge, resulting in a hysteretic rating curve, also known as the loop-rating curve (Jones, 1915). The use of a steady-flow rating curve for flood waves was considered to lead to major errors greater than 15% in discharge estimation (Dottori et al., 2009). As a solution, Jones dynamic rating curve approach was applied for calculating discharge during peak flows.

#### Rating curves

For gauging station Z.38, a rating curve was provided by the RID based on surveys in 2017 and 2018. At Khlong Kio, a rating curve was constructed manually. Khlong Kio is located downstream of Z.38, and no storage or extraction takes place in between both gauging stations. Meanwhile, lateral inflow was present. Hence, the condition was set that discharge at Khlong Kio must always equal or exceed

discharge at Z.38, while taking into account the lag time between both gauging stations. The Manning equation (Manning, 1891), in combination with a detailed survey of the cross-section at Khlong Kio was used to establish a rating curve at Khlong Kio. Discharge was measured at different stages serving as calibration points for the rating curve at Khlong Kio. A current meter and ADCP boat were used to survey discharge:

- By using a current meter, point velocities were measured at several widths and depths of the cross-section to construct a velocities-profile. Consequently, discharge was obtained after applying the area-velocity method (Herschy, 1993).
- An ADCP-boat (Acoustic Doppler current profiler) was used to measure velocities-profiles. Discharge was obtained by processing the ADCP data with the manufacture's software. Using the ADCP-boat was preferred over the current meter because of accuracy and less manual labor (Obergruber, 2002). Nevertheless, the current meter was used when the ADCP-boat malfunctioned during fieldwork.

Consequently, the rating curve at Khlong Kio was established by calibrating the Manning equation (Eq. 4) to match the stage-discharge measurements. In Eq. 4,  $Q$  is discharge [ $m^3/s$ ],  $n$  is the friction coefficient [ $s/m^{1/3}$ ],  $A$  is the wet cross-sectional area [ $m^2$ ],  $R$  is hydraulic radius [ $m$ ], and  $s$  is channel slope [ $m/m$ ]. During calibration, via trial-and-error of 'friction' and 'slope' parameters, respectively  $n$  and  $s$  were adjusted.

$$Q = \frac{1}{n} A R^{\frac{2}{3}} s^{\frac{1}{2}} \quad \text{Eq. 4}$$

#### *Jones dynamic rating curve approach*

Jones' formula was used as dynamic rating curve approach (for theory, see section 2.2.2) for calculating discharge during high flows observed at Z.38 and Khlong Kio. Jones' formula was calibrated by  $Sr$ , resulting in a hysteretic rating curve that intersects (or approached closely) the stage-discharge measurements at Z.38. So  $Sr$  was calibrated on the shape of the hysteresis.

#### *Quality control*

The rating curve and corresponding discharge at Khlong Kio were validated by plotting the discharge at Z.38 and Khlong Kio cumulatively. Consequently, it was checked whether discharge at Khlong Kio always equaled or exceeded the discharge from the upstream gauging station Z.38.

#### *4.1.3 Bathymetry: longitudinal profile*

Bathymetry data was available in the form of river cross-sections (y-z profiles) and bottom level (Jiradecha et al., 2011). This data set contained bottom-level and bank-level (both left and right side) in reference to MSL at 40 cross-section locations (number 13-38 and 40-53 in Figure 14). Hence, a longitudinal profile was obtained through linear interpolation of bottom- and bank-level between the y-z profiles. However, the longitudinal profile was outdated where floodwalls had been constructed. Therefore, the floodwall level was surveyed using point measurements at locations of the y-z profiles.

Single GPS (or GNSS) sensors in mobile phones were reviewed as not suitable for floodwall level survey, given the low precision with deviations up to tens of meters in z-direction (Eissfeller et al., 2007). This problem of random errors was counteracted by using a differential GNSS set up with two receivers. A differential GNSS has a precision of centimeters (Shum et al., 2010). As a result of the high precision, accuracy does not play a role because all measurements would have the same constant offset. By logging the positioning of a calibration point as well, a constant offset is easily removed afterward.

#### *GNSS set up with two receivers*

The GNSS set-up was built in collaboration with a colleague-student from Delft University of Technology, who described the exact setup and function for parallel research (Boer, 2019). Appendix A provides a summary of the GNSS set up.

The base station receiver was fixed on top of the Rayong Area Revenue office because that was the highest accessible building in the area. The 'rover' (second receiver) was placed on top of a cap (see Picture 3 and Picture 4 in Appendix A). While walking over the floodwall wearing the cap, the three-dimensional position of the rover antenna was logged every second (see Figure 14). In this way, an extra bias in z-direction equal to the length of the person wearing the cap was present and corrected for afterward. U-centre software (uBlox) was used for data processing.

#### Calibration & MSL referencing

Apart from walking along the floodwall with the GNSS rover antenna, dike levels of unchanged y-z profiles were surveyed as well. Consequently, those dike levels were used as calibration points for the GNSS data set. After calibration, both the original bathymetry data and the floodwall height had the same (MSL) reference frame.

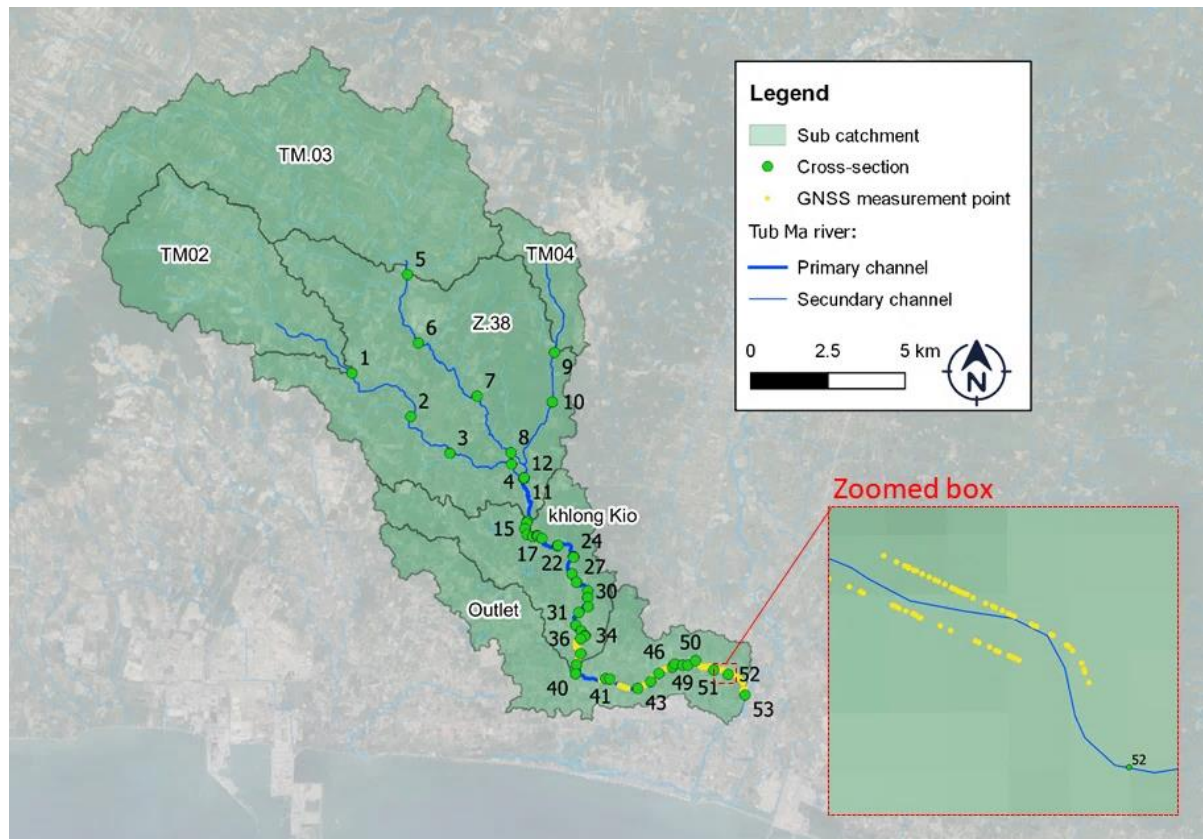


Figure 14: Aerial view of the numbered cross-section locations (in green) and the x-,y-,z- point measurements surveyed by the GNSS set up (in yellow).

#### 4.1.4 Bathymetry: cross-sections

The bathymetry of the Tub Ma river was mapped as y-z profiles at 53 cross-sections (see Figure 14). At 40 cross-section locations, bathymetry data was available from previous research (see section 4.1.3). Where floodwalls had been built, the available bathymetry data was updated. Floodwall level was obtained from fieldwork (see section 4.1.3) and applied to the y-z plots. The following procedure was applied to adjust the y-z plots for observed floodwalls:

1. Distance between left and right floodwall (cross-section width) was measured during fieldwork;
2. It was assumed that both floodwalls (left and right) were placed symmetrically to the midpoint of the cross-section;

The other 13 cross-sections (numbers 1-12 and 39 in Figure 14) were surveyed by hand. At each location, wet and dry cross-section was surveyed separately. For mapping the wet cross-section, a rope was spanned across the channel (perpendicular to the riverbanks) with markings on a fixed interval of

1 meter. Consequently, the water depth was measured at each marked interval along the rope by using a yardstick. The dry cross-section was mapped by measuring the cross-sectional width at several distances above water level.

#### Validation floodwall level

A sample of floodwall-adjusted cross-section plots was validated by comparing the plotted height above soil (distance top of floodwall - river bed, see Figure 15) with fieldwork measurements.

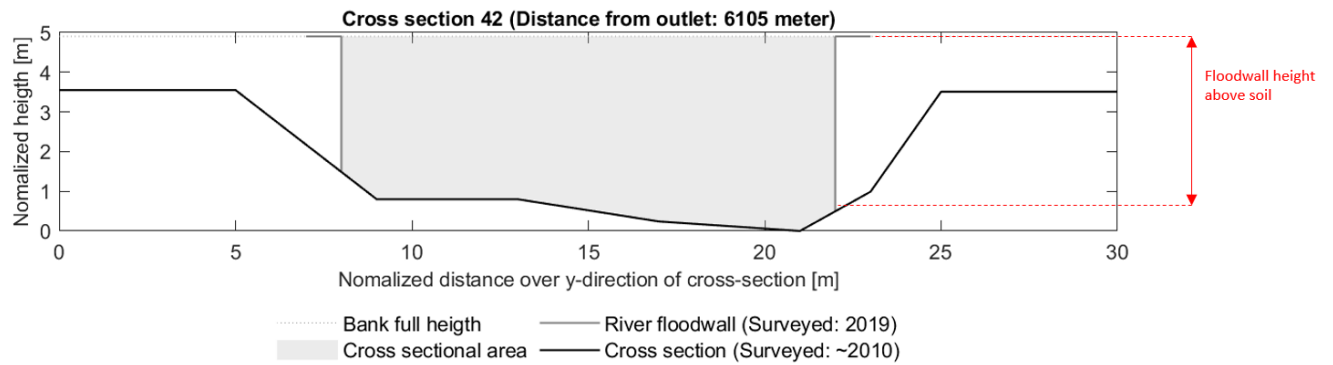


Figure 15: Illustration of the floodwall's height above soil, used as a validation parameter in this research.

#### 4.1.5 Structure geometries (weirs)

Between Z.38 and the outlet, no recent information about river weirs was available. Each historically known structure was searched for using satellite images from Google Maps, and by following the path of the river. The survey of the weirs consisted of mapping the exact location and measuring the dimensions.

Sedimentation around weirs generally takes place at the upstream side of the river (Kang et al., 2012). Therefore, the downstream side of the structure was set as 'real' bottom level. This 'real' bottom level was obtained by linear interpolation of the closest cross-section up- and downstream. Consequently, the crest-level was measured in reference to bottom level at the downstream side of the weirs.

Based on the distance between the weirs, water level slope was calculated (Figure 16). At the moment of survey, discharge was close to 0 m<sup>3</sup>/s. Hence, water level slope between the structures was expected to be close to 0 as well. The bottom level (and so crest level) of the weirs was adjusted such that water level slope ranged between 0.01 and 0 m/km.

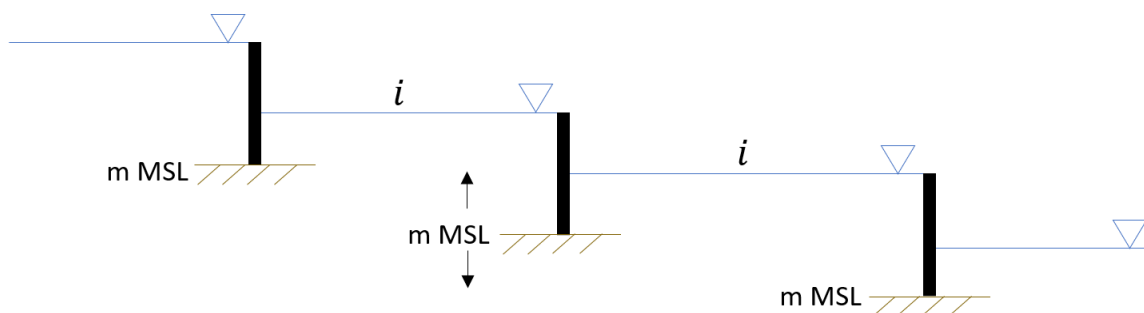


Figure 16: Visualization of validating MSL reference by water level slope between structures.

## 4.2 Flood early warning assessment

This section addresses the methodology for answering the first research question: “Do water level fluctuations from upstream tributaries relate to high discharge peaks in the downstream part of the river?”

### 4.2.1 Lag time: cross-association

Cross-association (Eq. 5) is a statistical technique to relate two sequences of nominal data at successive time lags (Davis, 1986). In this analysis, a relation is the condition that the nominal value of both series is the same for a given lag time. For determining the lag time of peak flows, cross-association was performed between water level downstream (Khlung Kio) and water level at all gauging stations upstream of Khlung Kio.

Water level times series retrieved from the Divers (see section 4.1.1) were used as input for cross-association (Eq. 5). Each time series was nominalized into a binary time series (true or false). For nominalization, a threshold value was set that classified discharge as 'true' (above threshold) or 'false' (below threshold). This threshold was manually set at a level where it outreached baseflow and noise from small rises in discharge. At successive time lags (corresponding to a celerity between 0.1 and 1.5 m/s), the number of matches between Khlung Kio and each upstream sequence was counted ( $m$ ) as well as the number of possible matches ( $n'$ ). Consequently, the degree of correspondence was given by the index of similarity ( $I_s$ ). Whereas the index of similarity is defined as the ratio of the number of matches over the possible number of matches (Davis, 1986). The retrieved index of similarity was tested on statistical significance using a Chi-squared-test.

$$I_s(t_{lag}) = \frac{m}{n'} = \frac{\text{number of matching pairs}}{\text{number of compared pair}} \quad \text{Eq. 5}$$

### 4.2.2 Matching peak flows

While the index of similarity takes into account all data points of a sequence, insight was also required in the degree of correspondence between individual peak flows. At each gauging station, all separate 'events' (contiguous water level above the threshold value) were searched and labeled by date-time. For each event at Khlung Kio, associated events at all the upstream gauging stations were matched based on their date-time labels and the expected lag time (see section 4.2.1).

### 4.2.3 Proportionality flood early warning locations

It was qualitatively described how the discharge of the three tested flood early warning gauging stations (TM.02, TM.03, TM.04) contributed to downstream flow, relative to each other. The rational method (Kuichling, 1889) predicts stormwater run-off based on catchment area, runoff-coefficient, and rainfall intensity. All three parameters from the rational formula were evaluated per sub-catchment.

#### Catchment area

The area of each sub-catchment was calculated by applying the watershed delineation method in QGIS using the USGS digital elevation model. The gauging locations were set as pour points for this analysis.

#### Run-off coefficient

Given the large degree of urbanization, it was presumed that the degree of impervious area dominantly determined the run-off coefficient of the sub-catchments. Therefore, the run-off coefficients of the sub-catchments were related to each other by considering the degree of urbanization through two methods:

As a first method, a demonstrated relation between road density and run-off was used (Endreny & Thomas, 2009). Road density [ $\text{km}/\text{km}^2$ ] was retrieved per sub-catchment by using a shapefile containing all roads in the Tub Ma catchment, provided by the RID.

Secondly, NDVI-analysis was used as an information extraction approach for estimating spatial representative run-off coefficients. High NDVI values indicate that the vegetation is denser and the higher vegetation density level shows a smaller run-off coefficient value (Suhardi & Entin, 2019;

Thanapura et al., 2007). Band 4 and 5 of Landsat 8 satellite images (retrieved from <https://earthexplorer.usgs.gov/>) were used for calculating NDVI. At the end of the rainy season, vegetation was in the greenest colored state while urban land use has the same surface all year round. Therefore, an image of November 5, 2018, was used because this was a cloud-free day at the end of the rainy season.

#### *Rainfall intensity*

For the two extreme events in 2018 and 2019, radar-rainfall data was available from parallel research (Methaprayun, 2020). This hourly precipitation data was averaged per sub-catchment and plotted in hydrographs. Consequently, the sub-catchment specific hydrographs were used as an indication of the spatial variability of the rainfall intensity during extreme events in Tub ma.

### **4.3 Hydraulic model Tub Ma river (tool)**

This section describes how available data and fieldwork observations were conceptualized into a model. During the set-up of the model, the requirements from the research question were applied as a guiding principle for assumptions and simplification.

#### *4.3.1 Choice of model*

For answering the research questions in this thesis, a channel routing model was required that captures dynamic flood wave properties caused by backwater effects from structures. For that reason, a hydraulic model was chosen and not a hydrological model (see background theory in section 2.3.1).

Based on the available data, a 1D model was preferred above a 2D model. In this way, the principle that “a model cannot be more complex than what is justified by the input data” was taken into consideration.

Sobek 2.16 (Deltares ©) was used to set up a 1D hydraulic model of the Tub Ma river. The RID had no preference for using a particular model. A selection of modeling suites was made based on the requirements for the use case. Consequently, Sobek was chosen because of the model's general reputation of being a 'stable model that does the job.' The Sobek-Rural 1DFlow module was most suitable for modeling a 1D channel network and for controlling pumping stations (Deltares, 2019).

#### *4.3.2 1D schematization*

Between gauging station Z.38 and the outlet, a model was built consisting of a single stream (see Figure 17). The upstream boundary corresponded to gauging station Z.38 and was modeled as a discharge boundary. The downstream boundary was located behind the floodgate and pumping station and was modeled as a water level boundary. Every 500 m (roughly the distance between two calculation steps), a node for lateral inflow was added.

The bathymetry of the stream was modeled by nodes, which represented the cross-sections (see section 4.1.4) and weirs (see section 4.1.5). Cross-section 1 to 13 were not used since they were located upstream of Z.38. Manning's  $n$  values were used for representing the friction applied to the flow (Manning, 1891). At the natural cross-sections, dense vegetation was observed, while almost no vegetation was present along the floodwalls. Based on this observation, a distinction was made between friction values for stream parts with and without floodwalls.

All weirs were added to the model and described by width, crest level, and opening dimensions (see section 4.1.5). At the outlet, the pumping station and flood gate were placed parallel. The floodgate is modeled as a sluice and was described by crest level and opening dimensions.

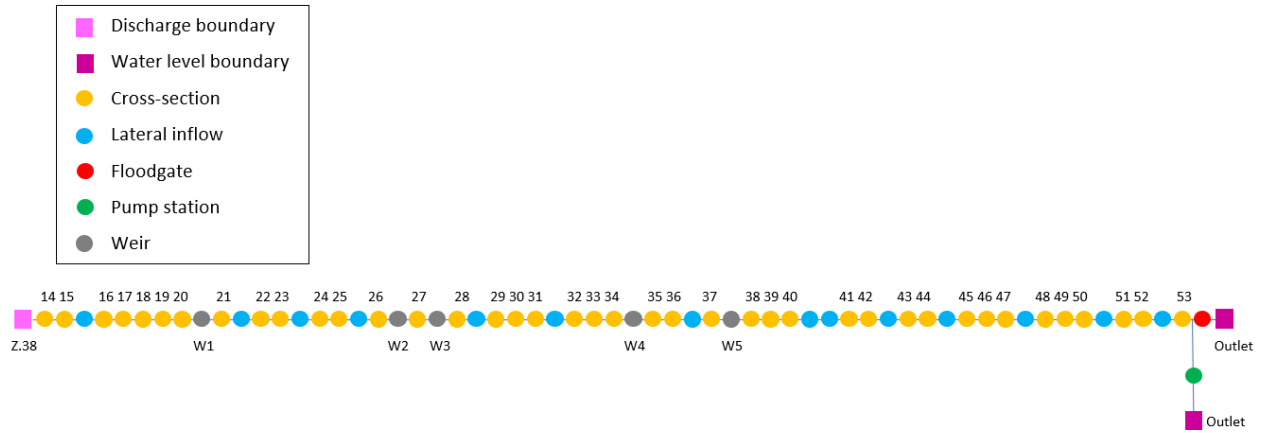


Figure 17: Overview of the model schematization (nodes).

### 4.3.3 Calibration

Discharge calculated from the time series logged by Divers (see section 4.1.1 and 4.1.2) were used for calibration of the hydraulic model. At Z.38, discharge was set as input. Behind the outlet, water levels were directly used as boundary condition; in that way, tidal fluctuations were automatically taken into account during calibration.

Consequently, the model was calibrated by roughness, using Manning's  $n$ -values. Between Z.38 and Khlong Kio, the model was calibrated on discharge. Between Khlong Kio and the outlet, calibration was performed by water level. Upstream of Khlong Kio most cross-sections were natural, while downstream of Khlong Kio the stream was mostly confined by floodwalls. For that reason, separate  $n$ -values were searched for the river segment up- and downstream of Khlong Kio. Calibration was performed through optimization by narrowing down the interval of tested Manning's  $n$ -values.

Nash-Sutcliffe Efficiency (Nash & Sutcliffe, 1970), or in short NSE (Eq. 6), was used as a single objective function assessing the goodness of fit. In Eq. 6,  $N$  is the sample size,  $Q_m(t)$  is the modelled time series and  $Q_o(t)$  is the time series observed in the field. NSE was chosen because this case study focused on high discharge rather than low flow. Afterward, a logarithmic plot was used to validate the goodness of fit visually. Infield observation of the cross-sections (i.e. bottom, vegetation) was linked to reasonable intervals of  $n$ -values based on literature. For the reliability of the model, it was checked whether the calibrated  $n$ -values lay within the intervals from literature.

$$NSE = 1 - \frac{\sum_{t=1}^N (Q_m(t) - Q_o(t))^2}{\sum_{t=1}^N (Q_o(t) - \bar{Q}_o(t))^2} \quad \text{Eq. 6}$$

### 4.3.4 Design storms

Peak discharges for different return periods were calculated for measurement location Z.38 (Jiradecha et al., 2011), see Table 1 (section 3.3). For those discharge values, synthetic design discharge hydrographs were developed based on the shape of the highest discharge events of 2018 and 2019. For this approach, the discharge hydrographs were normalized first. Consequently, the hydrographs were linearly scaled to match the peak discharges values of the different return periods.

#### Lateral inflow

As synthetic design discharge hydrographs were used as upstream boundary, lateral inflow also required a synthetic form. Since the design storms entailed discharge and not rainfall, a rainfall-runoff model for designing lateral inflow would not have been justified by the available data. Instead, lateral inflow was schematized as directly proportional to the rate of inflow (Nerc, 1975), with a proportionality factor  $\alpha$ . This simplification was justified through the results from the sensitivity analysis (see section 4.4.3).

A quick analysis of the rise in discharge between gauging station Z.38 and Khlong Kio showed that factor  $\alpha$  was different for each peak in the time series from 2019. For that reason, the lateral inflow was calculated as a proportion of baseflow. At both Z.38 and Khlong Kio, hydrograph separation was applied using HYSEP (USGS, 1996). Lateral inflow factor  $\alpha$  was determined for the whole period at which baseflow was present during the rainy season. Consequently, the lateral inflow between Z.38 and Khlong Kio was validated by plotting the cumulative discharge of both gauging stations, including lateral inflow. For the last part of the Tub Ma (from Khlong Kio to the outlet), factor  $\alpha$  was scaled according to the principles of the rational method. Thus,  $\alpha$  was set as a function of run-off area and run-off coefficient (see section 4.2.3).

## 4.4 Flood mitigation assessment

This section addresses the methodology for answering the second research question: “*What is the potential contribution of the outlet pumping station for the prevention of flooding through overbank flow?*”

### 4.4.1 Scenarios

Within the scope of a closed floodgate, two scenarios were set up that reflected the current pumping station operation strategy (see Appendix E), and a third scenario was set up reflecting flood early warning. So, for each scenario, the pumping station was started at a different time.

The design storms were set as an upstream discharge boundary. At the downstream boundary, water level was set at 1 m MSL at the start of the design storm while the floodgate was closed, equal to the minimum water level at which the pumping station can run.

### 4.4.2 Flood wave propagation

First, the design storms were run through the model with an open floodgate to gather insight into the performance of the stream (e.g. flood wave celerity, channel capacity). Because of the open floodgate, operational strategies of the pumping station were neglected. Consequently, the design storms were run through the model for each of the scenarios with a closed floodgate.

### 4.4.3 Sensitivity analysis

A sensitivity analysis was applied to test whether the conclusions from this research were affected by simplification or uncertainties. For the following independent variables, the effect on the outcomes of this research was tested:

- Pump capacity – The design pump capacity (20 m<sup>3</sup>/s, see section 3.3) was directly applied in the model. The actual pumping capacity is often lower, mainly because of friction at the inlet (Fathi-Moghadam & Drikvandi, 2012). In Tub Ma, observed vegetation and debris was likely to result in extra friction at the inlet of the pumping station. For that reason, the effect of a lower pumping capacity (15 m<sup>3</sup>/s instead of 20 m<sup>3</sup>/s) was assessed.
- Dike level height – The cross-sections confined by floodwalls had 0.5 m uncertainty in the z-direction (see section 5.1.4). For that reason, the effect of rising and lowering the floodwalls by 0.5 m was tested.
- Lateral inflow – The fractional lateral inflow was directly related to the design storms and maximum lateral inflow coincides with maximum discharge. However, given that the run-off ratio increased in the direction of the outlet (section 4.2.3), the maximum lateral inflow was likely to occur ahead of maximum discharge. For that reason, the scenarios were tested for a 5 hours forward time shift of the lateral inflow.

## 5 Results

In this chapter, the results and the interpretation of the results are presented. The structure of the chapters closely follows the structure of the preceding chapter 'Methodology'. The first section (5.1) presents and discusses the fieldwork results. Section 5.2 gives the results of the flood early warning assessment, addressing the first research question. Then, the schematization and calibration results of the hydraulic model are given in section 5.3. Lastly, the results of the flood mitigation assessment are presented and interpreted in section 5.4.

### 5.1 Fieldwork results

#### 5.1.1 Water level time series

Water level time series from August 28, 2019, until November 7, 2019, are plotted in Figure 39 and Figure 40 of Appendix B. The same data is plotted in Figure 18 for the period covering the highest water levels of 2019. From this figure, it was recognized that water level peaks around the flood early warning gauging stations (TM.02, TM.03, TM.04) coincide with each other in time. Also, Figure 18 indicated a travel time of half a day for the propagation of peaks from TM.02/03/04 to the outlet.

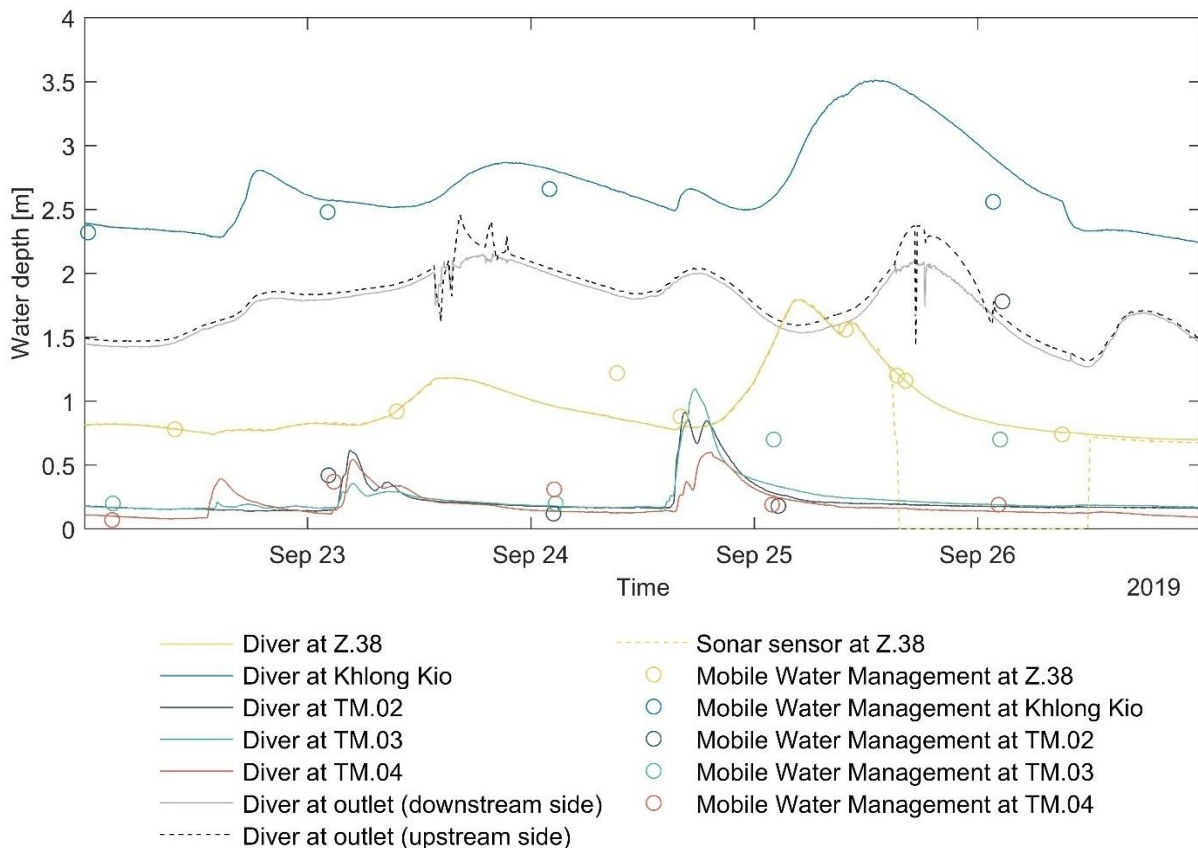


Figure 18: Water depth time series from the available devices at all gauging stations between September 22, 2019 until September 27, 2019. (Note: For this figure, water level was converted to water depth [m] based on the bottom level [m MSL] at the gauging station.)

The water level time series around the outlet of Tub Ma (plotted in Figure 19) revealed the presence of tidal fluctuations and a tidal range of roughly 1 m. Generally, the water level up- and downstream of Tub Ma's outlet was equal. Given that Rayong river is much larger than Tub Ma, the stage around the outlet was dominantly determined by stage in the Rayong river (including tidal forces). Up to the first half of September, the high-end of the tidal range was equal at both sides of the outlet, while the low-end of the tidal range was lower at the downstream side of Tub Ma's outlet. This observation was assumed to be the result of water flowing in during high tide; but being trapped in Tub Ma river during

low tide. Based on this assumption, the floodgate's crest level was observed as at -0.25 m MSL from Figure 19. Between September 30 and October 6, the water level at both sides deviated (Figure 19), indicating a closed floodgate. However, no information was available about the floodgate operation during those days. Therefore, this period was neglected for calibrating the model of Tub Ma river (see section 4.3.3).

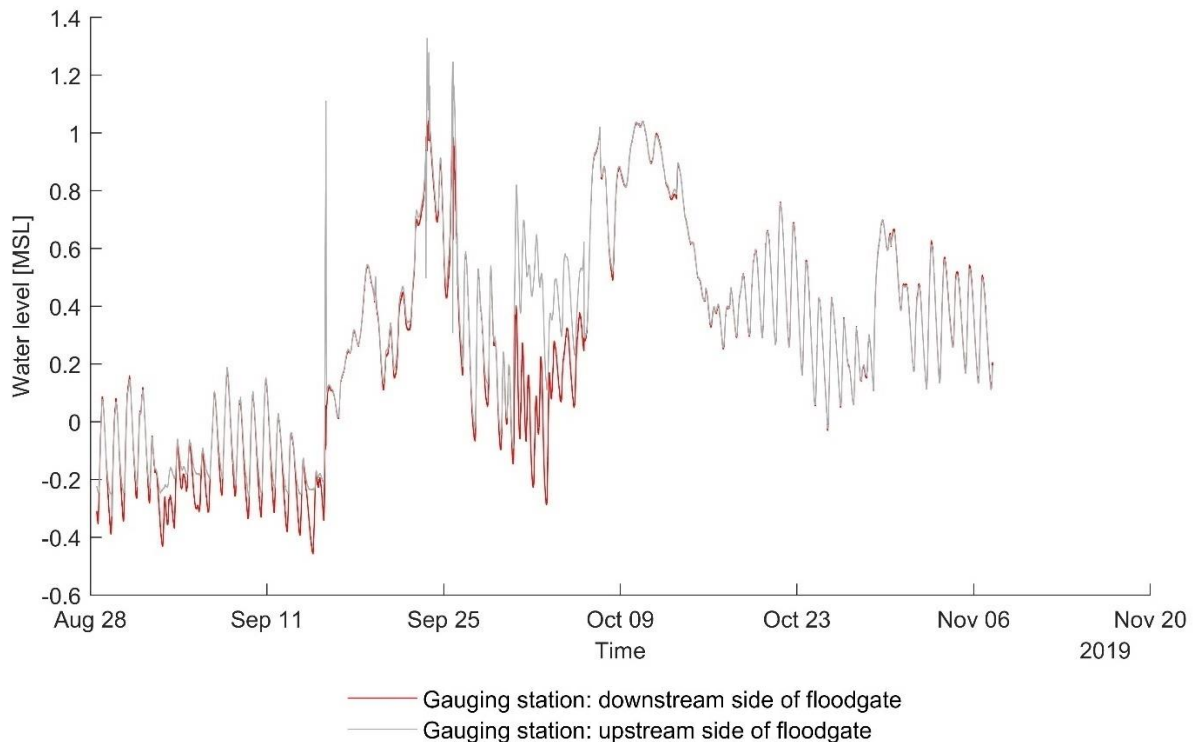


Figure 19: Water level time series from both gauging station at the outlet of Tub Ma.

#### Quality control – Double mass & residual mass analysis

All Divers have logged continuously, without temporary failures. The sonar sensor at gauging station Z.38 stopped logging on the day when the most extensive water levels occurred (September 26). Water level registration by Mobile Water Management (MWM) took place daily at Z.38, but with larger intervals and less regular at the other gauging stations.

Figure 20 (panel A-C) shows the results of benchmarking the MWM-observations at flood early warning gauging stations TM.02/03/04 against the measurements from Divers. The double mass curves were full of inflection points indicating non-systematic deviations between MWM and Diver measurements. Also, the fluctuations from the residual mass curve indicated a non-constant relation between the time series from MWM and the Diver. This low precision was the result of errors during the processing of the images by the 'Peilregistratie' application. These errors were induced by fouling covering the measurement lines on the staff gauge and by low photograph quality. Pictures were often of low quality because of: (1) poor lighting due to shadow; (2) accessibility of the staff gauge (image quality generally decreases by using the zoom function of a mobile phone); and (3) picture angle (photographs were taken while standing a few meters above the staff gauge on a bridge).

Panels D and E from Figure 20 are the results of benchmarking the sonar sensor and MWM time series against the time series retrieved from the Divers at gauging station Z.38. The sonar sensor at Z.38 had a high precision given stable slopes of the lines in panel A. However, the positive slope of the residual mass curve indicated consequent higher values (constant offset) measured by the sonar sensor compared to the Diver. For a short period of time, the sonar sensor did not survey any data, as indicated by the horizontal part of the double mass curve. In the field, it was observed that the sonar sensor was replaced after that time. After replacement, the constant offset between Diver and sonar sensor decreased given the decreased positive slope of the residual mass curve (Figure 20 panel D).

In panel E of Figure 20, two shifts were observed in the double mass curve, indicating a change in accuracy twice. During the start and end of the time series, the water level was relatively low, and fouling was present on the MWM staff gauges at those low stages. Fouling covered the measurement lines on the staff gauge, resulting in wrong water level readings by the image recognition module of the 'Peilregistratie' application. Nevertheless, the almost constant slope of the residual mass curve between those inflection points of the double mass curve indicated that fouling-errors are systematic over a range of low water levels Figure 20 (panel E).

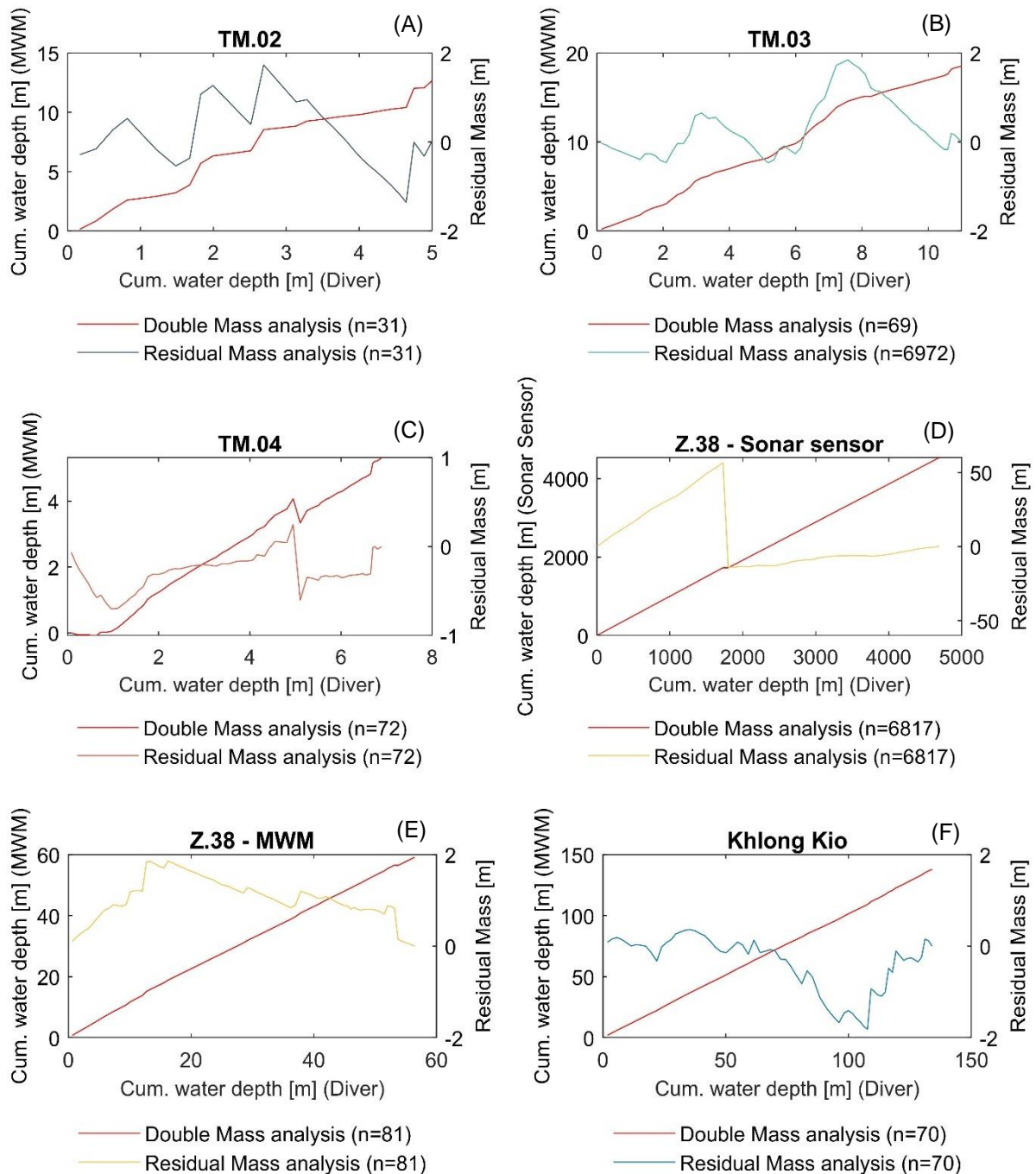


Figure 20: Double mass analysis and residual mass analysis between water depth time series of different monitoring devices. Diver and Mobile Water Management at gauging station TM.02 (panel A), Diver and Mobile Water Management at gauging station TM.03 (panel B), Diver and Mobile Water Management at gauging station TM.04 (panel C), Diver and sonar sensor at gauging station Z.38 (panel D), Diver and Mobile Water Management at gauging station Z.38 (panel E), Divers and Mobile Water Management at gauging station Khlong Kio (panel F).

At gauging station Khlong Kio (Figure 20 panel F), the straight double mass curve indicated a constant relation between the Diver and MWM time series. The consecutive downward and upward phase of the residual mass curve indicated respectively relatively low- and high values of the MWM measurements. However, no reason was found for this deviation regarding water level registration by Mobile Water Management. It was suggested that the Diver's position in the monitoring tube had changed position, e.g. after reading out the logged data.

#### Quality control – Absolute errors

Absolute deviations from benchmarking MWM and RID's sonar sensor against the Divers are presented in Table 3. Outliers were identified by removing 10%, 25%, and 50% maximum deviations. By removing the 50% largest deviations (last row, Table 3), an indication of *accuracy* was obtained, while information about *precision* was achieved by comparing the 50%, 75%, and 95% intervals from Table 3.

The Divers had a precision of  $\pm 2$  cm (Van Essen Instruments, 2016), so the deviations shown in Table 3 within 2 cm were neglected. Clearly, sonar sensor measurements were equally precise and as accurate as the data logged by the Divers. The precision of the MWM measurements differed per gauging station, which was highest at Z.38 and TM.04, and lowest at TM.02. The accuracy of the MWM measurements was within the order of 0 to 5 cm.

Table 3: Maximum absolute deviations in surveyed water level between Divers and Mobile Water Management/ sonar sensor after removing outliers.

Gauging station:	TM.02	TM.03	TM.04	Z.38	Z.38	Khlong Kio
Monitoring device:	MWM	MWM	MWM	Sonar	MWM	MWM
Maximum error after removing 10 % largest deviations [m]	0.77	0.11	0.11	0.02	0.13	0.35
Maximum error after removing 25 % largest deviations [m]	0.45	0.19	0.05	0.02	0.06	0.14
Maximum error after removing 50 % largest deviations [m]	0.05	0.05	0.02	0.02	0.02	0.08

#### Usefulness of gauging techniques

Mobile Water Management stage registration and the sonar sensor at Z.38 were both part of Tub Ma's local context, while the Divers were only brought in for research purposes. Citizen survey by MWM took place on a less than daily scale, while water level peaks at the flood early warning gauging stations (TM.02/03/04) were only present for a few hours (see Figure 18). So, for the survey of high water propagating through Tub Ma, a measurement interval of maximum 1 hour was required. Hence, the temporal scale of the MWM readings was too large for monitoring high water levels. Meanwhile, the 15-minute temporal scale of the sonar sensor was small enough to observe water level peaks.

#### 5.1.2 Discharge

##### Rating curves

The rating curve for gauging station Z.38 was directly retrieved from the RID. In this research, the accuracy of the Z.38 rating curve was not assessed. However, possible errors would have propagated as systematic errors since the rating curve at Khlong Kio was based on Z.38. Hence, errors in the Z.38 rating curve were not likely to result in a wrongly calibrated model.

The result of the calibrated Manning equation at Khlong Kio (cross-section 39, see Figure 53 in Appendix B) is displayed in Figure 21 panel A. At the stage (calibration point) for which discharge was surveyed using the current meter, the rating curve surpassed the calibration point. However, the survey took place during the falling limb of the flood wave. According to the hysteresis theory (see section 2.2), during the falling stage observed discharge is indeed smaller than the flow given by a stage-discharge relationship.

Figure 21 panel B shows that the stage-discharge relationship at Z.38 was much steeper compared to Khlong Kio. This difference was explained by the broader cross-section around gauging station Z.38. It was recognized that for the same error in stage-survey, the error in discharge is more substantial for a steeper rating curve.

Taking into account the Diver's precision of 2 cm, the consequent errors in discharge are negligible for low water levels. But given the increasing slope of both rating curves, errors in discharge due to stage-survey increased with the stage. However, stage-discharge relationships are generally known to be less accurate for the higher stages (Dottori et al., 2009). For higher flows, the uncertainty of the rating curve itself outweighed the propagated error from stage-survey.

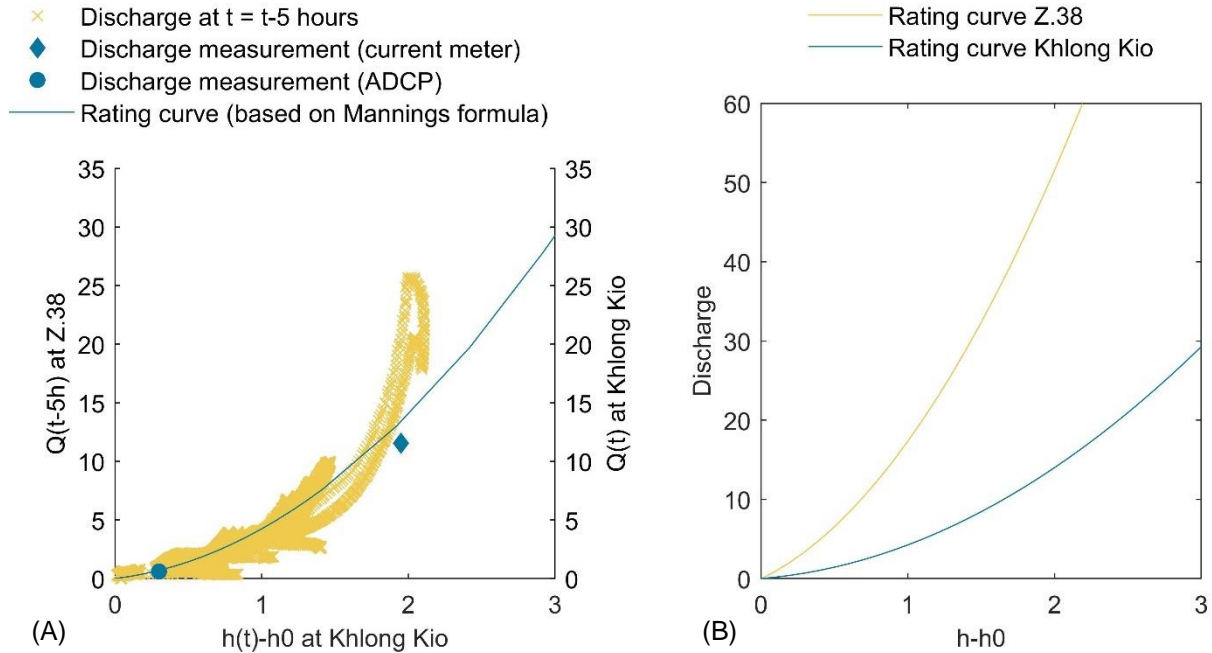


Figure 21, panel A: Establishment of the stage-discharge relationship at gauging station Khlong Kio. Panel B: Stage-discharge relationship at gauging stations Z.38 and Khlong Kio.

#### Dynamic rating curve approach

Panel A of Figure 22 shows the results of Jones' formula, calibrated on the shape of the hysteresis at gauging station Z.38. In Figure 22, a subsiding flood wave hysteresis makes a clockwise loop (Battjes & Labeur, 2017). Hence, the discharge measurements from RID must have been taken during the rising stage.

In Figure 41 (see Appendix B), discharge is plotted after direct use of the rating curve and plotted based on the dynamic rating curve approach. The same time series are shown in Figure 23 for a smaller time window that covers the highest water levels of 2019. By application of the dynamic rating curve approach, peak flow increased and shifted forward in time. Meanwhile, this time shift forward of the maximum discharge is larger for lower water levels. Figure 23 also showed that the increase in peak discharge by the dynamic rating curve approach was larger for higher water levels. As a consequence, lag time decreased between Z.38 and Khlong Kio by the application of the dynamic rating curve approach. Lag time plays an important role in the objective functions for model calibration (Nash & Sutcliffe, 1970). So, it was recognized that the application of the dynamic rating curve approach led to a more accurately calibrated hydraulic model than the use of a steady rating-curve.

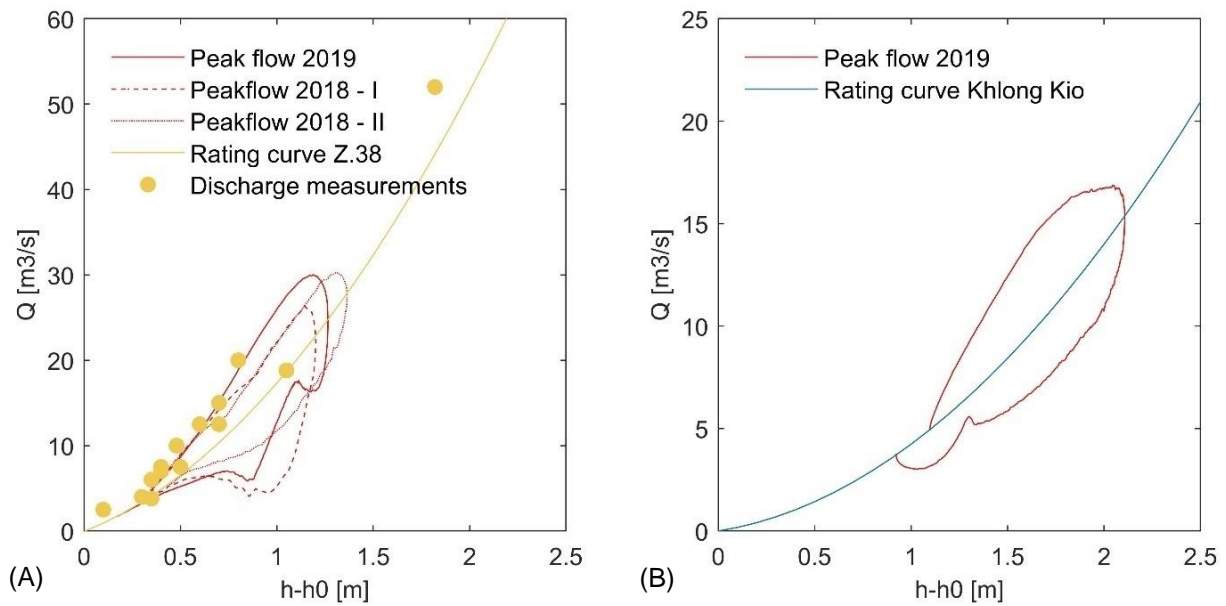


Figure 22: Hysteresis resulting from the dynamic rating curve approach and the original discharge measurements from the RID at gauging station Z.38 (panel A) and the result of the dynamic rating curve approach at Khlong Kio (panel B).

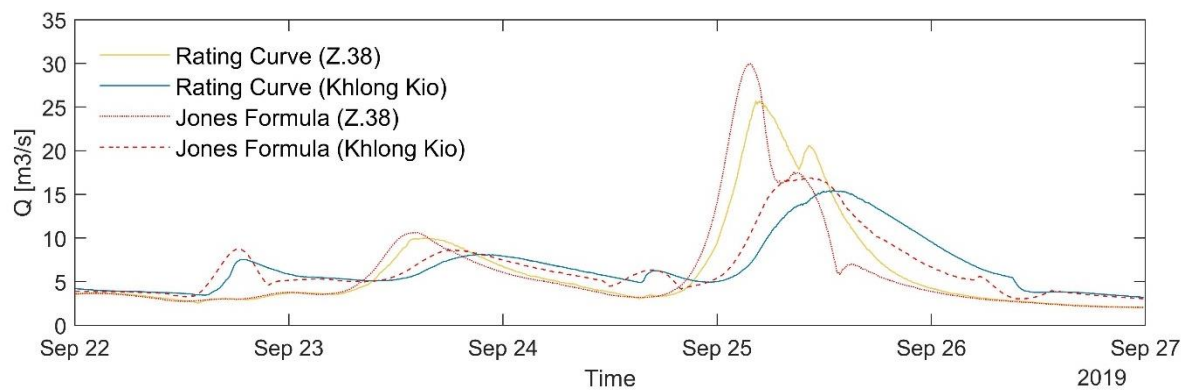


Figure 23: Discharge obtained from indirect measurements using Divers; by applying both a stage-discharge relationship (rating curve) and a dynamic rating curve approach (Jones' formula).

### 5.1.3 Bathymetry: longitudinal profile

#### GNSS set up and processing

The base station antenna found its position ( $12^{\circ} 40' 5.96917$ ,  $101^{\circ} 17' 48.00296$ ) after 24 hours, with a 95% confidence interval of 0.5 cm in latitude, 1.0 cm in longitude, and 1.5 cm in height. According to the U-centre software, the floodwall level was logged with a precision of 0.1 m. Given that the average height (bottom-dike) of cross-sections was 4 to 5 m, this was an insignificant error of  $\sim 2.5\%$ . The precision of the data set containing the bottom level was unknown (Jiradecha et al., 2011). However, in this research, the precision of the floodwall level was more important than the precision of the bottom level. Namely, errors in the floodwall level resulted in overbank flow taking place or not at a specific location, while errors in the bottom level mainly affected the storage capacity of the river.

The surveyed level of the floodwalls (plotted in Figure 24) indicated that the dike level had become more homogeneous in height. This was the result of building floodwalls. Due to the floodwalls, overbank flow was likely to occur over a longer stretch of the Tub Ma river instead of at a few critical points. Nevertheless, around Khlong Kio ( $\sim 7500$  m from the outlet), the floodwall was relatively low compared to floodwalls up- and downstream from this point. Hence, overbank flow was most likely to start around Khlong Kio.

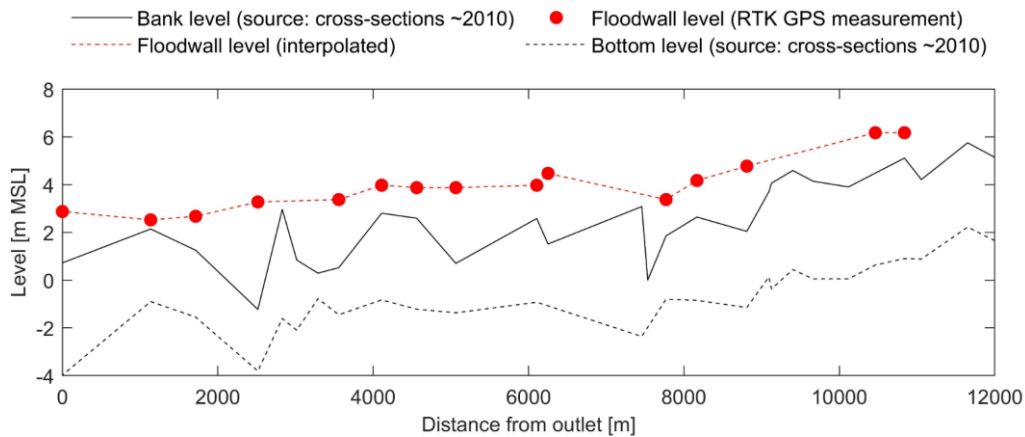


Figure 24: Longitudinal profile of Tub Ma between Z.38 and outlet.

#### 5.1.4 Bathymetry: cross-sections

The processed results from the cross-section survey are plotted as y-z profiles in Figure 44 until Figure 57 (Appendix C). From fieldwork, the distance between the left and right floodwall was found as a constant value of 14 m. Table 4 shows the results of validating the plotted cross-section using fieldwork measurements. The plotted values are in the same order of magnitude as the measured values. The plotted distance between the bottom and floodwall level (see Figure 15 in section 4.1.4) was around 0.5 m larger compared to what was surveyed. This was attributed to either sedimentation or measurement errors. In section 5.4.4, it was assessed how a possible error of 0.5 m affected the model results and whether it changed the conclusions from this research.

Table 4: Comparison of plotted distance and surveyed distance between the top of the floodwall and riverbed.

Cross-section (see Appendix C)	Plotted distance top of floodwall - river bed [m]	Surveyed distance top of floodwall - river bed [m]
29	3.8	3.4
44	4.5	4
46	4.2	4
50	4.9	4.5

#### 5.1.5 Structure geometries (weirs)

Between Z.38 and Khlong Kio, in total five structures were found and surveyed. The geometries, including crest level and bottom level are shown in Appendix D.

## 5.2 Flood early warning

### 5.2.1 Lag time

Figure 25 shows the cross-association results for water level between Khlong Kio and all gauging stations upstream of Khlong Kio. For Z.38, the index of similarity had a clear maximum at a lag time of 6 hours. Regarding the upstream locations, maxima were found at 13, 14, and 15 hours lag time for respectively TM.02, TM.03, and TM.04. So, the cross-association analysis indicated a time lag of 13 to 15 hours between discharge at the flood early warning gauging stations (TM.02/03/04) and discharge at Khlong Kio.

It was recognized that the curves of TM.02/03/04 (Figure 23) are relatively flat. This was explained by the fact that water level peaks at Khlong Kio covered more time steps compared to the short peaks at TM.02/03/04. Hence, for more than one lag time value, the events of Khlong Kio (peak above threshold) covered the whole event at TM.02/03/04, resulting in a relatively flattened curve. So, the relative flat parabolic curves were not the result of a large range of lag times but a consequence of change in shape of the peaks between TM.02/03/04 and Khlong Kio.

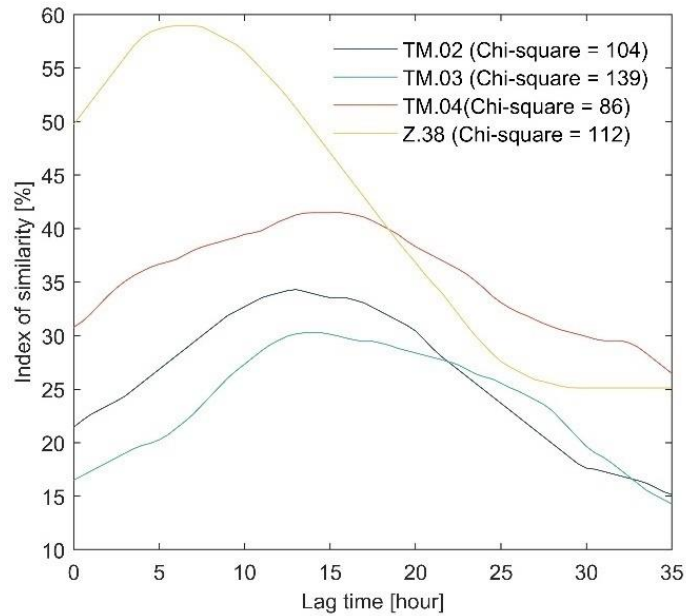


Figure 25: Cross-association results of water level between Khlong Kio and all gauging stations upstream of Khlong Kio for successive time lags.

A Chi-square test underlined with a 95% significance level that it was unlikely that the percentage of matched events (Index of similarity) was found without a relationship.

### 5.2.2 Matching peak flows

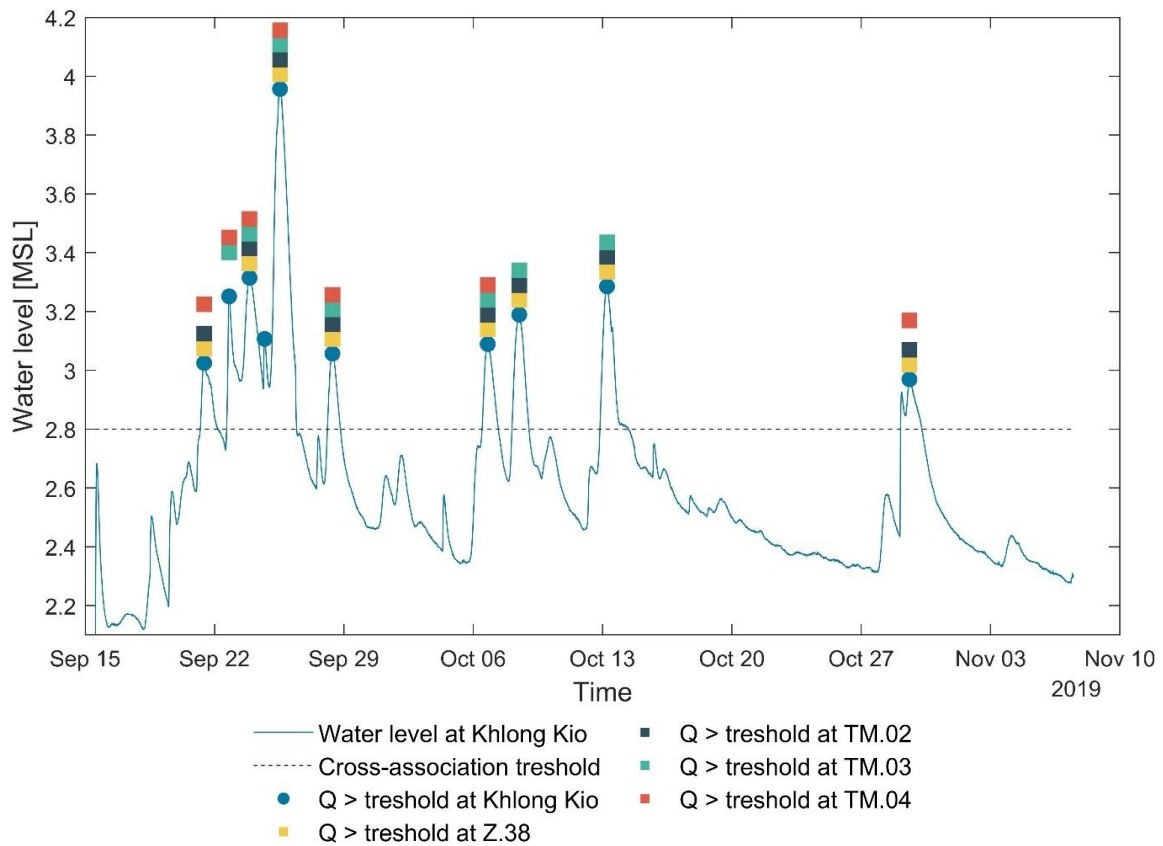


Figure 26: Matching results of events (contiguous water level above threshold) between Khlong Kio and all gauging stations upstream of Khlong Kio for the time lags found by cross-association.

Figure 26 visualized for each peak above threshold (event) at Khlong Kio, the presence of associated events from the upstream gauging stations. Either TM.02, either TM.03 or both together, showed an event for each event at Khlong Kio. So, it was concluded that TM.02 and TM.03 were more critical for flood early warning than TM.04. For the largest observed event at Khlong Kio (September 25, 2019), all gauging stations upstream of Khlong Kio showed an event (Figure 26).

5.2.3 Proportionality flood early warning locations

Catchment Area

All delineated sub-catchments are displayed in Figure 27. Associated surface areas are presented in Table 5. The three early warning gauging stations covered half (46%) of the total catchment area. However, this analysis revealed that sub-catchment areas of the three flood early warning gauging stations varied considerably. TM.03 was double as large as TM.02, and TM.04 was notably small. The outline from all sub-catchments together coincided well with the catchment boundary used by the RID.

Table 5: Sub-catchment areas of the Tub Ma basin.

Sub-catchment	TM.02	TM.03	TM.04	Z.38	Khlong Kio	Outlet
Area [km <sup>2</sup> ]	27.9	59.7	7.0	60.1	21.3	28.3

Run-off coefficient

The calculated values of the two parameters reflecting urbanization, NDVI and road density, are plotted against each other in Figure 28. A linear relation between both parameters was recognized. Given this linear relation, it was concluded that NDVI was related to road density and that both parameters reflect the degree of urbanization in Tub Ma well. TM.02/03/04 had the lowest run-off coefficients and were individually comparable. The run-off coefficient was largest in the Outlet sub-basin.

The three early warning gauging stations covered half (46%) of the total catchment area, but the run-off coefficients of those sub-catchments were relatively low compared to the downstream part of the catchment. So logically, the flood volume that could be predicted by TM.02/03/04 was less than 46%.

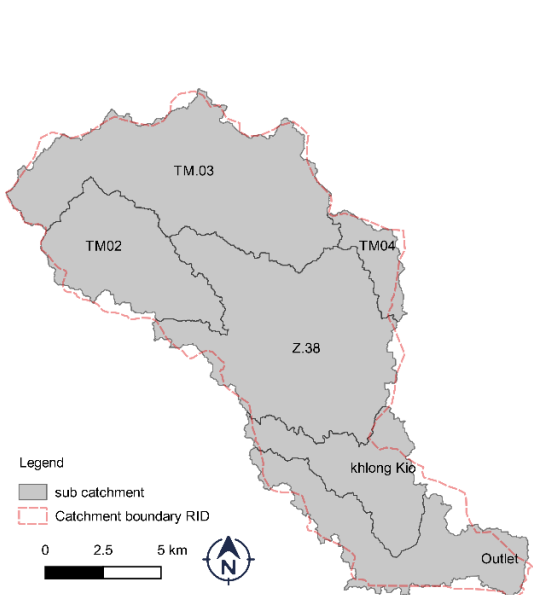


Figure 27: Delineated sub-catchments of the Tub Ma basin in reference to the RID’s catchment boundary.

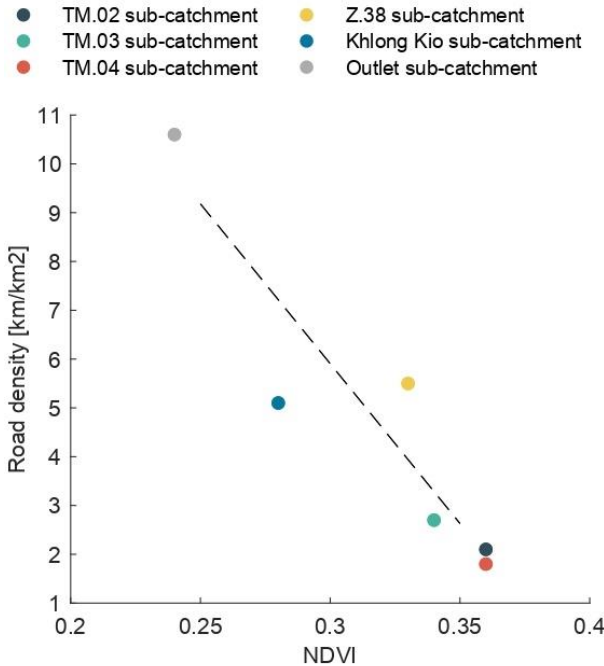


Figure 28: Road density and NDVI per sub-catchment, linear relation displayed by dotted line.

### Rainfall intensity

In a parallel research project (Methaprayun, 2020), it was demonstrated that the largest rainfall events in Tub Ma cover the whole catchment. However, the spatial variability of rainfall intensity in Tub Ma is large (Methaprayun, 2020).

In section 5.2.2 it was recognized that TM.04 gave fewer matches compared to TM.02 and TM.03. Meanwhile, it became clear that TM.04 has a relatively small surface compared to TM.02 and TM.03. So, given the observed spatial variability of rainfall, it is logical that the smallest sub-catchment (TM.04) had the highest probability of missing out a storm event.

## 5.3 Hydraulic model Tub Ma catchment

### 5.3.1 Calibration results

The model was calibrated over the periods September 15, until September 30, and October 6 until November 7. In between, water level was affected by a (part of the time) closed floodgate on which no information was available (see section 5.1.1). Before September 15, reservoirs between Z.38 and Klong Kio were filled as discharge at Z.38 was larger than discharge at Klong Kio. This period was applied as warm-up period for the model and thus also left out for calibration as well.

Between Z.38 and Klong Kio, the maximum NSE value of 0.89 was found for a Manning's  $n$  value of 0.14. Between Klong Kio and the outlet, the maximum NSE value of 0.91 was found for a Manning's  $n$  value of 0.10. The observed time series are plotted against the modeled series in Figure 61 (Appendix F). By the use of a log scale plot (panel C in Figure 61), the modeled flow recession was validated visually.

During fieldwork, a first guess was made of the cross-section friction by comparing observations with literature (Table 6). Consequently, modeled Manning's  $n$  values were benchmarked against the expected range of values. For the natural cross-sections, modeled friction was in line with the expectations. For the cross-sections with floodwalls, modeled friction was rougher than expected. This was explained by the theory of equifinality, the calibration parameter (Manning's  $n$ ) might have counter balanced errors in other parameters such as bed slope.

Table 6: Fieldwork observations of cross-sections, associated friction values from literature, and the calibrated Manning's  $n$  values.

	Fieldwork observation	Literature Manning's $n$ value (Chow, 1959)	Modeled Manning's $n$ value
<b>Natural cross-sections</b>	Dense vegetation (0.5 - 1.5 m) at the sides and a riverbed of sand, rocks (0.1- 0.5 m), and vegetation (0.5 – 1.0 m)	0.07 – 0.15	0.14
<b>Concrete floodwalls</b>	Rough concrete floodwalls on the sides, and fine sand on the riverbed with sometimes vegetation (0.5 – 1.0 m).	0.035 - 0.5	0.10

### 5.3.2 Design storms

Figure 29 shows the derived hydrographs of the design storms. The steep gradient of the rising limbs is characteristic of water running off fast in urban areas.

The sizes of the largest design storms were recognized as unrealistic since average velocity exceeds 1.5 m/s during bank full flow (see Table 7). In other words, the largest design storms simply not fitted through the cross-section of Z.38. So, for discharge associated with a return period of 50 and 100 years, water was expected to overflow upstream and around Z.38 already. This was explained by the assumption that such high flows were never surveyed and thus resulted from extrapolation by the RID.

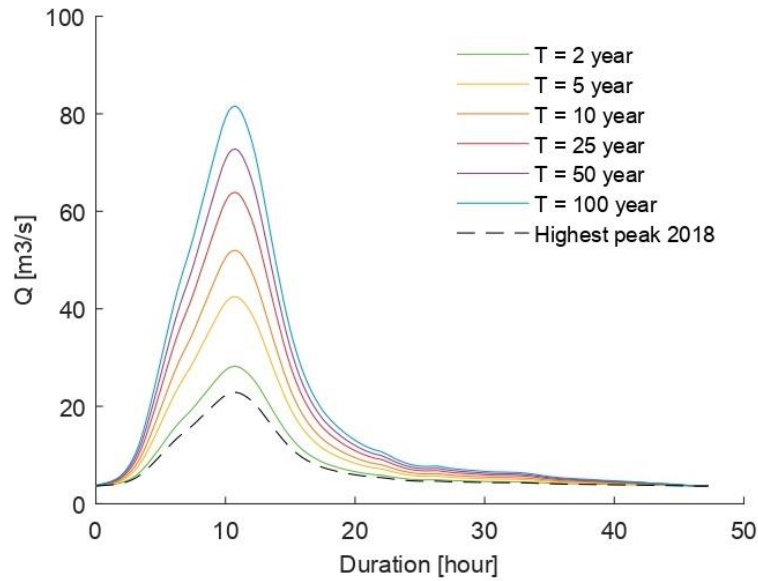


Figure 29: Synthetic design discharge hydrograph at Z.38 for design storms from Table 1.

Table 7: Average flow velocity at Z.38 based on design discharge while assuming bank full flow.

Return period [year]	2	5	10	25	50	100
Average flow velocity in cross-section [m/s]	0.61	0.92	1.13	1.39	1.58	1.77

#### Fractional lateral inflow

Figure 30 shows the result of baseflow separation using HYSEP. In general, baseflow at gauging station Khlong Kio was 11% larger compared to Z.38. ( $\alpha = 1.11$ ) However, between the 22nd and 30th of September  $\alpha$  was much larger. During this period, local inflow at Khlong Kio interfered with falling limbs of larger peaks around Khlong Kio. As a result, baseflow was overestimated during this period; so  $\alpha$  was overestimated as well during that period.

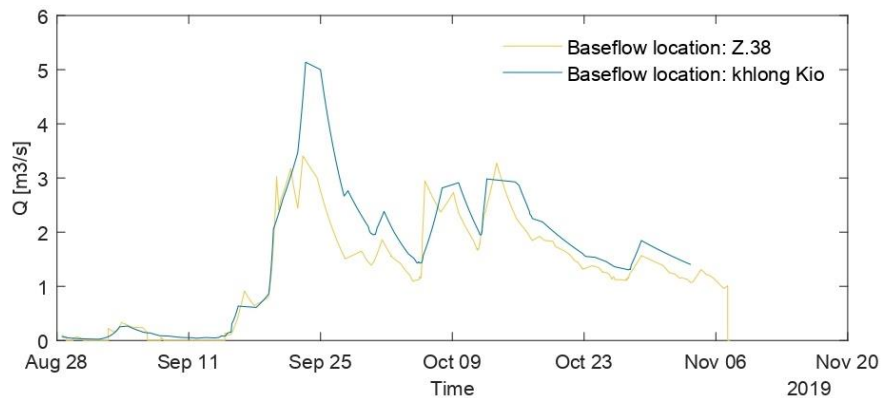


Figure 30: Baseflow after hydrograph separation using HYSEP.

Figure 31 shows the cumulative discharge at Z.38 and Khlong Kio. In addition, discharge from Z.38 was plotted including 11% fractional lateral inflow. From Figure 31, it was observed that the cumulative flow of Z.38 including baseflow ran parallel to the curve of Khlong Kio. Both discharge curves were equal except for the jumps in the gauged discharge at Khlong Kio. These jumps were the result of local events in the Khlong Kio sub-catchment. Logically, jumps from local inflow were not balanced by fractional lateral inflow.

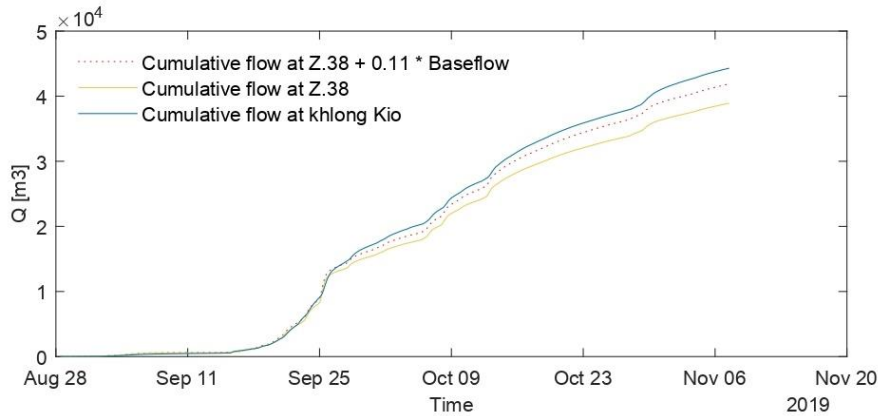


Figure 31: Cumulative discharge after application of the dynamic rating curve approach on water level time series retrieved from Divers, and after applying later inflow between Z.38 and Khlong Kio.

Between Khlong Kio and the outlet, the lateral inflow  $\alpha$  was multiplied by 1.32 since the outlet sub-catchment is 32% larger than the Khlong Kio sub-catchment. In addition,  $\alpha$  was increased to take into account the larger run-off fraction around the outlet (see section 5.2.3). Based on the difference in NDVI this was estimated as a 5% increase (Suhardi & Entin, 2019).

## 5.4 Flood mitigation assessment

### 5.4.1 Scenarios

From the operational description in Appendix E, two scenarios were recognized, reflecting outlet control based on water level information from Z.38 (scenario A) and outlet control based on water level information from the outlet (scenario B). A third scenario (C) was outlet control based on flood early warning. First, it was calculated at which time the pumping station was started according to each scenario.

- **Scenario A** – From Figure 29, the time at which water level reached 8.6 m MSL was read (Table 8). Consequently, 1 hour (see Appendix E) was taken into account as the time between notification and mitigation.

Table 8: Pumping station operation time (hours after start design storm) based on scenario A.

Design storm	T <sub>2</sub>	T <sub>5</sub>	T <sub>10</sub>	T <sub>25</sub>	T <sub>50</sub>	T <sub>100</sub>
H <sub>Z.38</sub> = (8.6m MSL)	t = 7:40 h	t = 5:10 h	t = 4:45 h	t = 4:20 h	t = 4:10 h	t = 4:00 h
t <sub>start pump</sub>	t = 8:40 h	t = 6:10 h	t = 5:45 h	t = 5:20 h	t = 5:10 h	t = 5:00 h

- **Scenario B** - As water level was 1 m MSL at the start of the model simulation, t<sub>start pump</sub> was set equal to the start of the simulation for scenario B.
- **Scenario C** – The lag time between the flood early warning gauging stations and Z.38 was 6.5 hours (see section 5.2.1). Meanwhile, it was read from Figure 29 that peak discharge at Z.38 occurred after 10.5 hours. With this information, it was calculated that the peak discharge of the design hydrographs would have occurred 4 hours (10.5 - 6.5 = 4) after the start of the design storm event (see Figure 32). Hence, t<sub>start pump</sub> was set equal to 4 hours for scenario C. In reality, flood early warning is based on exceedance of a threshold value, so notification would be given earlier than 4 hours. Meanwhile, the time between notification and mitigation is neglected. These two simplifications were assumed to balance each other out.

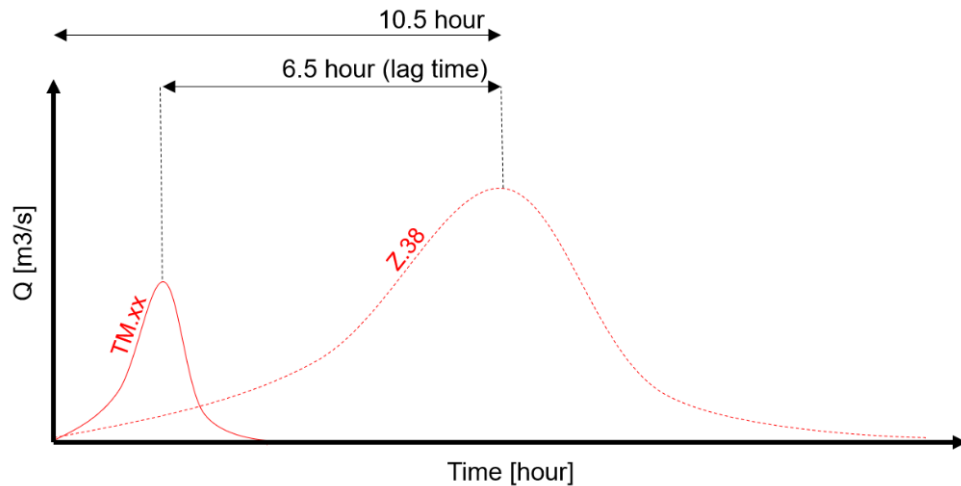


Figure 32: Visualization of lag time between TM.02/03/04 retrieved from cross-association.

Pumping station operation based on water level at the outlet (scenario B) resulted in the largest mitigation time. Information from flood early warning (scenario C) did lead to an earlier decision for operating the pumping station compared to making use of water level information from Z.38 (scenario A). However, it was observed that scenario B reflected the actual operation strategy (see Appendix E). Hence, flood early warning (scenario C) did not result in an earlier (nor different) decision for operating the pumping station.

#### 5.4.2 Flood wave propagation - open floodgate

In Figure 33, flood wave propagation between Z.38 and the outlet is plotted for an open floodgate. By these results, Tub Ma was recognized as a fast-responding flow regime hardly damping out unsteady flow. The cumulative flow at the outlet (panel A, Figure 33) showed that the fraction of inflow arriving at the outlet in the first 5-10 hours is negligible. Consequently, once discharge at the outlet became significant, it rose towards maximum discharge capacity within 2-3 hours (panel B, Figure 33). However, discharge at the outlet stayed just below pump capacity when water from overbank flow was removed from the system (panel C, Figure 33). So, the maximum discharge at the outlet was suppressed by the channel capacity as well, instead of pump capacity only. Nevertheless, in reality, not all water from overbank flow becomes inundation water, a part would still discharge towards the outlet in the form of overland flow. Taking note of this, pump capacity and channel capacity were recognized as equivalent regarding maximum discharge.

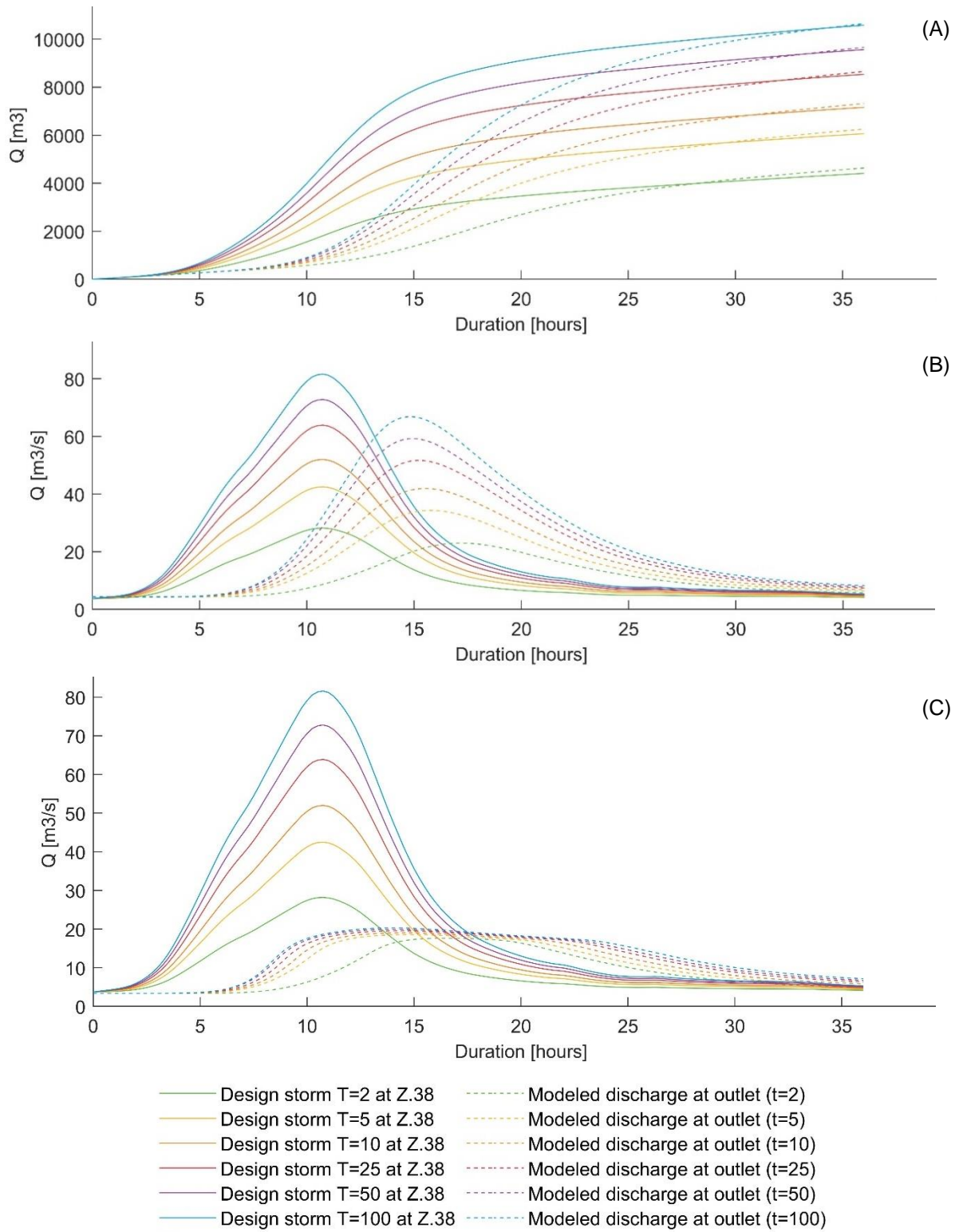


Figure 33: Propagation of design storms from Z.38 to the outlet without overbank flow (panel A and B), and after removing water from the system by overbank flow (panel C).

### 5.4.3 Flood wave propagation – scenarios pumping station operation

In Figure 34, cumulative inflow at Z.38 is plotted together with the cumulative pump discharge at the outlet. In Appendix F, the same figure is plotted for each of the other design storms. In these cumulative plots a sequence of three sequential episodes (see Figure 34) was recognized:

1. First, between 0 and ~8 hours, inflow around the outlet was smaller than the pump capacity. During this first episode, the pumping station was always started but the exact start time differed per scenario. Before the start of the pumping station, the inflow was stored in the Tub Ma river. Logically, water level rose by storing water in Tub Ma.

After 9 hours (Figure 34), the cumulative discharge was equal for all three scenarios. In scenario A and C, the pumping station started later, but the pump capacity was sufficient to pump out the discharge that was stored in Tub Ma before.

So, during the first episode, the three scenarios showed a trade-off between start time and pumping capacity. In the scenarios where the pumping station was started earlier, average pumping discharge was lower compared to the scenarios with a late start of the pumping station.

2. During the second episode (between 9 and 25 hours in Figure 34), the pump was running equally in all three scenarios. During this episode, discharge at the outlet constantly equaled maximum discharge. However, the maximum discharge was determined by both the water supply (capacity of Tub Ma channel) as well as the pump capacity. Since the pump capacity ( $18 \text{ m}^3/\text{s}$ ) was smaller than maximum capacity ( $20 \text{ m}^3/\text{s}$ ), the Tub Ma channel itself was the limiting factor. Though, the capacity of the pumping station and channel are almost equal.

Nevertheless, this episode revealed the maximum capacity of the channel. Logically, overbank flow took place when inflow exceeded maximum flow capacity during this episode.

3. During the third and last episode (starting around 25 hours in Figure 34) the water stored in Tub Ma channel was discharged until the water level reached +1 m MSL again. Afterward, the pump was operated to maintain this water level. So, at the end of this episode, the curves from inflow at Z.38 and pump discharge ran parallel since they both equaled baseflow. The difference between the endpoint of both lines roughly equaled flood volume since storage was brought back to the same level of the start of the event. For the exact flood volume (Figure 37), the lateral inflow was taken into account as well.

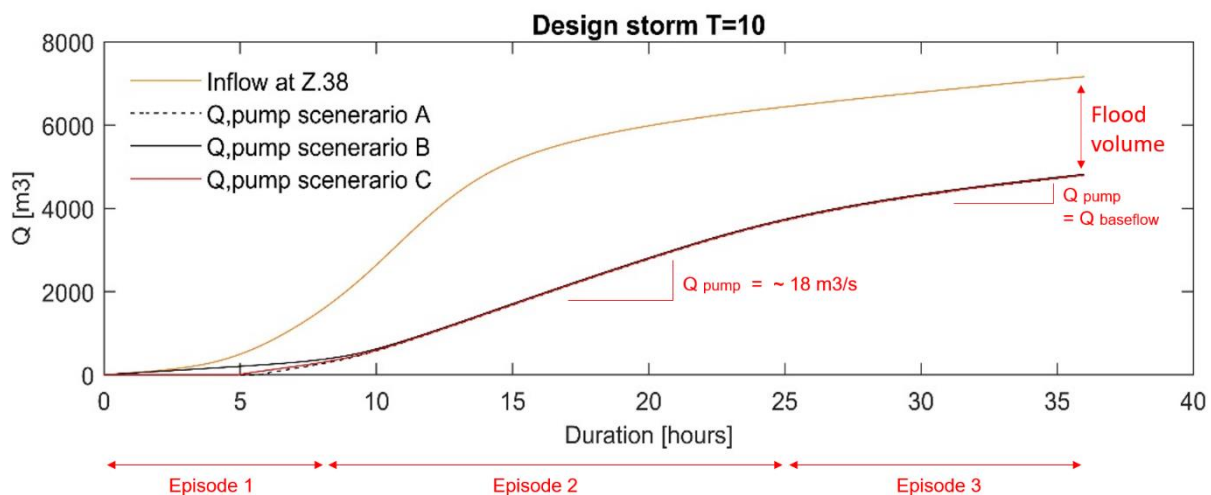


Figure 34: Cumulative inflow at Z.38 and cumulative pump discharge at the outlet.

The difference in total mitigation time between the scenarios was limited to the operation hours in episode 1, because during episode 2 the pump operation was already the same for all scenarios. During episode 1, timely operation of the pumping station does prevent flooding due to overbank flow. However, inflow was smaller than channel capacity during episode 1, so flooding was the result of filled in-river storage. Given that the 'worker' from the outlet checks water level hourly (see Appendix E), it was not

likely that maximum storage capacity in the river was reached without a notification from the worker to the RID Warning Centre. Hence, the actual mitigation time for scenarios A and C would have been larger.

From Figure 35, the cumulative pump discharge was compared for all return periods. The curves belonging to the different return periods started slightly deviating during episode 2 (so roughly after 8 hours). This indicated that for return periods with a higher discharge Tub Ma's maximum discharge capacity increased. The increased discharge capacity was recognized as the result of an increased water level gradient.

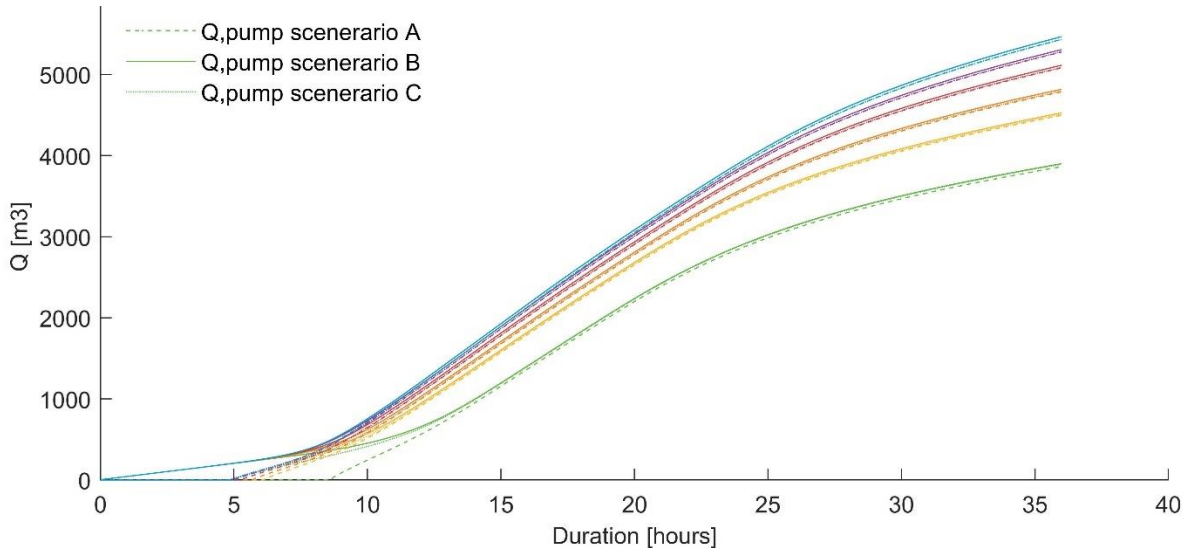


Figure 35: Cumulative pump discharge at the outlet for all scenarios and all design storms. Each design storm belongs to a separate color, equal to Figure 29 and Figure 33.

#### Overbank flow & flood volume

For each design storm, the total flood volume (Figure 37) was almost equal for each scenario. Also, the duration of overbank flow was almost equal along the longitudinal river profile (see Figure 36, Figure 64 and Figure 65 in Appendix F). Nevertheless, the duration of overbank flow around the outlet was shorter for the scenarios that started the pumping station earlier. From this observation, it was concluded that the small differences in flood volume between scenarios (Figure 37) were the result of overbank flow before the pumping station started (episode 1). This overbank flow took place because no storage capacity was left in Tub Ma during scenarios B and C. However, this is not realistic: when the storage capacity in Tub Ma was fully used, water level at the outlet equaled bank level. That water level would have been reported by outlet's 'Worker' to the RID Warning Centre (see Appendix E). Hence, the pumping station would have been started earlier in scenario A and C, and overbank flow around the outlet would be reduced.

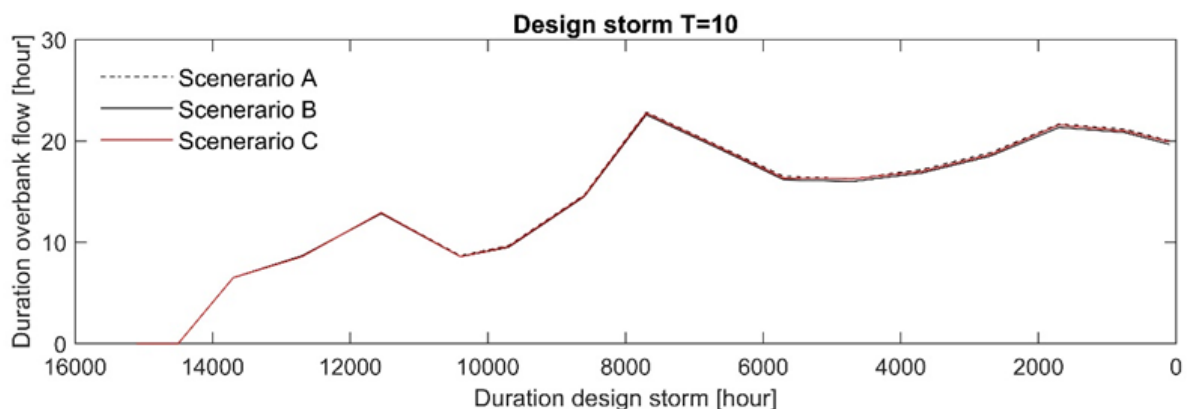


Figure 36: Duration of overbank flow along the longitudinal profile of Tub Ma.

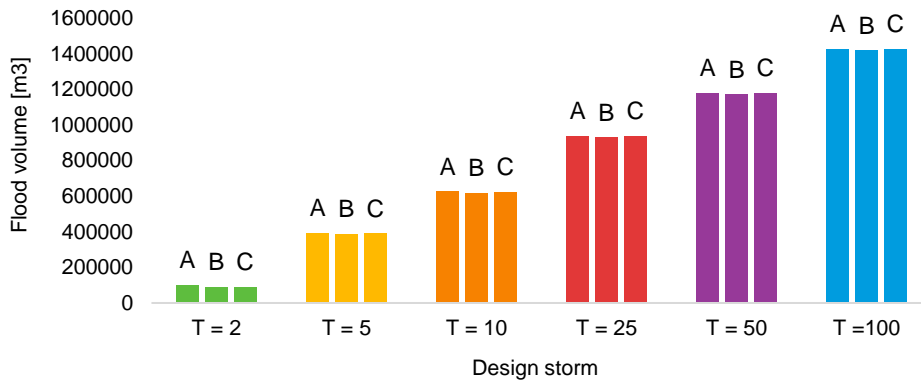


Figure 37: Flood volume per scenario for each design storm.

#### 5.4.4 Sensitivity analysis

In Figure 66, Figure 67 and Figure 68 (Appendix F), the cumulative pumping discharge is plotted for each of the adjusted parameters of the sensitivity analysis. By decreasing the pump capacity from 20 m<sup>3</sup>/s to 15 m<sup>3</sup>/s, the total pumped volume decreases (Figure 66), and the flood volume increased by 10-15%. After rising the floodwall level by 0.5 m, pumping discharge increased up to design discharge in episode 2 (see Figure 34). This resulted in a significant decrease in flood volume: >50% decrease for the three smallest return periods and 20% decrease for the other design storms (T=25, T=50, and T=100). Shifting the lateral inflow 5 hours forward in time had small effects: the total pumped volume increased by ~5%.

For all simulations of the sensitivity analysis, the differences between modeled scenarios were negligible. Since this research assessed the differences between scenarios, the tested simplification and uncertainties did not affect the outcomes of the research.

#### 5.4.5 Validation

On June 30, 2020, River flooding took place in Tub Ma. Kasetsart University was able to retrieve information about water levels during this event and about the operation (time) of the pumping station.

From this information, it was found that the hydrograph from Z.38 was closely linked to the design storm in this research (see Figure 38). Secondly, it turned out that the RID was already aware of floods, while they were not able to start the pumping station. The RID Warning Center had to wait for a rise in water level around the outlet before the pumping station could be set in operation. This storyline underlined the conclusion that the operation of the pumping station is restricted to the water level at the outlet.

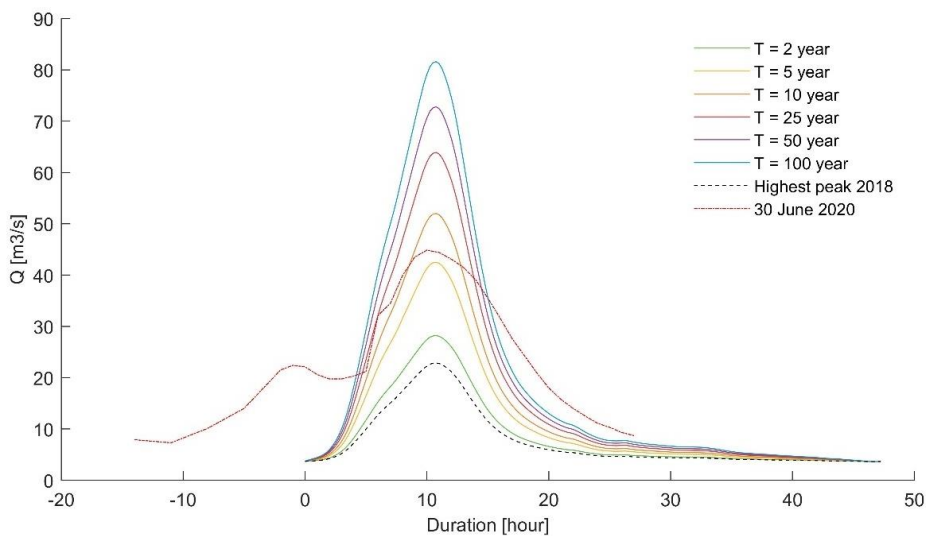


Figure 38: Inflow hydrograph at gauging station Z.38 for the design storms and the event of June 30, 2020.

## 6 Discussion

This chapter starts with a discussion on the research limitations. Consequently, the outcomes of the research are reflected on and discussed.

### 6.1 Research limitations

#### 6.1.1 *Limitations in data collection*

The analyses in this research were based on time-series retrieved between August and November 2019, which was an unusually dry period. Since flood wave celerity increases with increased flood wave size (see section 2.2.1), it is likely that the maximum potential lead time was overestimated in this research. However, due to the physical constraint of water level reaching the pumping station inlet level, the overestimation of lead time did not affect the conclusions in this report.

As a second consequence of using time-series from 2019, the applied model was calibrated on relatively low discharge values. It was observed in the field that large vegetation (1 – 1.5 m) in the cross-sections can bend during high discharge. So, it is likely that for extreme discharge values, friction is lower, and flood wave propagation speeds up. Nevertheless, a faster responding flow regime would not influence the conclusions in the report because water level increased already too fast for effective mitigation.

Flood waves were surveyed by stage only, while flood wave propagation is associated with unsteady flow. During the passing of flood waves, maximum discharge occurs ahead of the maximum stage. Meanwhile, model calibration is sensitive for the correct timing of maximum discharge. A direct survey of unsteady flow holds less uncertainty than the application of a dynamic rating curve approach such as Jones' formula. So, for further research in rivers systems where flood waves occur, it is recommended to survey a second parameter addressing unsteady flow, like flow velocity or water level slope. For example, surface flow velocities could be monitored using LSPIV (large-scale particle image velocimetry method) (Gerritsen, 2020). LSPIV could be integrated into the Mobile Water Management application since the method makes use of short videos.

#### 6.1.2 *Limitations of the applied model*

By the use of a 1D hydraulic model, submerged floodplains were left out of consideration. Water flowing over the dikes was removed from the system. However, in reality, part of the flood volume would still discharge towards the outlet. So, the calculated flood volume in the 1D model was larger than the inundation volume would be in reality. Nevertheless, this simplification did not affect the conclusions since flood volume was not part of the research scope.

The SOBEK model was simplified for the specific use case of this research, and the simplifications were validated by a sensitivity analysis. The sensitivity analysis indicated that the conclusions are not affected by the schematization of lateral inflow, floodwall level, and design pumping capacity. Nevertheless, when using the same model for new use-cases in further research, the simplifications and schematization require reconsideration.

The synthetic flood design hydrographs (design storms) for the largest return periods were thought to be unrealistic. The discharge for a return period of 50 and 100 years did not fit through the cross-section of gauge station Z.38, given that the average velocity would exceed 1.5 m/s during bank full flow. Meanwhile, the maximum discharge for other return periods was expected to be increased due to climate change and ongoing urbanization. Since all design storms lead to the same conclusion, reconsideration of the design discharge values was not required for this research. Hence, the return periods were recognized as 'labels' rather than actual return periods.

The scope of this research was spatially limited to the Tub Ma channel, while the outlet capacity of Tub Ma also depended on the water level in Rayong River. For this research, the water level in Rayong river was assumed higher than Tub Ma, and discharge was only possible by pumping. This assumption reflected the situation during past events. However, in the search for alternative measures for decreasing flood risk, measures that lower the water level in Rayong river were left out due to this spatial

scope. For further research, it is recommended to also assess the possibilities to lower the water level in the Rayong river.

## 6.2 Usefulness of a flood early warning system in Tub Ma

### 6.2.1 Flood early warning information

Fluctuations in water level at gauge stations TM.02, TM.03 and TM.04, tested as the flood early warning locations, were related to water level fluctuations downstream in Tub Ma river. So, water levels in the three upstream tributaries of Tub Ma are precursors for fluvial flooding downstream.

The flood wave travel time between gauging stations TM.02, TM.03, TM.04 and Khlong Kio was found to be 13-15 hours. Flood wave travel time was directly applied as the hydrological parameter indicating maximum potential lead time. Hence, the maximum potential lead time for early warning was 13-15 hours. However, the time series used for this calculation contained no significant flood waves. Since flood wave celerity increases with increased flood wave size (see section 2.2.1), the maximum potential lead time for large flood waves will be less than the 13-15 hours found in this research.

Most of the flood wave volume (roughly  $\frac{3}{4}$ ) originated from the basin area downstream of gauge stations TM.02, TM.03, TM.04. The three early warning gauging stations covered half (46%) of the total catchment area. Nevertheless, the run-off in the early warning sub-catchments was small compared to the downstream part of Tub Ma basin. Hence, extensive extrapolation would have been required for the forecasting of flood volume. Given the spatial variable character of heavy rainfall in Tub Ma, predicted flood(wave) volume would hold a significant degree of uncertainty. As a consequence, volume forecasting using water level at gauge stations TM.02/03/04 requires coping with false alarms as well as the underestimation (or even missing) of flood events.

In this case study, false alarms do not affect the usefulness of the flood early warning system. The adverse effects of false alarms depend on the decision connected to the notification (WMO, 2018). In Tub Ma, the effect of false alarms was limited to the unnecessary operation of the pumping station. Furthermore, time-to-time (unnecessary) operation even increases reliability since the decision-makers and mechanical operators become more experienced. Also, it was recognized that a sequence of false alarms might lead to distrust of early warning notifications (Girons Lopez et al., 2017). Those at risk or those who are designated to make a decision may not respond proactively to the warnings if the information channel is not fully trusted (WMO, 2018). However, distrust of the early warning system can be avoided by pre-identifying and communicating an expected false-alarm ratio (WMO, 2018).

Also, considering the underestimation (or even missing) of flood events; the flood early warning system was appraised as useful. Underestimation of flood wave volume results from spatial rainfall variability and was linked to locally heavy rainfall in the downstream part of the catchment. Meanwhile, the downstream part of the catchment was also the area subjected to fluvial flooding. In this situation where the location of the most torrential rainfall equals the location of flooding, physical observation of the rainfall event becomes a second communication channel for notification, on top of the positioned early warning system (WMO, 2018). Hence, where the early warning system lacks adequate notification, citizens and e.g. the workers located at the outlet would have been warned by observing heavy rainfall themselves.

The local 'monitoring and analyzation' of stage at the flood early warning locations is not (yet) useful for timely notification. Water level peaks in Tub Ma's upstream tributaries only appeared during a few hours, while local stage-survey by citizens (using Mobile Water Management) took place on a less than daily scale. As a result, most events were not observed as they took place between two measurements. So, for a reliable warning system, the monitoring time scale needs to match the interval at which a hazard parameter appears. For flood early warning purposes, a monitoring scale of 0.5 or 1 hour was required at gauging stations TM.02, TM.03, TM.04.

### 6.2.2 Flood mitigation based on flood early warning

#### *Flood mitigation capabilities of the pumping station*

It was recognized that after 20 years of urbanization, most of the catchment's non-linear- and threshold processes of the hydrological cycle were replaced by overland flow (direct run-off) and artificial drainage. Accordingly, it was observed that the Tub Ma basin had a fast responding system behavior: rapidly rising river discharge after rainfall, but almost no baseflow between two events. The transition from baseflow to the peak discharge from a flood wave took only hours. From these characteristics, Tub Ma river was evaluated as an open drain more than a natural channel.

Hydraulic modeling of flood wave propagation through Tub Ma indicated that the discharge capacity at the most constraining cross-section (around Khlong Kio) approximately equaled the pumping capacity of the outlet structure. From this observation, two causes of fluvial flooding were recognized when inflow exceeds discharge capacity. Firstly, in-river storage capacity was filling up, and fluvial flooding occurred through water spilling over the floodwalls. Secondly, overbank flow occurred where inflow exceeds channel capacity, which started around Khlong Kio.

Flood volume resulting from spilling was smaller when the pumping station is started earlier. Timely operation of the pumping station ensured maximum available in-river storage capacity when inflow starts exceeding pump capacity. Around the stream segments where inflow exceeds channel capacity, the flood volume was not affected by the time at which the pumping station was started. Because by the time overbank flow occurred, the pumping station was already running at full capacity, and the in-river storage was filled up. Hence, the maximum possible reduction of flood volume was storage created by early operation of the pumping station. This reduction of flood volume was around 5%, and therefore recognized as negligible.

#### *Pumping station operation based on flood early warning*

The decision to operate the pumping station was not confined to a notification but was also physically constrained by the water level (not) exceeding the pump-inlet level. As a result of this physical limitation, the pumping station was started roughly at the same time for all operation strategies, including flood early warning. So, information from a flood early warning system led not to a different decision regarding the operation of the pumping station.

For the hypotheses from the Research motivation (see 1.1), it was tested whether on-time operation of the outlet structure would prevent or reduce fluvial flooding. Increased water level gradient and flow velocity due to the operation of the pumping station was tested to dampen flood waves and to reduce overbank flow. This research demonstrated that for river systems with little baseflow and rapidly rising discharge, it was physically not possible to start a pumping station ahead of flood waves in a river system that is empty. Consequently, the pumping station was not able to influence the hydraulic conveyance (e.g. by gradient and flow velocity) to dampen flood waves.

### 6.2.3 Usefulness of a flood early warning system in Tub Ma

For the specific use-case of flood mitigation through pumping station operation, flood early warning does not lead to a different operational decision, and a flood early warning system is not beneficial. However, flood early warning systems are designed to decrease disaster risk (UNDRR, 2015), and not for (flood) hazard mitigation solely.

The scope of this study was limited to mitigation only, while disaster risk reduction requires an assessment that includes: hazards, exposure, vulnerability, and capacity (WMO, 2018). Risk can change depending on the actual impacts and consequences of hazards: e.g. decreasing vulnerability by preparedness. In this research, flood early warning was linked to two specific components of the elements 'hazard' (fluvial flooding) and 'capacity' (pumping station operation). While flood early warning was not of added value for these two specific components, it can be useful for decreasing disaster risk.

## 7 Conclusion & recommendations

This research assessed whether flood early warning would lead to improved control of the catchment outlet structure to prevent fluvial flooding in Tub Ma. This thesis has demonstrated that for a catchment with varying data availability and quality, a short period of dedicated data survey and data-processing results in applicative conclusions and recommendations.

### 7.1.1 Flood early warning information

**Do water level fluctuations from upstream tributaries relate to high discharge peaks in the downstream part of the river? (research question 1)**

Yes, water levels in the upstream tributaries of Tub Ma are an information source for the forecasting of discharge (peaks) downstream. Water level based early warning enables a maximum potential lead time of 13-15 hours. Nevertheless, this maximum potential lead time will decrease by increasing flood wave magnitude. Forecasted flood wave volume connected to the early warning is uncertain but useful: false alarms have no adverse effects, while underestimated/missed alarms are backed up by heavy rainfall at the flood-prone location, serving as a second warning channel.

### 7.1.2 Flood mitigation

**What is the potential contribution of the outlet pumping station for the prevention of flooding through overbank flow? (research question 2)**

Due to a flow regime of limited baseflow and rapidly rising discharge, the pumping station is not able to timely influence the hydraulic conductivity for the prevention of overbank flow. Meanwhile, the pumping station discharge capacity approximately equals the discharge capacity of the most constraining cross-section of the Tub Ma river. So, flood mitigation is limited to the generation of in-river storage prior to flood events. Consequently, overbank flow occurs when inflow exceeds pumping capacity.

### 7.1.3 Conclusion

**Does flood early warning lead to improved control of the catchment outlet structure for preventing fluvial flooding in Tub Ma? (Main research question)**

Due to the fast-changing flow regime of Tub Ma, timely operation of the pumping station is physically limited by inflow and by the water level not exceeding the inlet level. With and without information from flood early warning, the pumping station is started roughly at the same time, equal to the time water level exceeds the inlet level. So, for the specific use-case of flood mitigation through pumping station operation, flood early warning does not lead to a different operational decision.

### 7.1.4 Recommendations for decreasing flood risk in Tub Ma

As this study showed a lead time of 13-15 hours, useful applications of a flood early warning system are likely within a broader scope of disaster *risk* reduction in Tub Ma. For example, an early warning system can decrease risk when it results in the decision to evacuate or to bring belongings to safe places. Hence, it is recommended to assess the usefulness of a flood early warning system for all elements of the disaster *risk*.

For the reduction of fluvial flooding, structural measures are recommended that decrease the discharge in Tub Ma (e.g. bypass channel) or structural measures that flatten the discharge curve (.e.g. temporal storage or slowing down the run-off processes). In Appendix G, these measures are shortly evaluated.

Also, this research underlined that water level at the outlet is the most important information for flood mitigation by operation of the pumping station. Hence, it is recommended to validate regularly the water level survey at the outlet.

## 8 Bibliography

- Battjes, J. A., & Labeur, R. J. (2017). *Unsteady Flow in Open Channels*. Cambridge University Press. <https://doi.org/10.1017/9781316576878>
- Boer, M. (2019). *Elevation modelling using dualfrequency Global Navigation Satellite System receivers*. Delft University of Technology.
- Box, G. E. P. (1979). Robustness in the Strategy of Scientific Model Building. In *Robustness in Statistics*. <https://doi.org/10.1016/b978-0-12-438150-6.50018-2>
- Candela, A., Brigandi, G., & Aronica, G. T. (2014). Estimation of synthetic flood design hydrographs using a distributed rainfall-runoff model coupled with a copula-based single storm rainfall generator. *Hazards Earth Syst. Sci.*, *14*, 1819–1833. <https://doi.org/10.5194/nhess-14-1819-2014>
- Carpenter, T. M., Sperflage, J. A., Georgakakos, K. P., Sweeney, T., & Fread, D. L. (1999). National threshold runoff estimation utilizing GIS in support of operational flash flood warning systems. *Journal of Hydrology*, *224*(1–2), 21–44. [https://doi.org/10.1016/S0022-1694\(99\)00115-8](https://doi.org/10.1016/S0022-1694(99)00115-8)
- Chi Choi, C. (2013). *Coupled Hydrologic And Hydraulic Models And Applications*. MS. <https://doi.org/10.17077/etd.1azzcpjl>
- Chow, V. (1959). *Open-channel hydraulics*. McGraw-Hill.
- climate-data.org. (2020). *Rayong climate: Average Temperature, weather by month, Rayong water temperature - Climate-Data.org*. <https://en.climate-data.org/asia/thailand/rayong-province/rayong-4309/>
- Davis, J. . (1986). *Statistics and data analysis in geology* (2nd Editio). John Wiley & Sons.
- Deltares. (2019). *SOBEK 1D/2D modelling suite for integral water solutions User Manual*. [https://content.oss.deltares.nl/delft3d/manuals/SOBEK\\_User\\_Manual.pdf](https://content.oss.deltares.nl/delft3d/manuals/SOBEK_User_Manual.pdf)
- Devia, G. K., Ganasri, B. P., & Dwarakish, G. S. (2015). A Review on Hydrological Models. *Aquatic Procedia*. <https://doi.org/10.1016/j.aqpro.2015.02.126>
- Dottori, F., Martina, M. L. V, Todini, E., Dottori, F., Martina, M. L. V, & Todini, E. (2009). A dynamic rating curve approach to indirect discharge measurement Hydrology and Earth System Sciences A dynamic rating curve approach to indirect discharge measurement. *Hydrol. Earth Syst. Sci.*, *13*, 847–863. <https://doi.org/10.5194/hessd-6-859-2009>
- Eissfeller, B., Ameres, G., Kropp, V., & Sanroma, D. (2007). Performance of GPS , GLONASS and Galileo. *Eisfeller et Al*.
- Endreny, T. A., & Thomas, K. E. (2009). Improving Estimates of Simulated Runoff Quality and Quantity Using Road-Enhanced Land Cover Data. *Journal of Hydrologic Engineering*, *14*(4), 346–351. [https://doi.org/10.1061/\(ASCE\)1084-0699\(2009\)14:4\(346\)](https://doi.org/10.1061/(ASCE)1084-0699(2009)14:4(346))
- Fathi-Moghadam, M., & Drikvandi, K. (2012). Manning coefficient, Vegetation, Flexibility, Non-Submerged; Manning coefficient, Vegetation, Flexibility, Non-Submerged. *International Journal of Hydraulic Engineering*, *2012*(1), 1–4. <https://doi.org/10.5923/j.ijhe.20120101.01>
- Foley, J. A., DeFries, R., Asner, G. P., Barford, C., Bonan, G., Carpenter, S. R., Chapin, F. S., Coe, M. T., Daily, G. C., Gibbs, H. K., Helkowski, J. H., Holloway, T., Howard, E. A., Kucharik, C. J., Monfreda, C., Patz, J. A., Prentice, I. C., Ramankutty, N., & Snyder, P. K. (2005). Global consequences of land use. In *Science*. <https://doi.org/10.1126/science.1111772>
- Gerritsen, G. H. (2020). *Flood wave monitoring using LSPIV A methodology for monitoring flood*

waves in an equatorial urban stream with fast response time.  
<http://resolver.tudelft.nl/uuid:5d856ba9-a207-4b61-8bb7-703322fe3154>

- Gill, M. A. (1978). Flood routing by the Muskingum method. *Journal of Hydrology*, 36(3–4), 353–363. [https://doi.org/10.1016/0022-1694\(78\)90153-1](https://doi.org/10.1016/0022-1694(78)90153-1)
- Girons Lopez, M., Di Baldassarre, G., & Seibert, J. (2017). Impact of social preparedness on flood early warning systems. *Water Resources Research*, 53(1), 522–534. <https://doi.org/10.1002/2016WR019387>
- Hamel, P. (2013). Source-control stormwater management for mitigating the impacts of urbanisation on baseflow: A review. *Journal of Hydrology*. <https://doi.org/10.1016/j.jhydrol.2013.01.001>
- Hayami. (1951). On the Propagation of Flood Waves. *Bulletin of Disaster Prevention Research Institute, Kyoto University*, 1.
- Heijnen, P. W. (2019). *Beslissen onder onzekerheid*.
- Hersch, R. (1993). The velocity-area method. *Flow Measurement and Instrumentation*. [https://doi.org/10.1016/0955-5986\(93\)90004-3](https://doi.org/10.1016/0955-5986(93)90004-3)
- Hirsch, R. M. (1977). *The interaction of channel size and flood discharge for basins undergoing urbanization Publication: Long-Term Changes in Sediment and Nutrient Delivery from Conowingo Dam to Chesapeake Bay: Effects of Reservoir Sedimentation View project*. <https://www.researchgate.net/publication/242558928>
- Hrachowitz, M., Fovet, O., Ruiz, L., Euser, T., Gharari, S., Nijzink, R., Freer, J., Savenije, H. H. G., & Gascuel-Oudou, C. (2014). Process consistency in models: The importance of system signatures, expert knowledge, and process complexity. *Water Resources Research*, 50(9), 7445–7469. <https://doi.org/10.1002/2014WR015484>
- Jarden, K. M., Jefferson, A. J., & Grieser, J. M. (2016). Assessing the effects of catchment-scale urban green infrastructure retrofits on hydrograph characteristics. *Hydrological Processes*, 30(10), 1536–1550. <https://doi.org/10.1002/hyp.10736>
- Jiradecha, C., Surakit, K., & Pinthong, P. (2011). *Feasibility Study of Survey, Design for Flood Solution in Rayong Municipality Area, Choeng Noen Subdistrict, Tubma Subdistrict and Noen Phra Subdistrict, Mueang District, Rayong Province*.
- Jones, B. E. (1915). A method of correcting river discharge for a changing stage. *U.S. Geological Survey Water Supply Paper*, 375-E, 117–130.
- Julien, P. Y., Ghani, A. A., Zakaria, N. A., Abdullah, R., & Chang, C. K. (2010). Case Study: Flood Mitigation of the Muda River, Malaysia. *Journal of Hydraulic Engineering*, 136(4), 251–261. [https://doi.org/10.1061/\(ASCE\)HY.1943-7900.0000163](https://doi.org/10.1061/(ASCE)HY.1943-7900.0000163)
- Kang, M. K., Choi, I. Y., Park, J. H., & Choi, J. H. (2012). Investigation of the Effect of Weirs Construction in the Han River on the Characteristics of Sediments. *Journal of Korean Society of Environmental Engineers*, 34(9), 597–603. <https://doi.org/10.4491/ksee.2012.34.9.597>
- Karaim, M., Elsheikh, M., & Noureldin, A. (2018). GNSS Error Sources. In *Multifunctional Operation and Application of GPS*. InTech. <https://doi.org/10.5772/intechopen.75493>
- Khedari, J., Sangprajak, A., & Hirunlabh, J. (2002). Thailand climatic zones. *Renewable Energy*. [https://doi.org/10.1016/S0960-1481\(01\)00005-2](https://doi.org/10.1016/S0960-1481(01)00005-2)
- Komori, D., Nakamura, S., Kiguchi, M., Nishijima, A., Yamazaki, D., Suzuki, S., Kawasaki, A., Oki, K., & Oki, T. (2012). *Characteristics of the 2011 Chao Phraya River flood in Central Thailand*. 6, 41–46. <https://doi.org/10.3178/HRL.6.41>

- Kuichling, E. (1889). The Relation Between the Rainfall and the Discharge of Sewers in Populous Districts. *Transactions of the American Society of Civil Engineers*, XX(1), 1–56.
- Lee, J. G., & Heaney, J. P. (2003). Estimation of urban imperviousness and its impacts on storm water systems. *Journal of Water Resources Planning and Management*. [https://doi.org/10.1061/\(ASCE\)0733-9496\(2003\)129:5\(419\)](https://doi.org/10.1061/(ASCE)0733-9496(2003)129:5(419))
- Luxemburg, W. M. J., & Coenders, A. M. J. (2017). *CIE4440, Lecture Notes And, Hydrological Processes Measurements*.
- Manning, R. (1891). *On the flow of water in open channels and pipes: Institute of Civil Engineers of Ireland Transactions*, v. 20.
- Marin, C. T., Bouten, W., & Sevink, J. (2000). Gross rainfall and its partitioning into throughfall, stemflow and evaporation of intercepted water in four forest ecosystems in western Amazonia. *Journal of Hydrology*, 237(1–2), 40–57. [https://doi.org/10.1016/S0022-1694\(00\)00301-2](https://doi.org/10.1016/S0022-1694(00)00301-2)
- Markar, M. S., Clark, S. Q., Yaowu, M., & Jing, Z. (2006). Evaluation of hydrologic and hydraulic models for real-time flood forecasting use in the Yangtze River catchment. *Australasian Journal of Water Resources*, 10(1), 93–102. <https://doi.org/10.1080/13241583.2006.11465284>
- Masselink, G., & Short, A. D. (1993). The effect of tide range on beach morphodynamics and morphology: a conceptual beach model. *Journal of Coastal Research*.
- Mergen, B., & Longshore, D. (2001). Encyclopedia of Hurricanes, Typhoons, and Cyclones. *Environmental History*. <https://doi.org/10.2307/3985097>
- Merz, B., Hall, J., Disse, M., & Schumann, A. (2010). Fluvial flood risk management in a changing world. In *Nat. Hazards Earth Syst. Sci* (Vol. 10). <http://www.nat-hazards-earth-syst-sci.net/10/509/2010/www.nat-hazards-earth-syst-sci.net/10/509/2010/>
- Methaprayun, M. (2020). *การเพิ่มประสิทธิภาพในการประเมินน้ำฝนเรดาร์ในลุ่มน้ำที่มีข้อมูลฝนอย่างจำกัด [Enhancement of Radar Rainfall Estimates in a Data Scarce Catchment]*. M.Eng. Thesis. Kasetsart University, Bangkok, Thailand.
- Meyer, A., Fleischmann, A. S., Collischonn, W., Paiva, R., & Jardim, P. (2018). Empirical assessment of flood wave celerity–discharge relationships at local and reach scales. *Hydrological Sciences Journal*, 63(15–16), 2035–2047. <https://doi.org/10.1080/02626667.2018.1557336>
- Mitsubishi Research Institute. (2015, March). *Natural Disaster Risk Assessment and Area Business Continuity Plan Formulation for Industrial Agglomerated Areas in the ASEAN Region*. <http://data.worldbank.org>
- Mobile Water Management. (2020). *Mobile Water Management - We READ Water*. <https://mobilewatermanagement.nl/>
- Nash, J. E., & Sutcliffe, J. V. (1970). River flow forecasting through conceptual models part I - A discussion of principles. *Journal of Hydrology*, 10(3), 282–290. [https://doi.org/10.1016/0022-1694\(70\)90255-6](https://doi.org/10.1016/0022-1694(70)90255-6)
- Nerc, N. (1975). *Flood studies report* (1st ed.). Hydrological Studies.
- Oberg, K. (2002). In Search of Easy-to-Use Methods for Calibrating ADCPs for Velocity and Discharge Measurements. *Hydraulic Measurements and Experimental Methods 2002*, 1–11. [https://doi.org/10.1061/40655\(2002\)4](https://doi.org/10.1061/40655(2002)4)
- Parker, D., & Fordham, M. (1996). An evaluation of flood forecasting, warning and response systems in the European Union. In *Water Resources Management* (Vol. 10, Issue 4, pp. 279–302). Springer Netherlands. <https://doi.org/10.1007/BF00508897>

- Price, R. K. (2009). Volume-conservative nonlinear flood routing. *Journal of Hydraulic Engineering*. [https://doi.org/10.1061/\(ASCE\)HY.1943-7900.0000088](https://doi.org/10.1061/(ASCE)HY.1943-7900.0000088)
- Reszler, C., Blöschl, G., & Komma, J. (2008). Identifying runoff routing parameters for operational flood forecasting in small to medium sized catchments. *Hydrological Sciences Journal*. <https://doi.org/10.1623/hysj.53.1.112>
- Savenije, H. H. G. (2009). HESS opinions: "The art of hydrology." In *Hydrology and Earth System Sciences*. <https://doi.org/10.5194/hess-13-157-2009>
- Sellin, R. H. J. (1969). *Flow in channels* (1st ed.). Macmillan and Co LTD.
- Shum, C. K., Lee, H., Abusali, P. A. M., Braun, A., de Carufel, G., Fotopoulos, G., Komjathy, A., & Kuo, C. (2010). Prospects of Global Navigation Satellite System (GNSS) reflectometry for geodynamic studies. *Advances in Space Research*, 47(10), 1814–1822. [https://www.academia.edu/13562374/Prospects\\_of\\_Global\\_Navigation\\_Satellite\\_System\\_GNSS\\_reflectometry\\_for\\_geodynamic\\_studies](https://www.academia.edu/13562374/Prospects_of_Global_Navigation_Satellite_System_GNSS_reflectometry_for_geodynamic_studies)
- Sieweke, J. (2013). River.Space.Design. Planning Strategies, Methods and Projects for Urban Rivers. *Journal of Landscape Architecture*. <https://doi.org/10.1080/18626033.2013.864134>
- Siripong, A. (2010). Detect the coastline changes in Thailand by remote sensing. *International Archives of the Photogrammetry, Remote Sensing and Spatial Information Sciences - ISPRS Archives*.
- Skublics, D., & Rutschmann, P. (2014). Hochwasserrückhalt durch natürliche Hochwasserretention entlang der bayerischen Donau. *WasserWirtschaft*. <https://doi.org/10.1365/s35147-014-0986-5>
- Sloto, R., Crouse, M., & Eaton, G. (1996). *HYSEP: A COMPUTER PROGRAM FOR STREAMFLOW HYDROGRAPH SEPARATION AND ANALYSIS*. <https://www.water-research.net/Waterlibrary/geologicdata/estbaseflow.pdf>
- Suhardi, G., & Entin. (2019). Estimation of Runoff Coefficient Using Satellite Imagery in Welang Watershed Pasuruan District Indonesia. *International Journal of Civil Engineering and Technology*, 10(6), 155–162. <http://www.iaeme.com/IJCIET/index.asp155http://www.iaeme.com/ijciet/issues.asp?JType=IJCIE T&VType=10&IType=6http://www.iaeme.com/IJCIET/issues.asp?JType=IJCIE T&VType=10&IType=6>
- Thai Meteorological Department. (2018). *Showing results for TMD tropical cyclones low pressure cells Search instead for TMD tropical cycles low pressure cells Search Results Web results Severe weather in Thailand*. <https://www.wmo.int/pages/prog/amp/pwsp/documents/CountryReportThailandSWFDP-SeA.pdf>
- Thanapura, P., Helder, D. L., Burckhard, S., Warmath, E., O'Neill, M., & Galster, D. (2007). Mapping urban land cover using quickbird NDVI and GIS spatial modeling for runoff coefficient determination. In *Photogrammetric Engineering and Remote Sensing* (Vol. 73, Issue 1, pp. 57–65). American Society for Photogrammetry and Remote Sensing. <https://doi.org/10.14358/PERS.73.1.57>
- UNDRR. (2015). *Sendai Framework for Disaster Risk Reduction 2015 - 2030*. [https://www.preventionweb.net/files/43291\\_sendaiframeworkfordrren.pdf](https://www.preventionweb.net/files/43291_sendaiframeworkfordrren.pdf)
- Van Essen Instruments. (2016). *PRODUCT MANUAL Diver®*. [www.vanessen.com/manuals](http://www.vanessen.com/manuals)
- Verkade, J. S., & Werner, M. G. F. (2011). Estimating the benefits of single value and probability forecasting for flood warning. *Hydrol. Earth Syst. Sci*, 15, 3751–3765. <https://doi.org/10.5194/hess-15-3751-2011>
- Vitousek, P. M., Mooney, H. A., Lubchenco, J., & Melillo, J. M. (1997). Human domination of Earth's

ecosystems. *Science*. <https://doi.org/10.1126/science.277.5325.494>

Werner, M., Winsemius, H. ., & Robinson, B. (2011). *A framework for establishing flow forecasting requirements: application in the Zambezi river basin*.

WMO. (2018). *Multi-hazard Early Warning Systems: A Checklist , Outcome of the first Multi-hazard Early Warning Conference*.

Worldbank. (2018). *Land area (sq. km) - Thailand | Data*.  
<https://data.worldbank.org/indicator/AG.LND.TOTL.K2?locations=TH>

Worldbank. (2020). *Thailand Overview*. <https://www.worldbank.org/en/country/thailand/overview>

Worldometer. (2020). *Thailand Population (2020) - Worldometer*. <https://www.worldometers.info/world-population/thailand-population/>

Zhao, S., Peng, C., Jiang, H., Tian, D., Lei, X., & Zhou, X. (2006). Land use change in Asia and the ecological consequences. *Ecological Research*. <https://doi.org/10.1007/s11284-006-0048-2>

Zhu, F., Hu, Z., Liu, W., & Zhang, X. (2019). Dual-Antenna GNSS Integrated with MEMS for Reliable and Continuous Attitude Determination in Challenged Environments. *IEEE Sensors Journal*, 19(9), 3449–3461. <https://doi.org/10.1109/JSEN.2019.2891783>

Zhu, T., Lund, J. R., Jenkins, M. W., Marques, G. F., & Ritzema, R. S. (2007). Climate change, urbanization, and optimal long-term floodplain protection. *Water Resources Research*. <https://doi.org/10.1029/2004WR003516>

## Appendix A. Summary of differential GNSS set up

This appendix provides a short background on the GNSS set up that was used for mapping the longitudinal river bathymetry.

### *GPS versus GNSS*

For the past two decades, precise three-dimensional positioning was mostly retrieved by the Global Positioning System or in short, GPS (Shum et al., 2010). The GPS system is developed by the United States of America and consists currently of 31 operational satellites. Meanwhile, Russia, China and the European Union have their own satellite constellations, respectively called GLONASS, Beidou, and Galileo (Shum et al., 2010). In contrast to GPS-receivers, GNSS- receivers can make use of satellites of all of these constellations. So at any time, more satellites are available for three-dimensional positioning through GNSS resulting in more accurate positioning (Shum et al., 2010).

### *Differential GNSS*

In this research, a differential GNSS set up was used. Differential GNSS makes uses of two instead of one receiver. One receiver is located at a fixed location and called 'base station', the second receiver is called the 'rover'. Both receivers communicate with each other by using the internet, which is available through hotspots from mobile phones. Over this internet connection, RTCM (Radio Technical Commission for Maritime) data was transmitted containing detailed information about the GNSS network such as perturbations in the ionosphere and troposphere (F. Zhu et al., 2019)

Using one GPS or GNSS receiver, tropospheric errors and the ionospheric errors result in large errors (a couple of meters) in the z-direction of the three-dimensional positioning (Karaim et al., 2018). However, when two GNSS receivers are relatively close to each other (within a couple of km), the tropospheric error and the ionospheric error in both receivers can be assumed identical. A positional offset between the base station's known position and the position according to the current satellite constellation can, therefore, be assumed to be the same at the rover's location. After correcting the rover's position according to the satellites for the offset retrieved from the base station, the three-dimensional positioning becomes accurate and precise up to 0.5 cm (Shum et al., 2010)

### *Equipment*

For the base station as well as the rover, the following equipment was used:

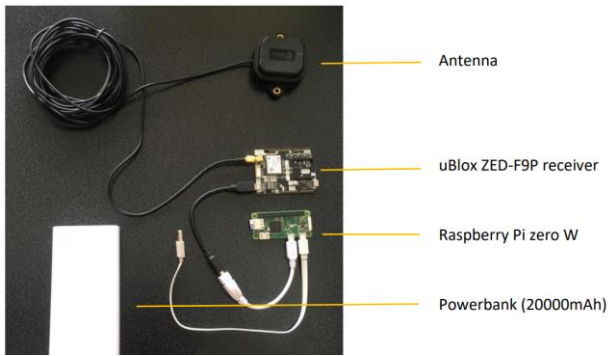
- GNSS receiver - uBlox ZED-F9P-00B-02
- Antenna - uBlox ANN-MB-00-00
- Raspberry Pi zero W
- Powerbank
- Wi-Fi connection from mobile phone's hotspot
- Watertight box
- Jumper cables

The set-up is displayed in Picture 1.

### *Set up*

The base station receiver was fixed on top of the Rayong Area Revenue office because that was the highest accessible building in the area (Picture 2 and Picture 3). A high building was required to protect the satellite connection from being blocked by surrounding buildings.

The rover was placed on top of a cap (see Picture 3 and Picture 4). While walking over the floodwall wearing the cap, the three-dimensional position of the rover antenna was logged every second. In this way, a bias in z-direction equal to the length of the person wearing the cap was present and corrected for afterward.



Picture 1: Set up of base station / rover (Boer, 2019).



Picture 2: 'Base station' receiver, on top of Rayong Area Revenue -building in Rayong.



Picture 3: 'Base station' antenna, on top of Rayong Area Revenue -building in Rayong.



Picture 4: 'Rover' antenna for GNSS receiver, on top a cap to survey floodwall level while walking.

*Recommendation for further research*

At some point, the base station stopped working due to the failure of the internet connection. It turned out the combination of heat from the mobile phone, powerbank, and incoming solar radiation had resulted in overheating. For further research, it is recommended to search for a solution to prevent overheating of the equipment.

## Appendix B. Fieldwork results: time series

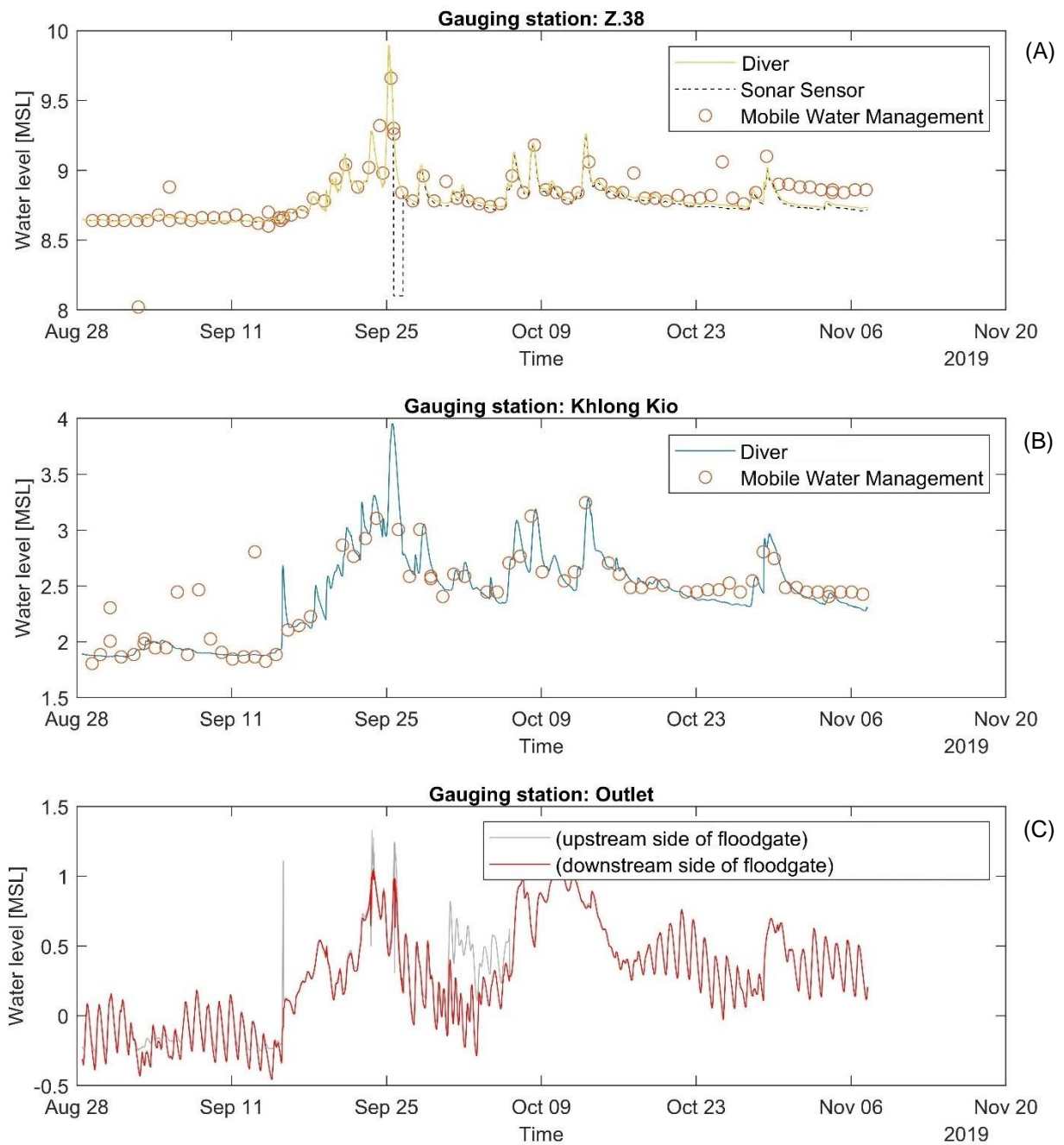


Figure 39: Water level time series from the available monitoring devices per gauging station.

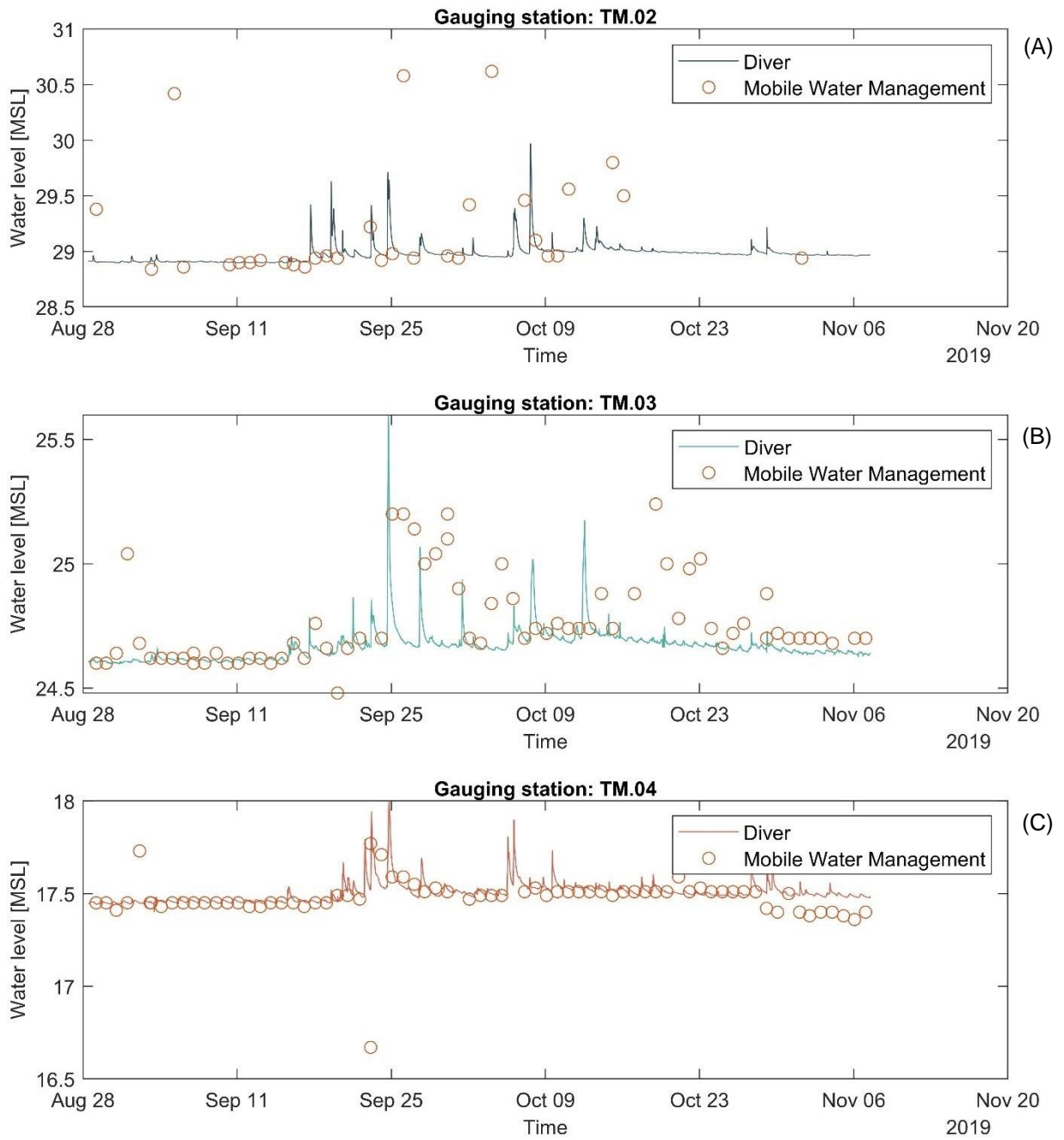


Figure 40: Water level time series from the available monitoring devices per gauging station.

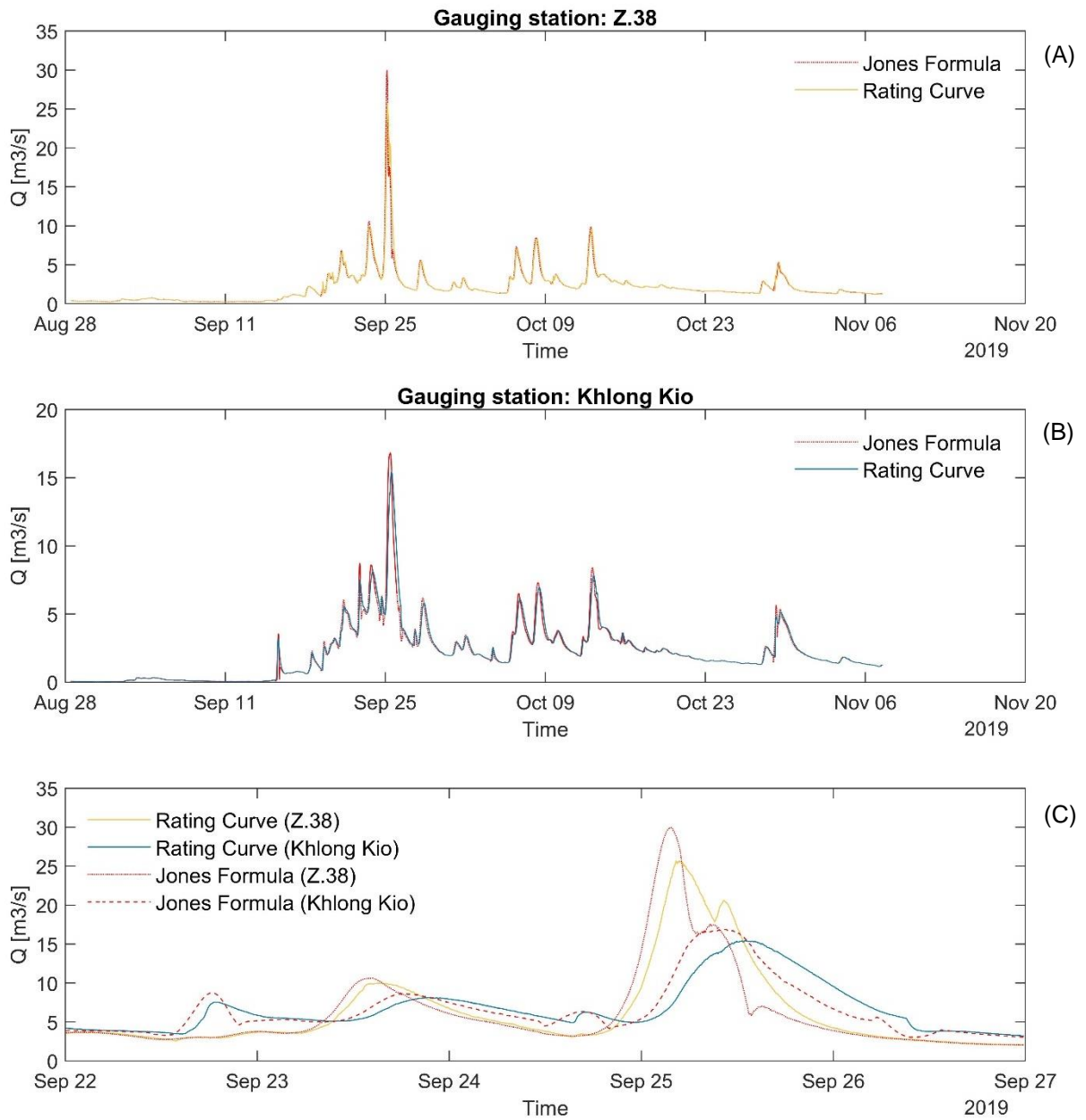


Figure 41: Discharge obtained from indirect measurements using Divers; by applying both the stage-discharge relationship (rating curve) and the dynamic rating curve approach (Jones' formula).

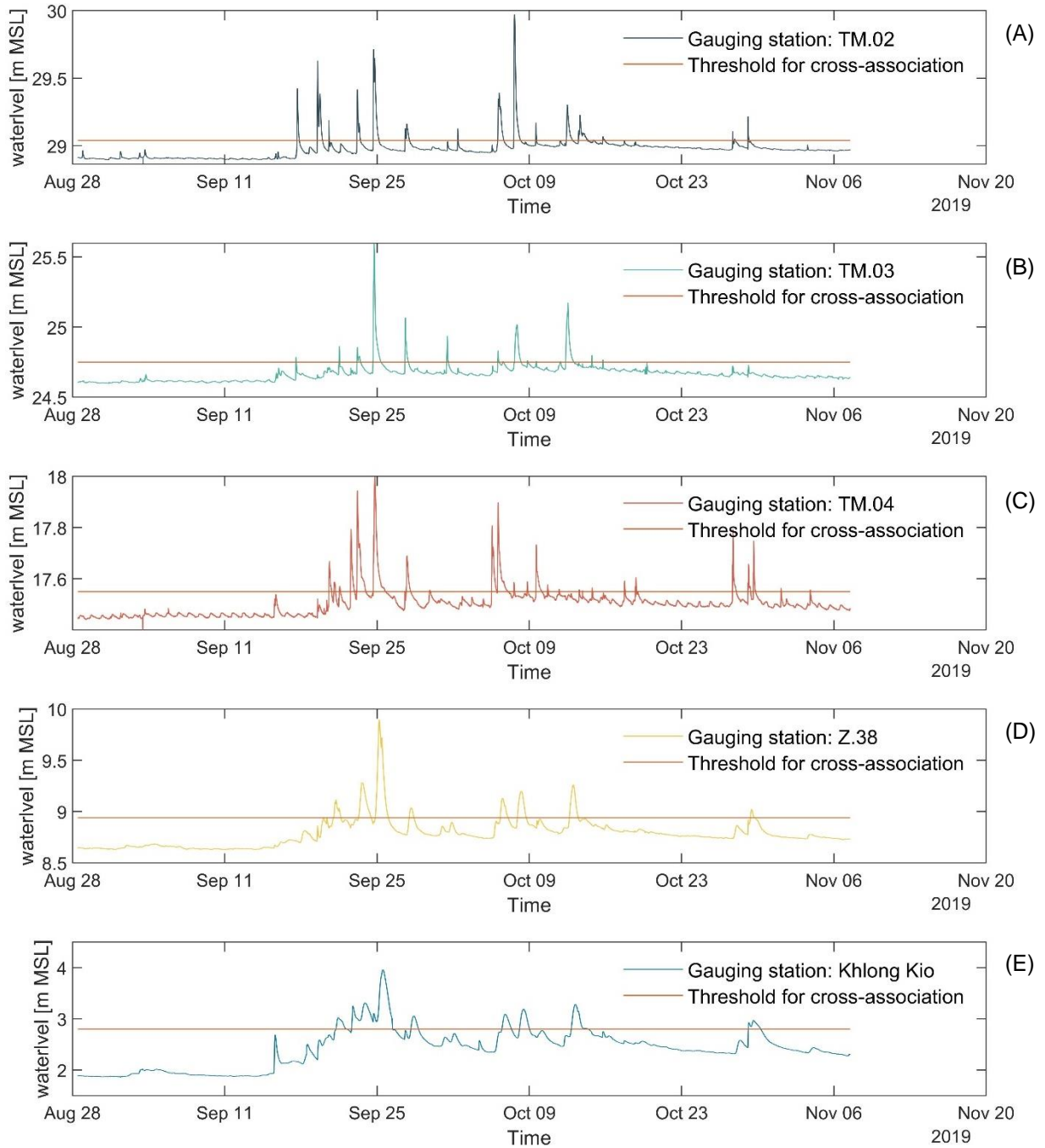


Figure 42: Water level threshold values used for cross-association analysis.

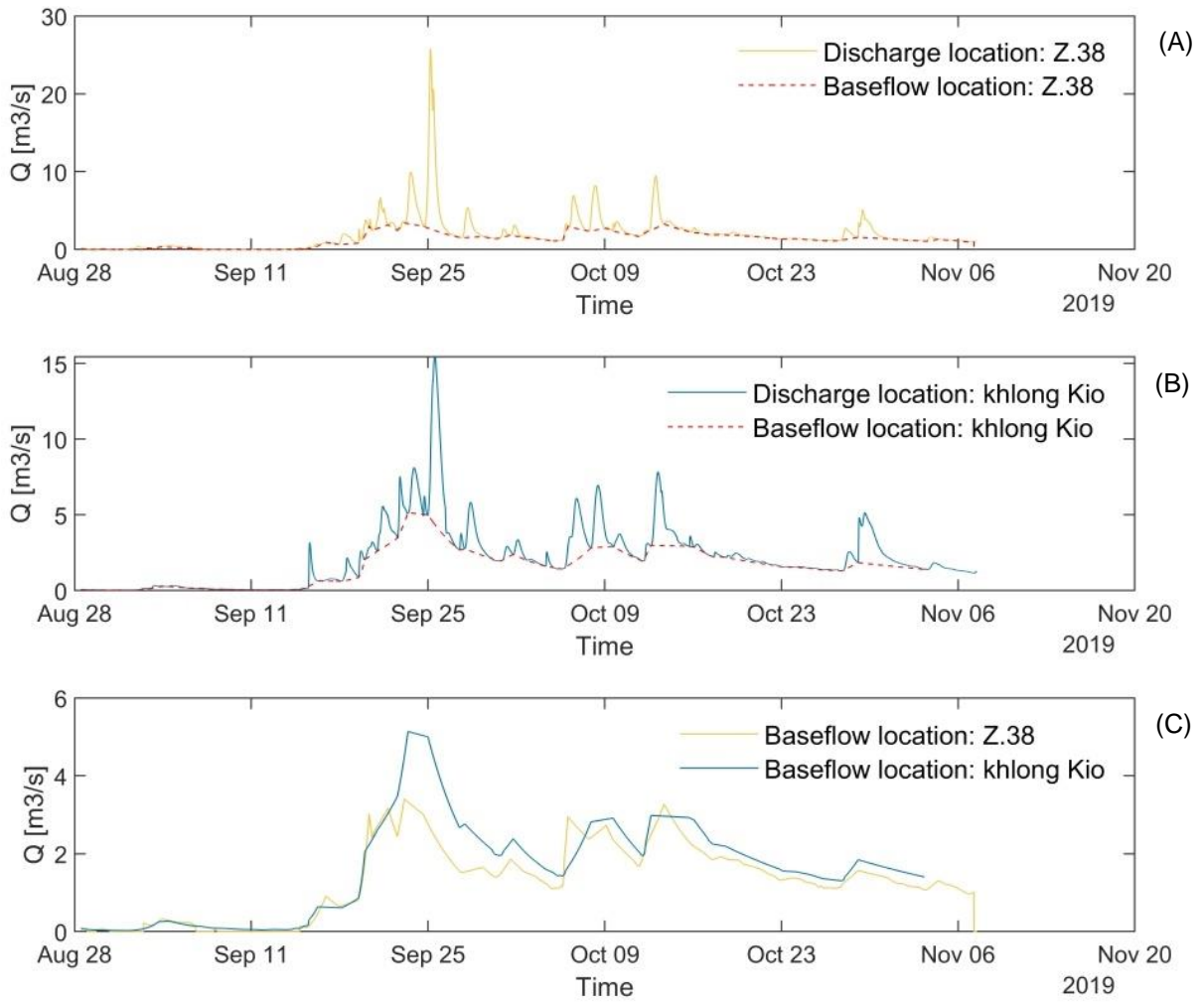


Figure 43: Baseflow separation by HYSEP (Sloto et al., 1996).

# Appendix C. Fieldwork results: bathymetry

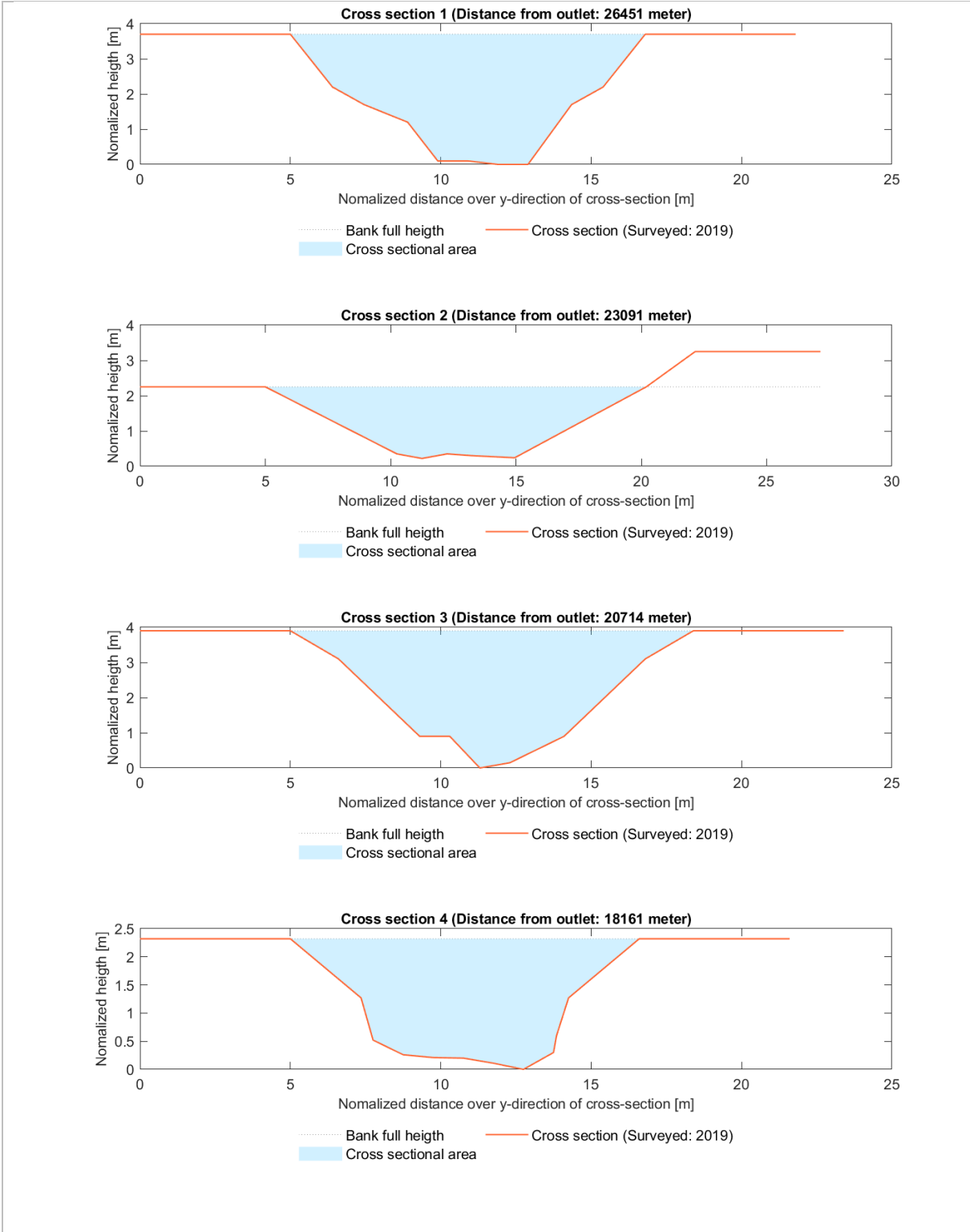


Figure 44: Cross-sections 1 to 4.

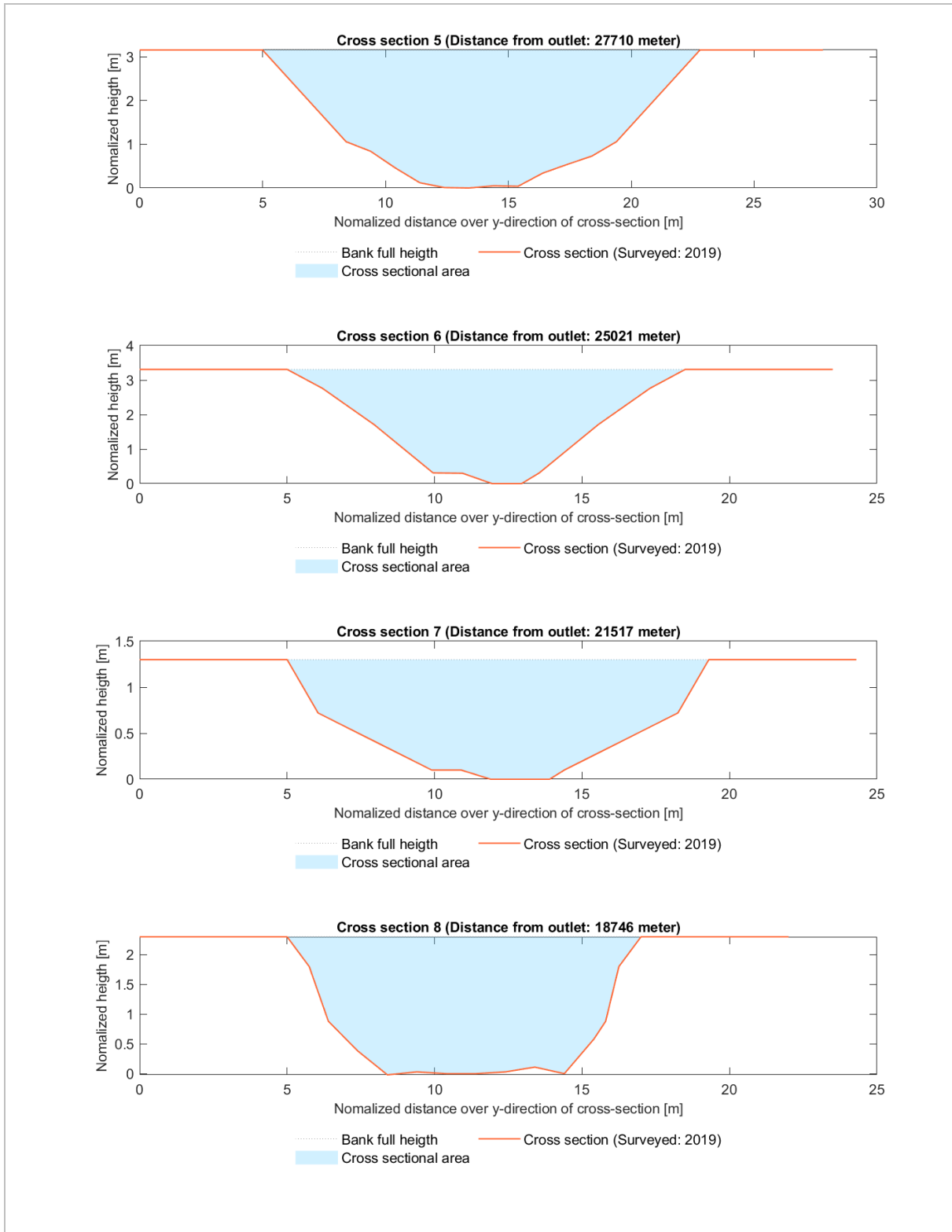


Figure 45: Cross-sections 5 to 8.

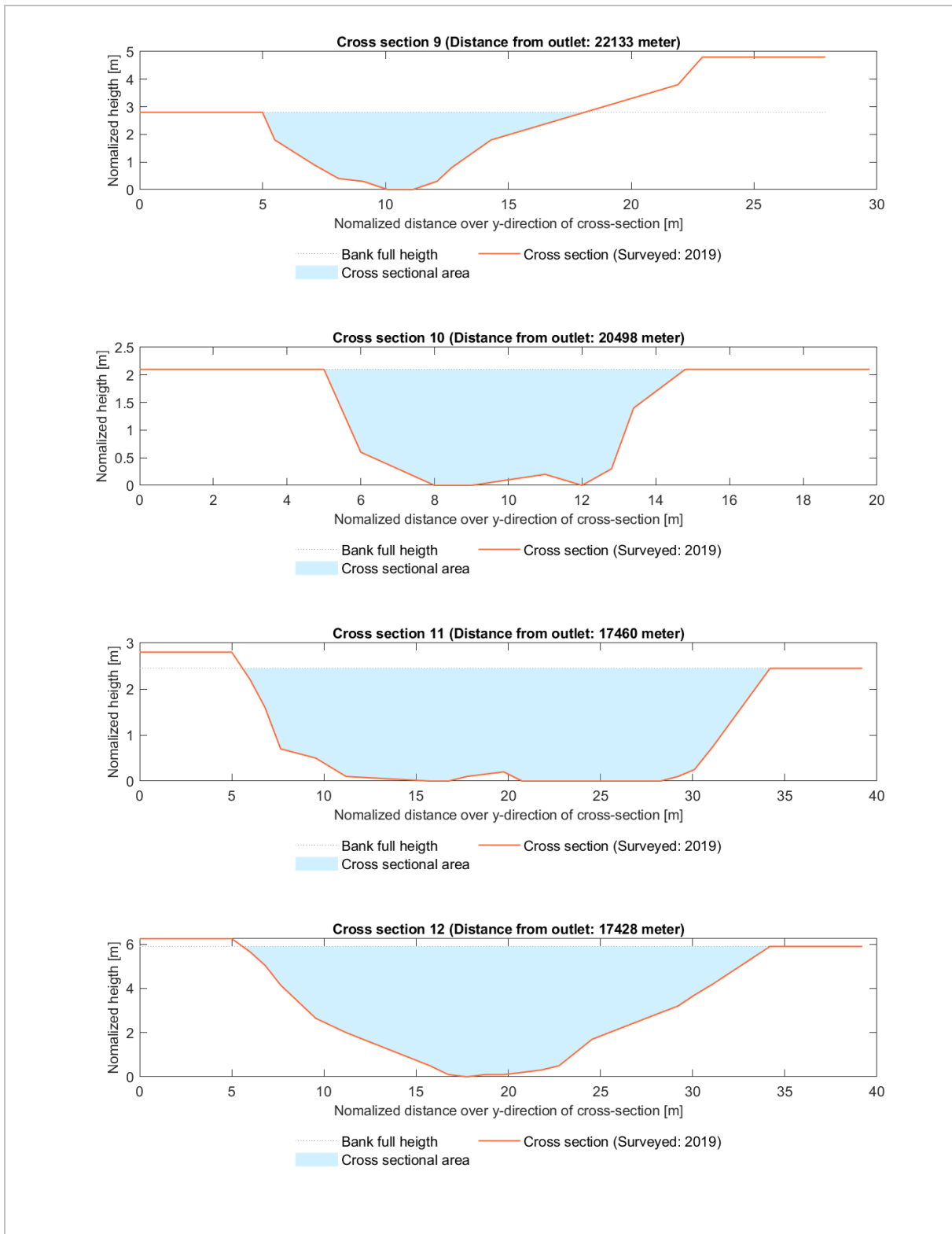


Figure 46: Cross-sections 9 to 12.

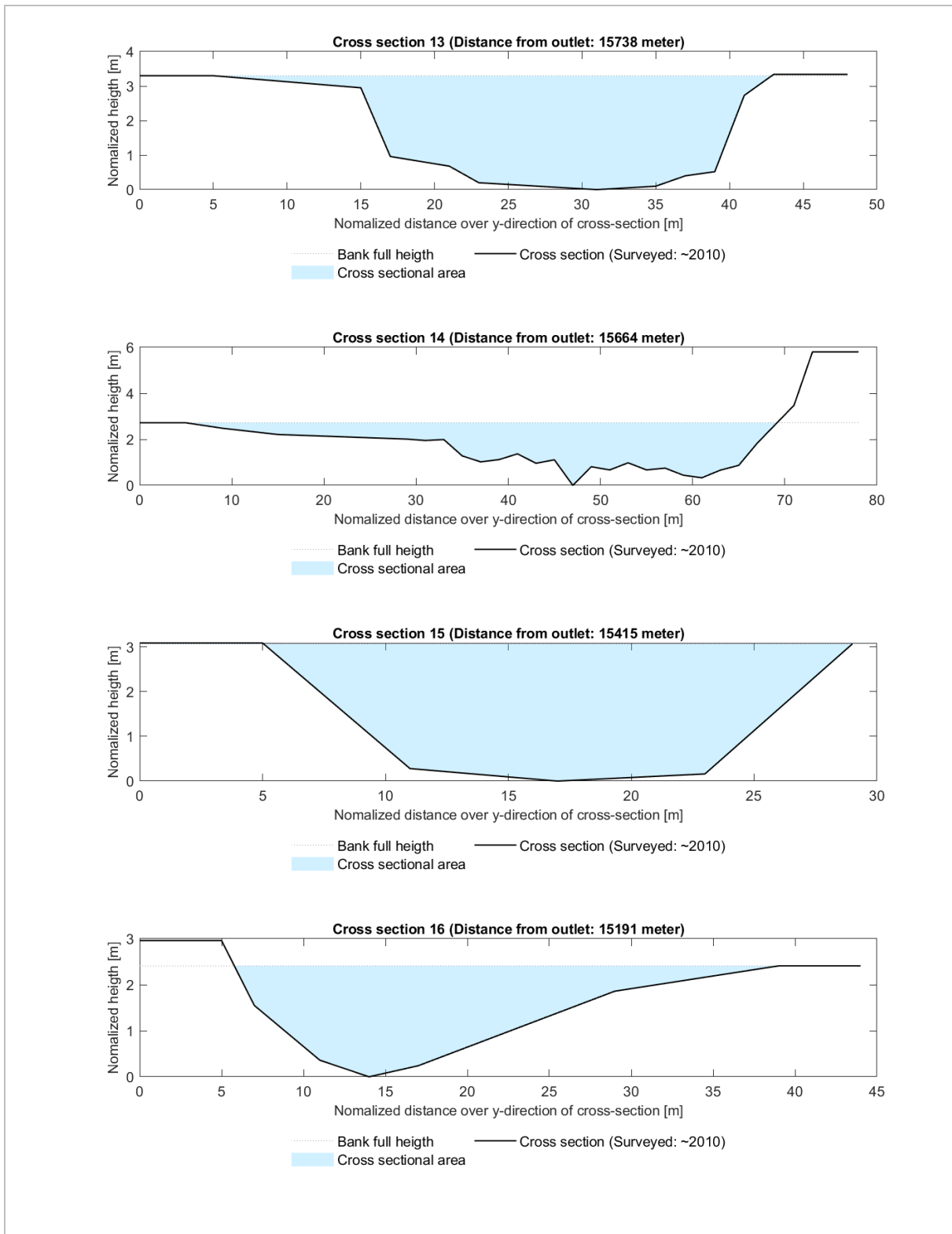


Figure 47: Cross-sections 13 to 16.

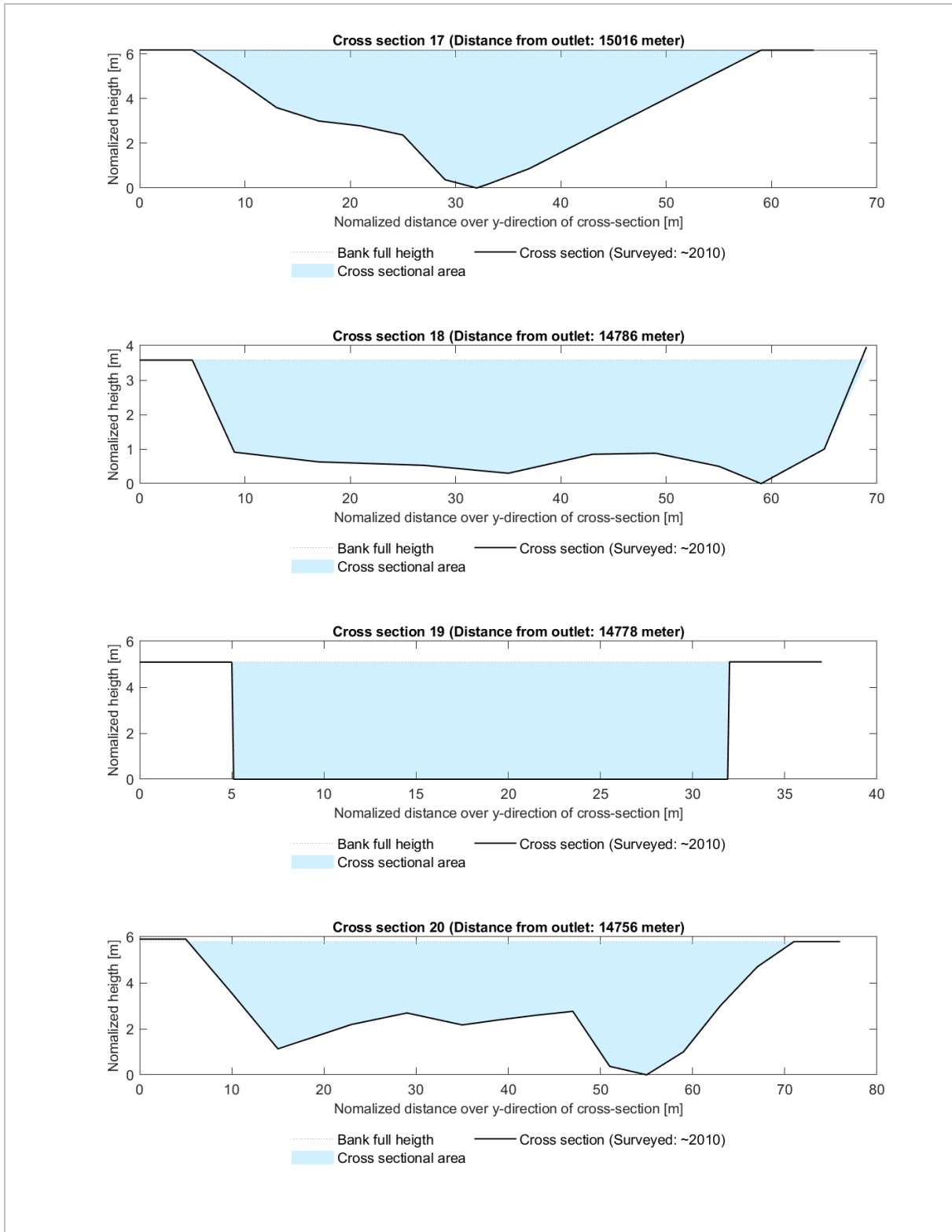


Figure 48: Cross-sections 17 to 20.

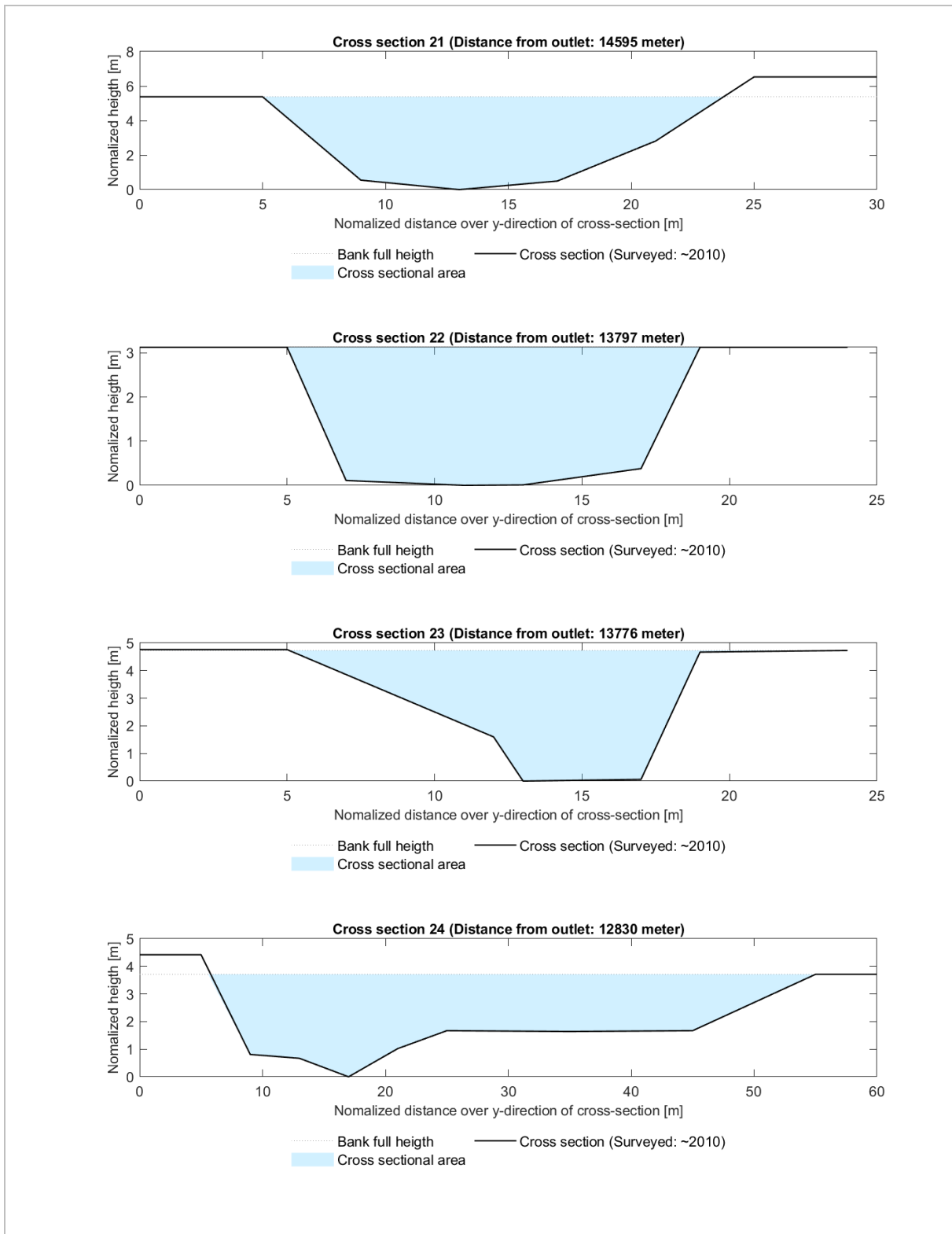


Figure 49: Cross-sections 21 to 24.

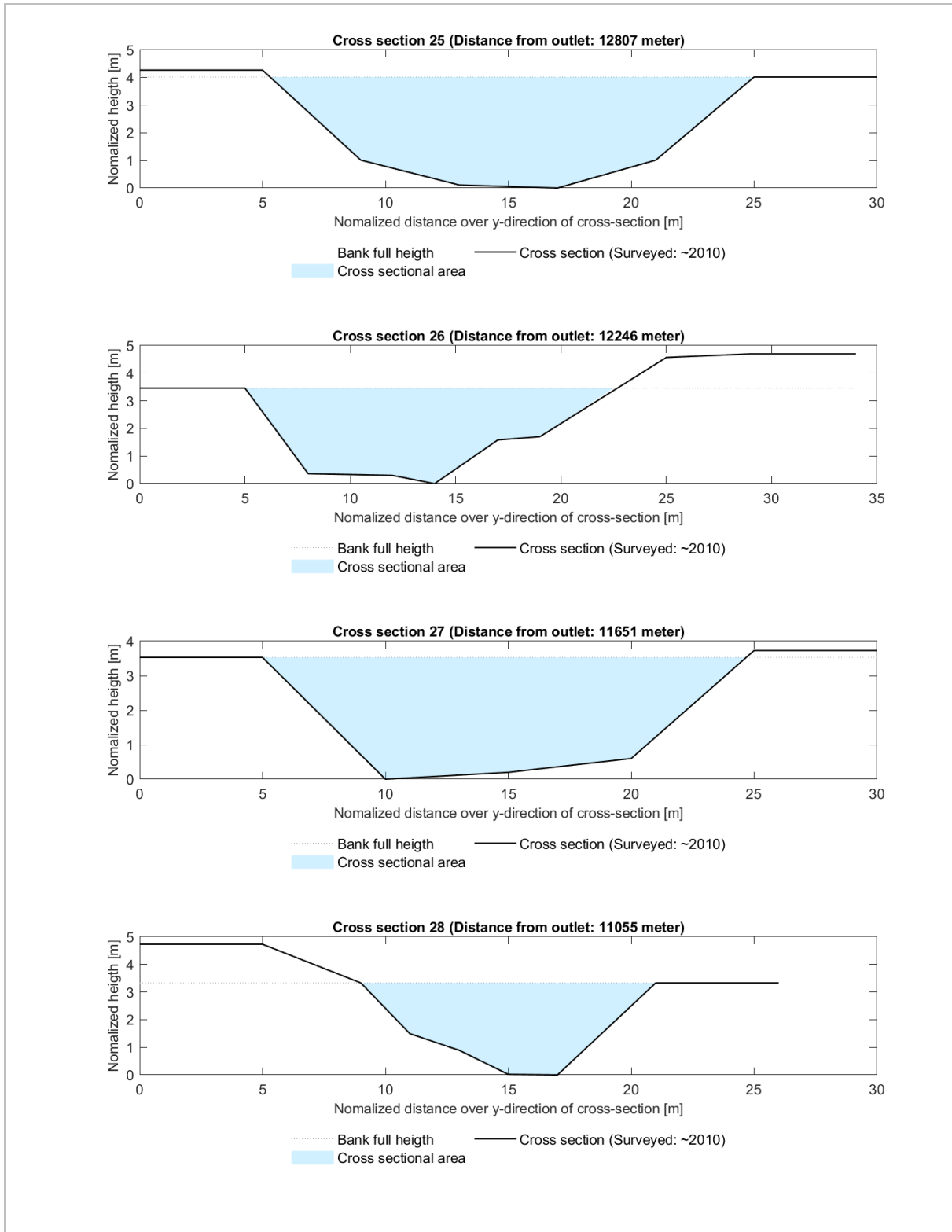


Figure 50: Cross-sections 25 to 28.

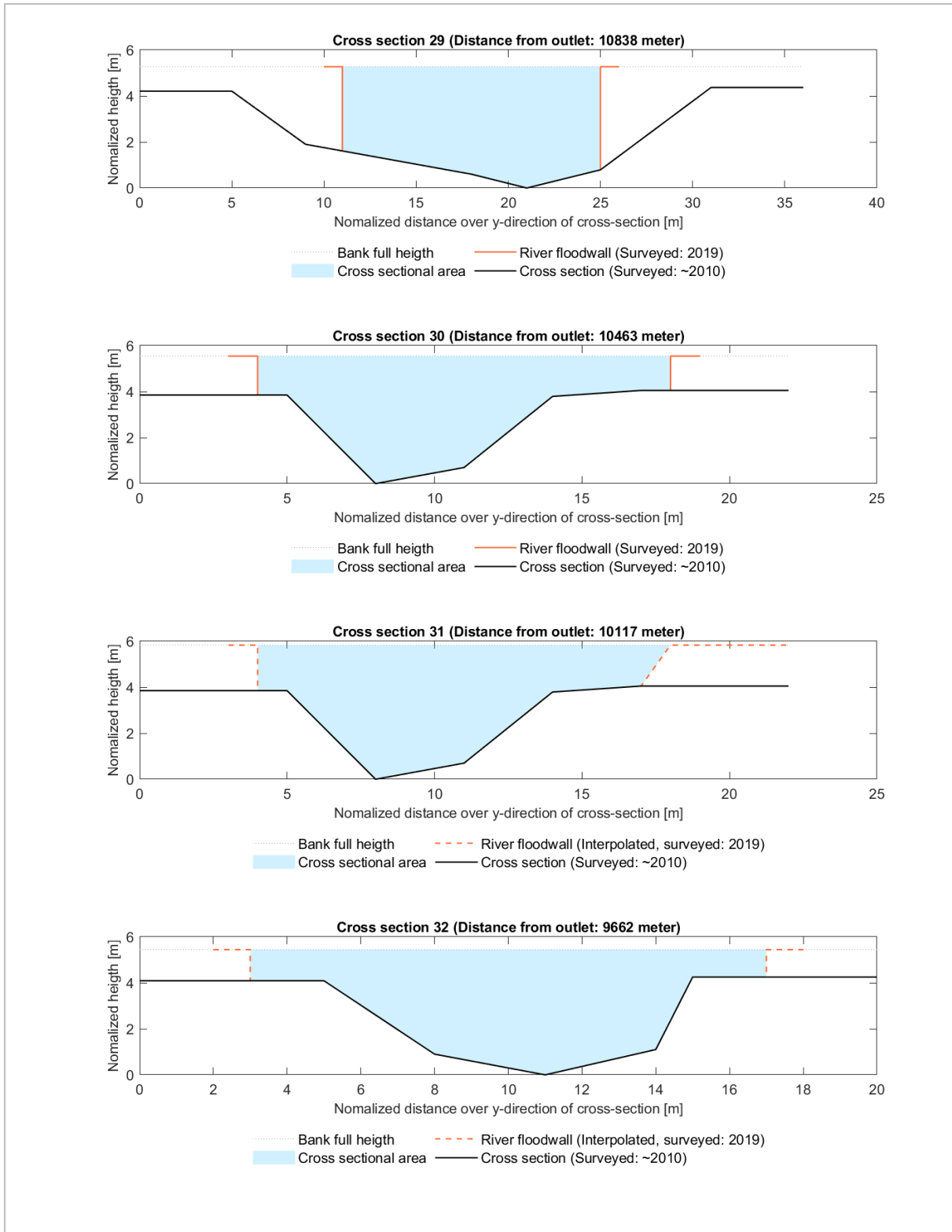


Figure 51: Cross-sections 29 to 32.

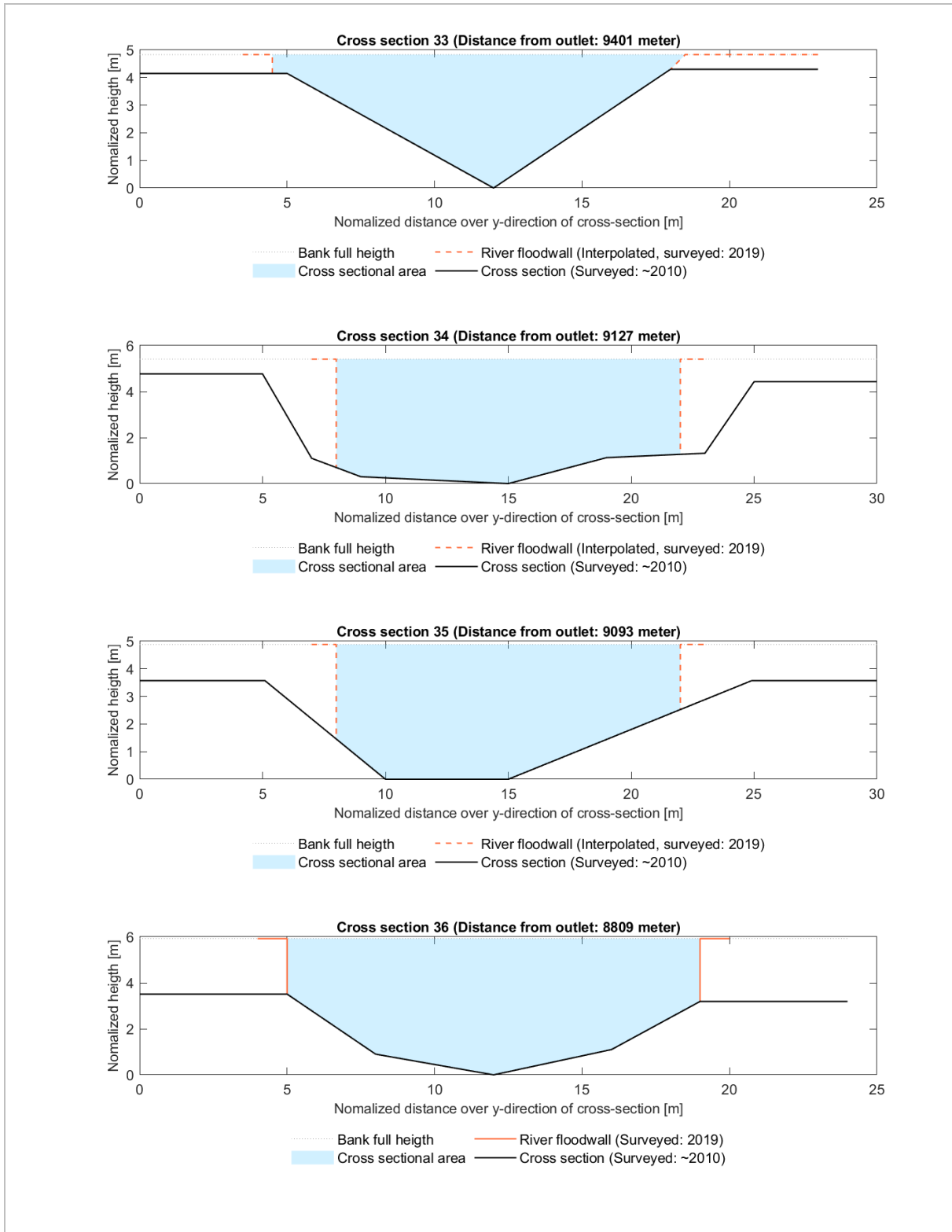


Figure 52: Cross-sections 33 to 36.

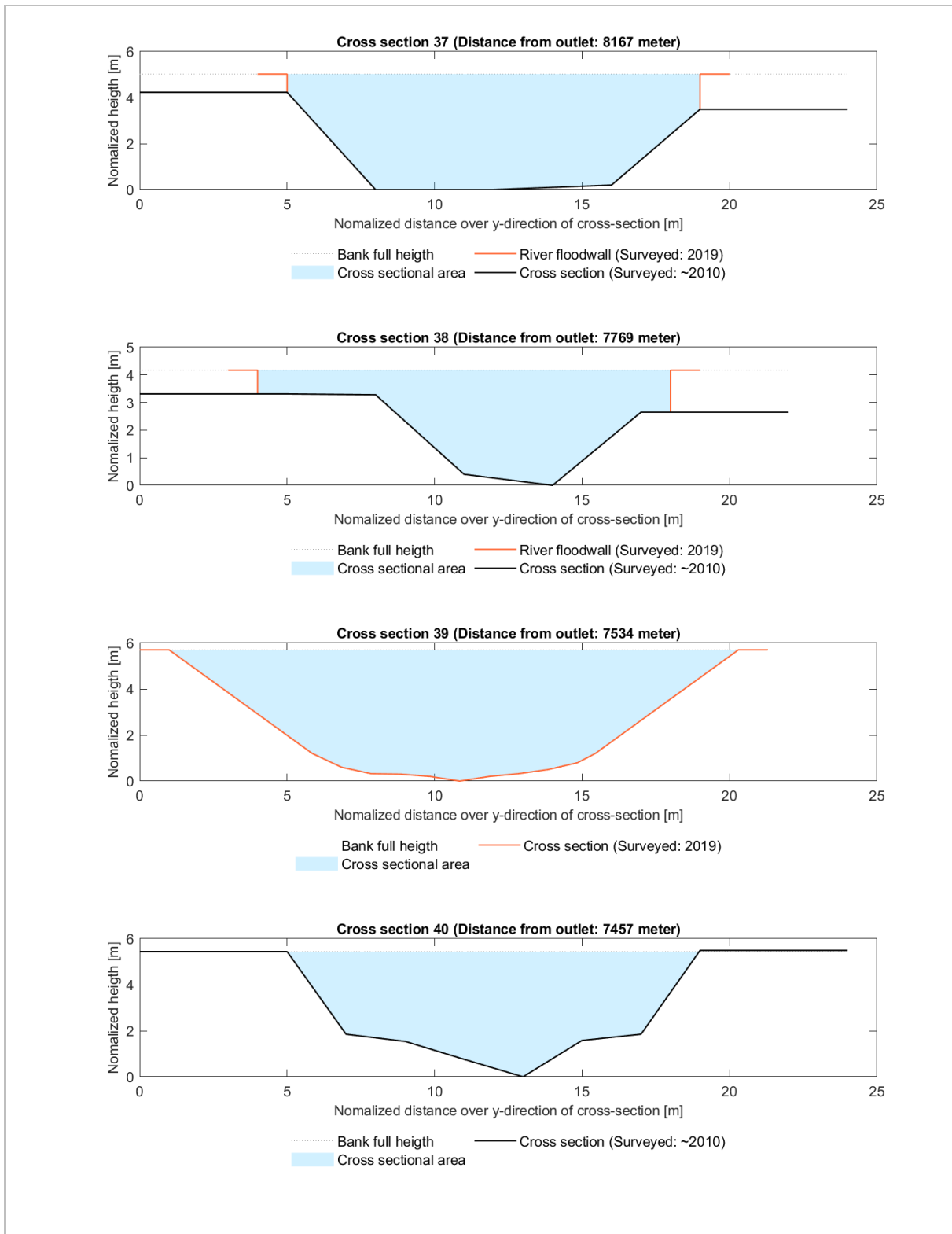


Figure 53: Cross-sections 37 to 40.

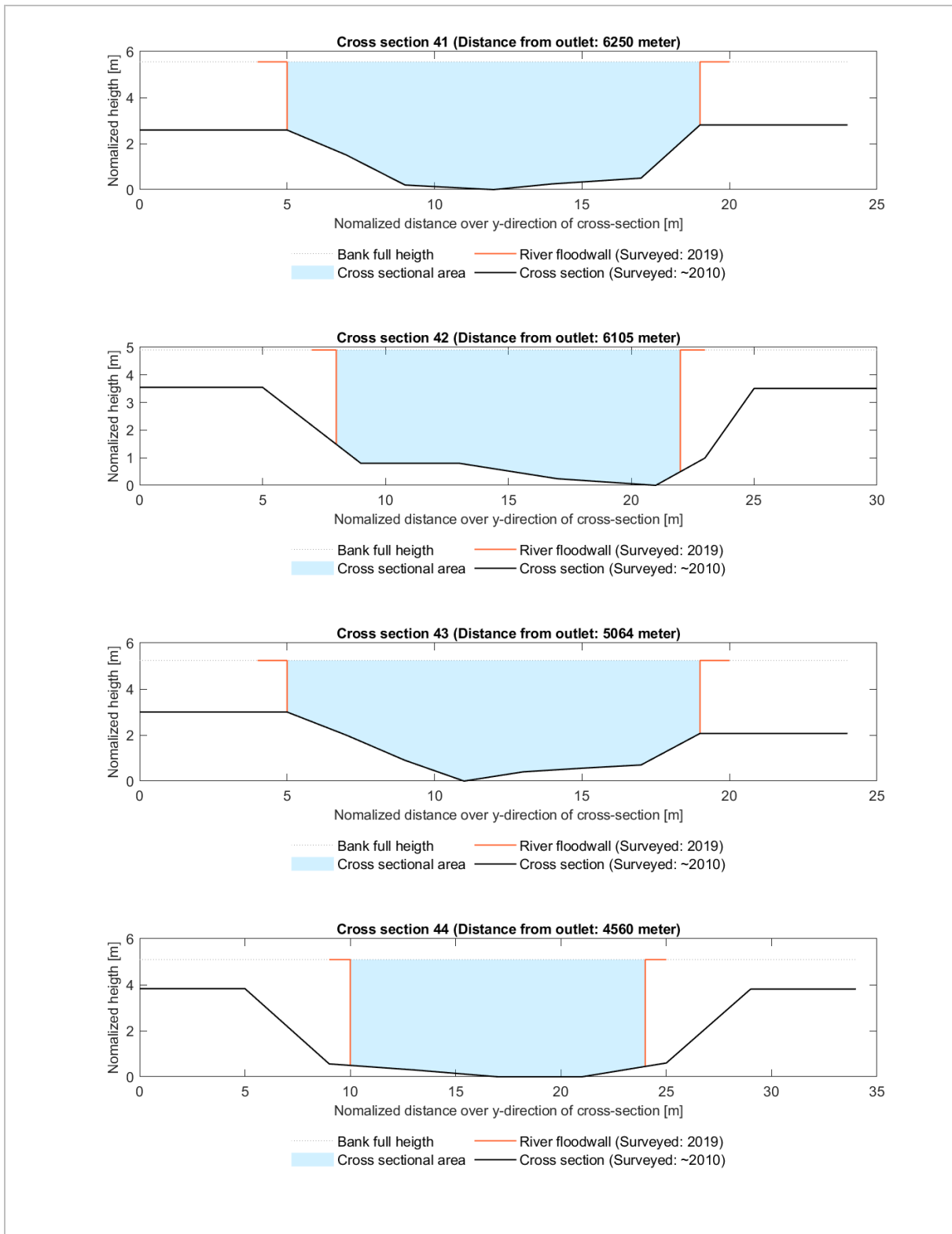


Figure 54: Cross-sections 41 to 44.

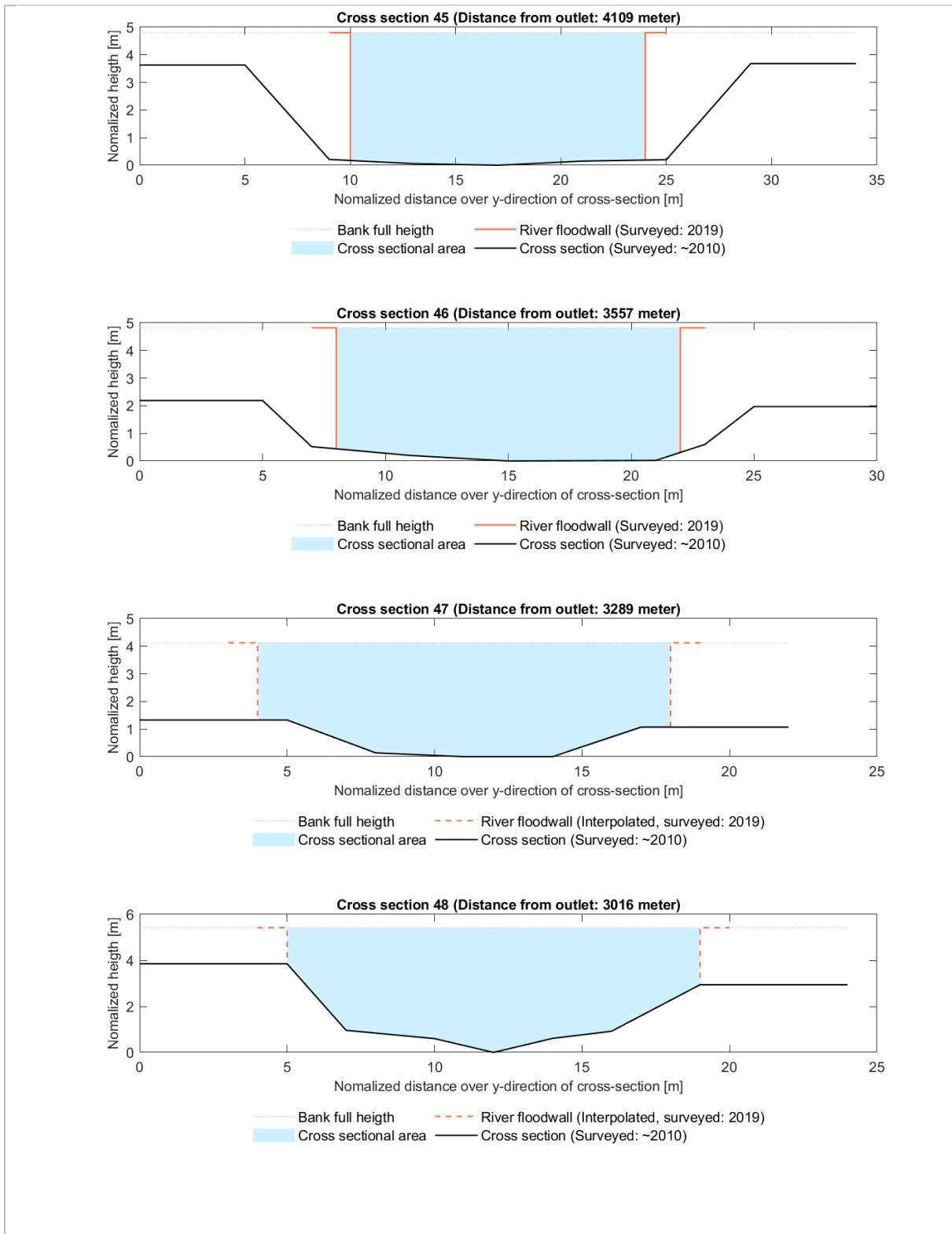


Figure 55: Cross-sections 44 to 48.

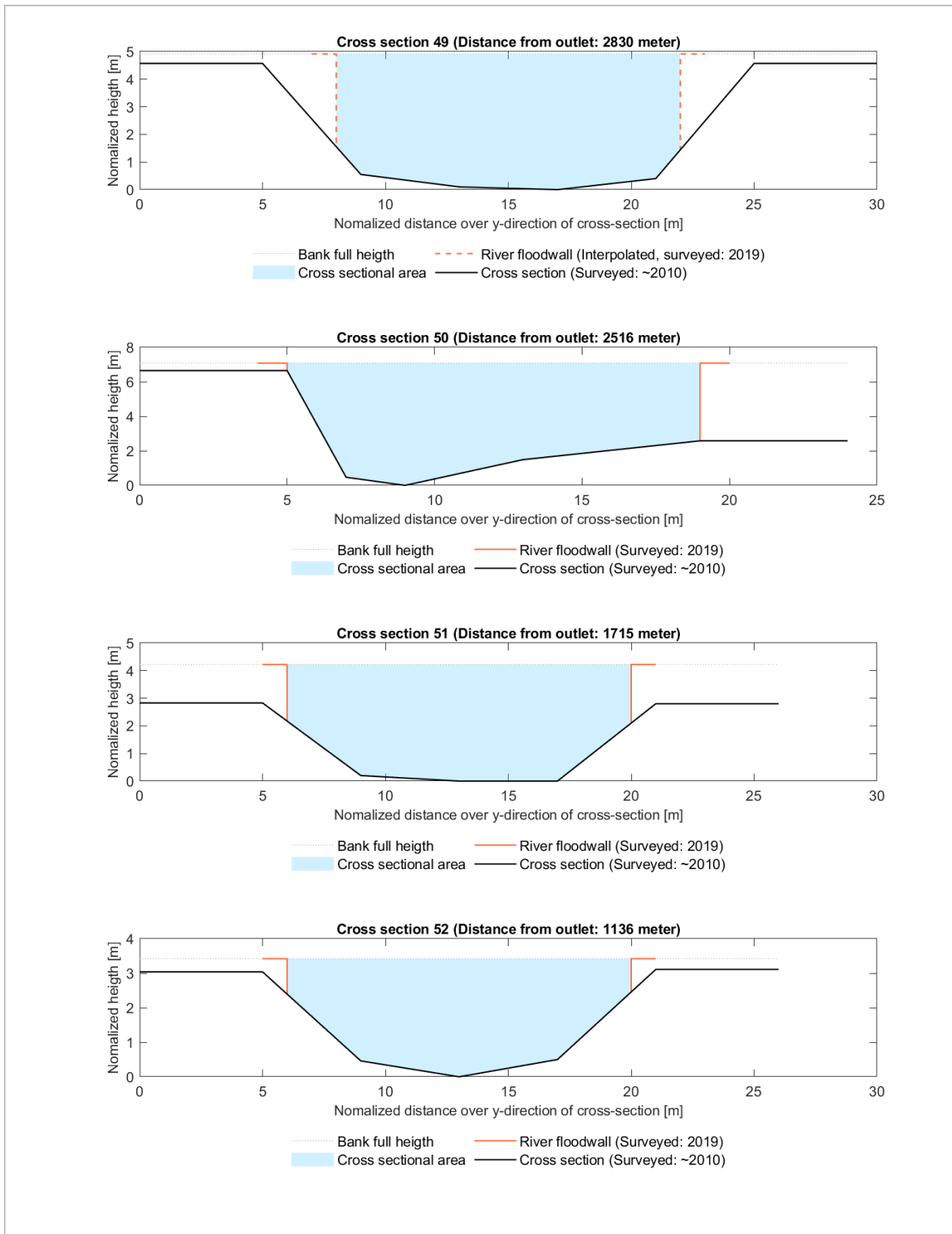


Figure 56: Cross-sections 49 to 52.

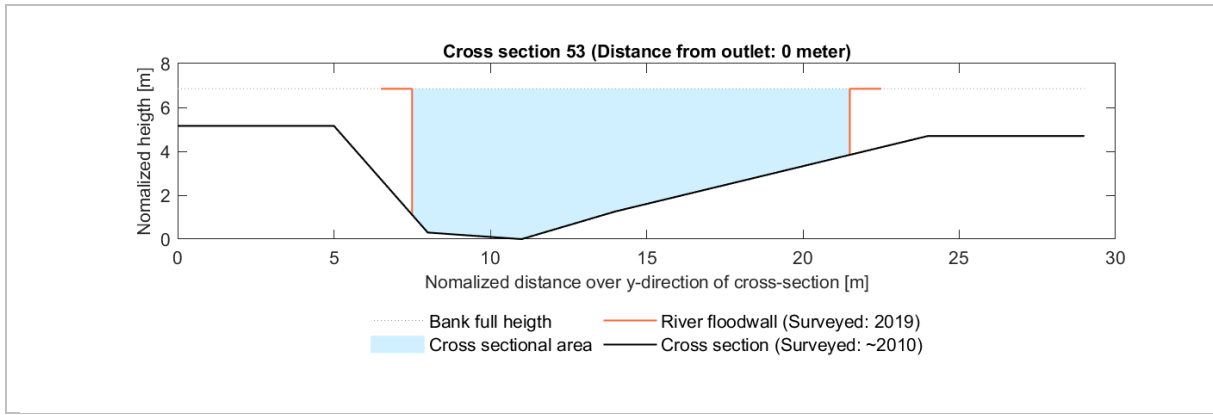


Figure 57: Cross-section 53.

# Appendix D. Fieldwork results: structure geometries

Table 9: Geometries of weirs in Tub Ma river, downstream of gauging station Z.38.

	Weir 1	Weir 2	Weir 3	Weir 4	Weir 5
Longitude	12.73355	12.73355	12.73355	12.73355	12.73355
Latitude	101.23177	101.23177	101.23177	101.23177	101.23177
Crest level [m MSL]	8.95	4.07	3.89	1.73	1.0
Opening width [m]	8.4	0.1	0.45	0.1	0.32
Opening length [m]	43.5	2.3	1.35	1.6	2
Opening height [m]	0	0.8	0.9	1.5	0.7
Number of openings	1	4	5	10	4
Channel width [m]	43.5	12.1	8.56	19	9.1

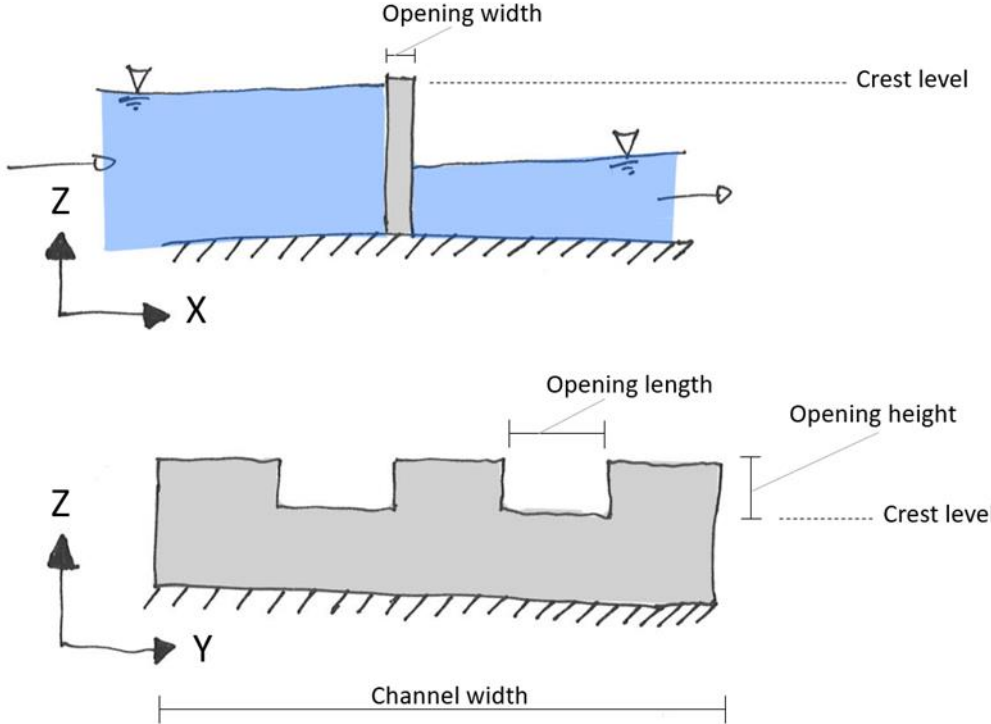


Figure 58: Visualization of the parameters describing weir geometries.

## Appendix E. Assessment of information & decision chain

This Appendix is a description of the operational governance of Tub Ma's pumping station. By doing that, the element "warning dissemination & communication" of the checklist for early warning systems (see section 2.1 for background information) was addressed. The operational strategies of the outlet pumping station were assessed by a number of conversations and interviews since no written guidelines were available within the RID.

### Outlet control in general

Given the much smaller discharge capacity of the pumping station compared to the floodgate, the latter was always preferred. Therefore, the floodgate was open (with the pumping station out of operation), except for the case when water level in Rayong river exceeded water level in Tub Ma. So, the operation of the floodgate was based on the water level in the Rayong river. Only when the floodgate was closed, the operation of the pumping station became relevant. Hence, the scope of this chapter is a closed floodgate.

### Decision event tree (theory of action)

First, all actors were identified that are part of the decision process regarding operation of the pumping station. In this context, actors were defined as persons (or a group of persons) that have 'freedom of action' (Heijnen, 2019). The decision to operate the pumping station was based on information from two different actors:

- The first actor was the 'RID Warning Center': a group of RID officers (i.a. Head of Engineering and Director of RID) that individually had the right to make a decision, depending on who is available. Only the members of the RID Warning Center had the authority to give orders for the operation of the outlet.
- The second actor was the 'worker' who lived and worked at the outlet. The worker's job was to monitor the water level at the outlet hourly. This worker was recognized as an actor because of his 'freedom of action' (Heijnen, 2019). Namely, the worker had to decide to report or to not report to the RID Warning Centre.

Consequently, a decision event tree (Heijnen, 2019) forms the basis for mapping how water level information and weather forecasts led to the decision to operate the pumping station. Starting at both actors, two different paths lead to the same outcome: the decision to operate or to not operate the pumping station. The associated decision event trees are shown in Figure 59 for the RID Warning Center and in Figure 60 for the worker at the outlet. Both decision event trees applied to the situation at which natural discharge was not possible because of a closed floodgate.

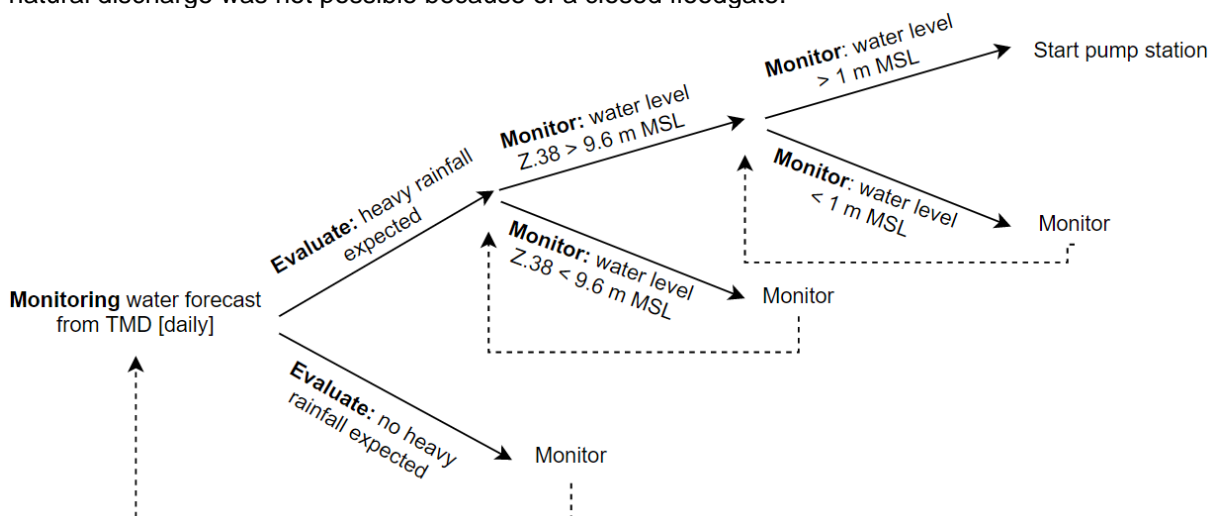


Figure 59: Decision event tree for 'RID Warning Center (scenario A).

The decision event tree from Figure 59 was called 'scenario A' in this research. The RID Warning Center took notice of the weather forecast from the Thai Meteorological Department (TMD). The forecast was monitored through different persons and channels on an irregular basis. However, it was believed that a forecasted storm event would always lead to notification of the RID Warning Center, in one way or the other. Consequently, the water level was hourly monitored at gauging station Z.38 and interpreted using the information in Table 10. This information was used for the final decision of starting the pumping station while taking into account the water level at the outlet as well. According to the Head of Engineering, it generally took 1 hour to start the pumping station after reading a water level at Z.38 of 9.6 m MSL or larger.

Table 10: Interpretation of water level at Z.38 by the RID Warning Center.

Water level at Z.38 staff gauge	Interpretation by RID Warning Center
1.5 m (9.6 m MSL)	Awareness level
1.8 m (9.9 m MSL)	Prepare for flooding
2.0 m (10.1 m MSL)	Flooding

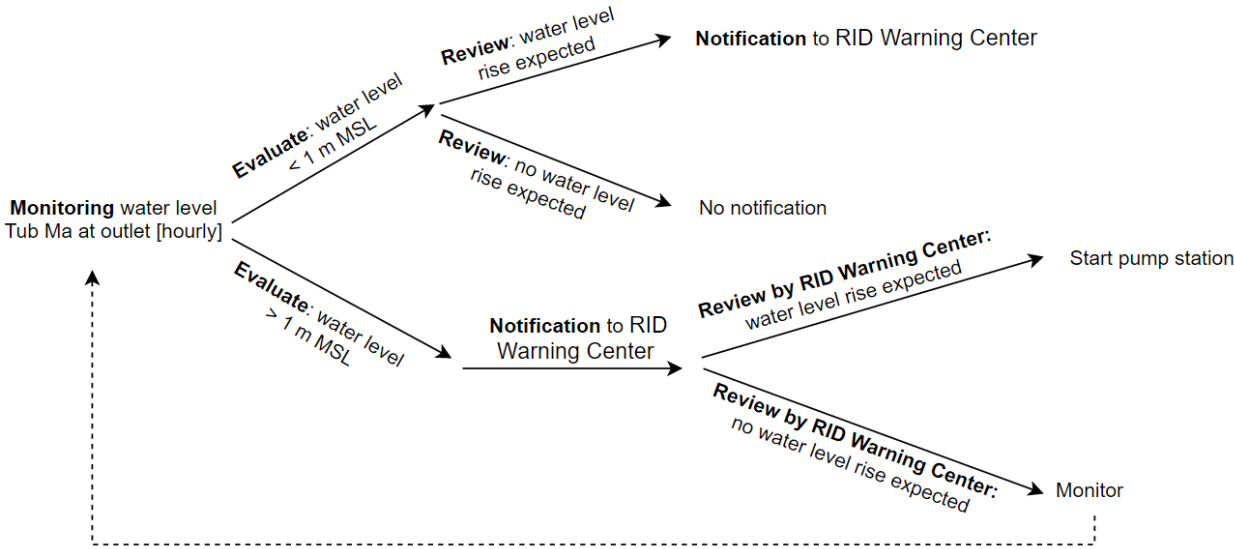


Figure 60: Decision event tree for the 'worker' around Tub Ma outlet (scenario B).

The decision event tree from Figure 60 was called 'scenario B' in this research. This tree started by regularly monitoring water level at the outlet by a worker. This worker had the task to report to the RID Warning Center when the water level was exceeding 1 m MSL or when the water level was rapidly rising. Based on this notification, the RID Warning Center aimed to keep the water level at 1 m MSL by the use of the pumping station (or reopening of the floodgate).

*Decision making in practice*

While the decision event tree described the theoretical operational strategy, operation in practice was assessed as well. During September 22 and September 25, 2019, a Line group chat was used to share information on water levels and rainfall, and to communicate decisions. This communication was analyzed to map decision making in practice.

The line group chat revealed that in practice, the pump station was entirely operated based on the water level at the outlet. Communication was dominated by the RID Warning Center asking for the water level at the outlet, and the worker sending pictures of the outlet's staff gauge. This communication feedback loop was recognized as a manual version of automatic switch-on, switch-off levels. As soon as the water level was high enough to operate the pumping station (> 1 m MSL), the RID Warning Center gave orders to do. The time it required to decide upon action was less than 15 minutes. Meanwhile, water level at Z.38 was surveyed but not used for decision making since operation of the pump was restricted by the (minimum) water level at the outlet. Instead, water level information from Z.38 was used for flood-forecasting but did lead to a decision.

## Appendix F. Model results

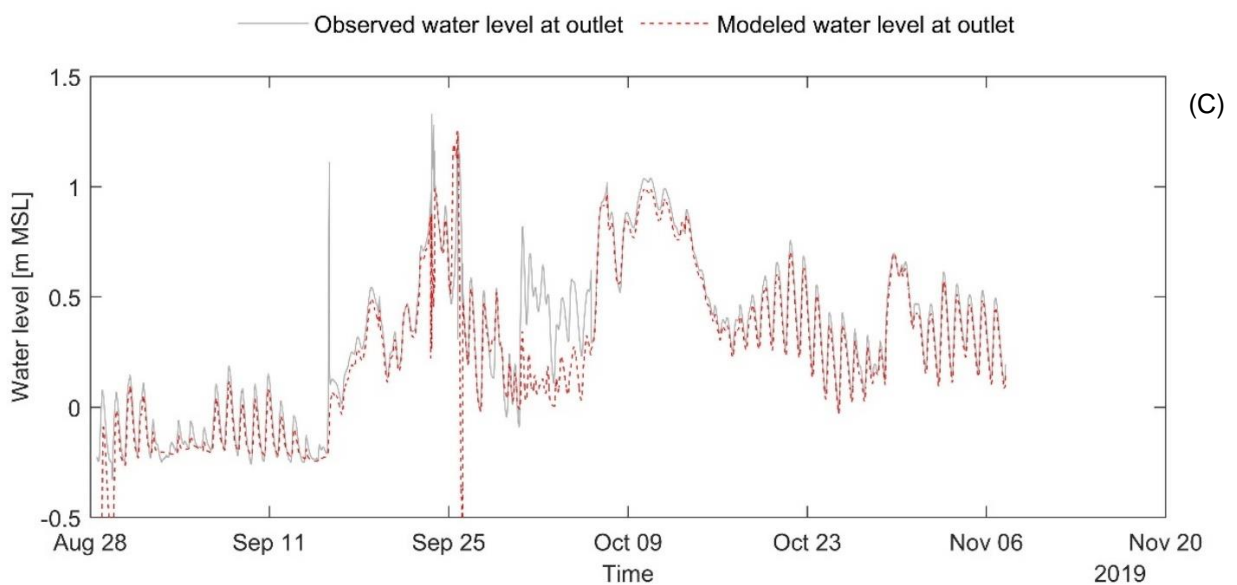
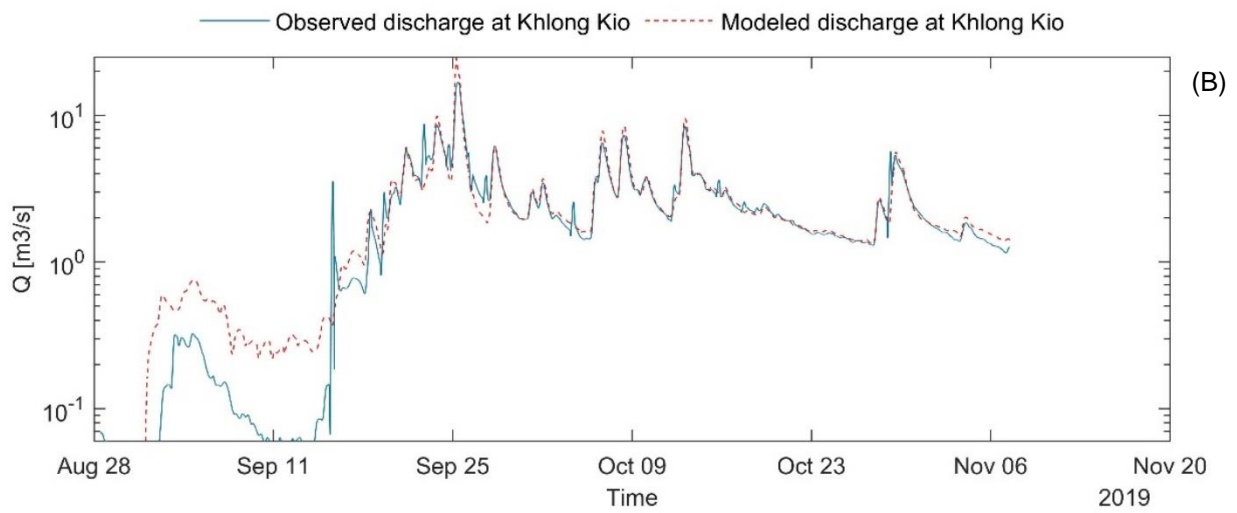
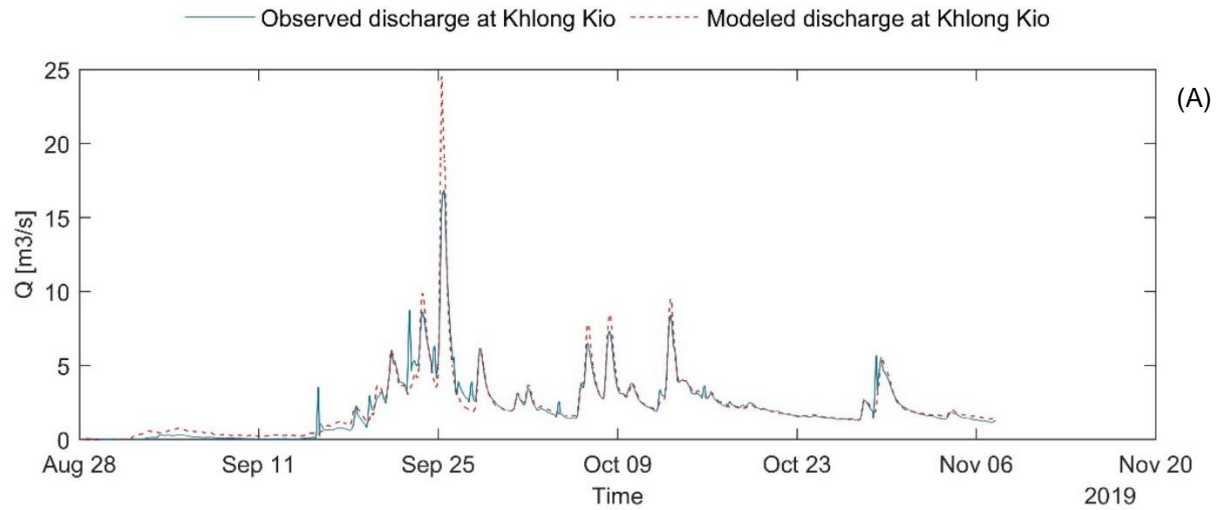


Figure 61: Results of model calibration on discharge at Khlong Kio (panel A and B) and water level at the outlet (panel C).

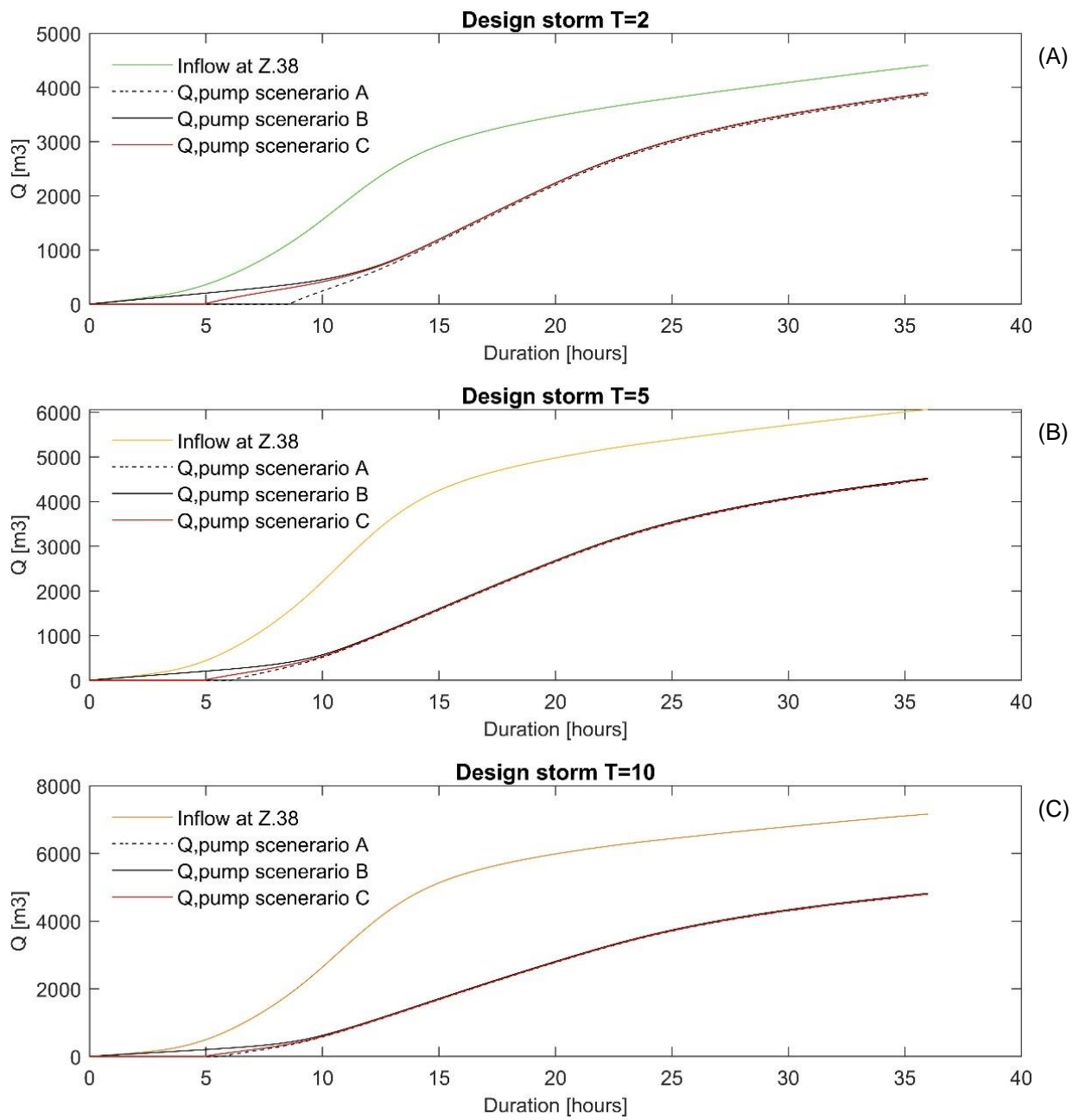


Figure 62: Cumulative inflow at Z.38 and cumulative pump discharge at the outlet.

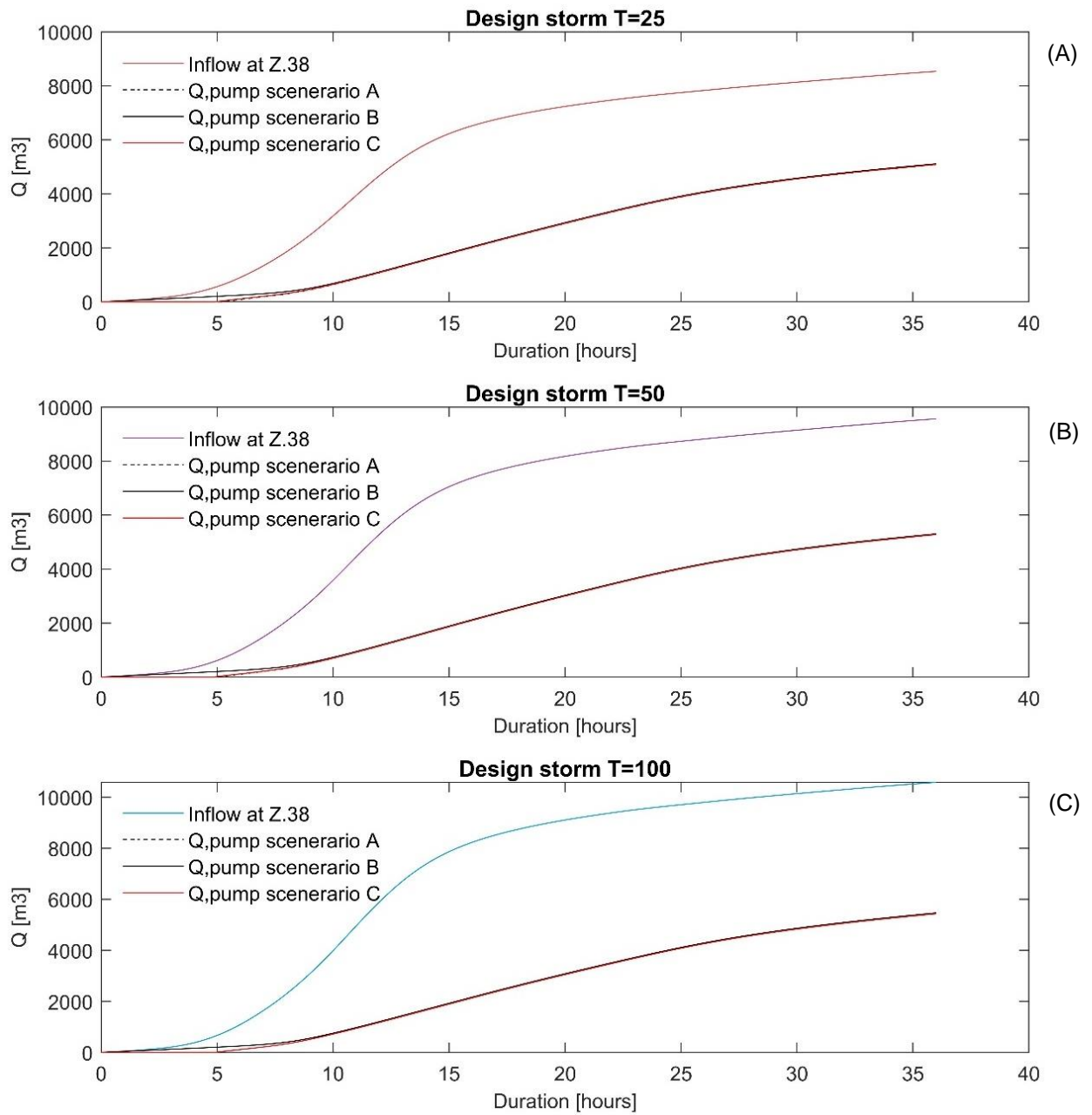


Figure 63: Cumulative inflow at Z.38 and cumulative pump discharge at the outlet.

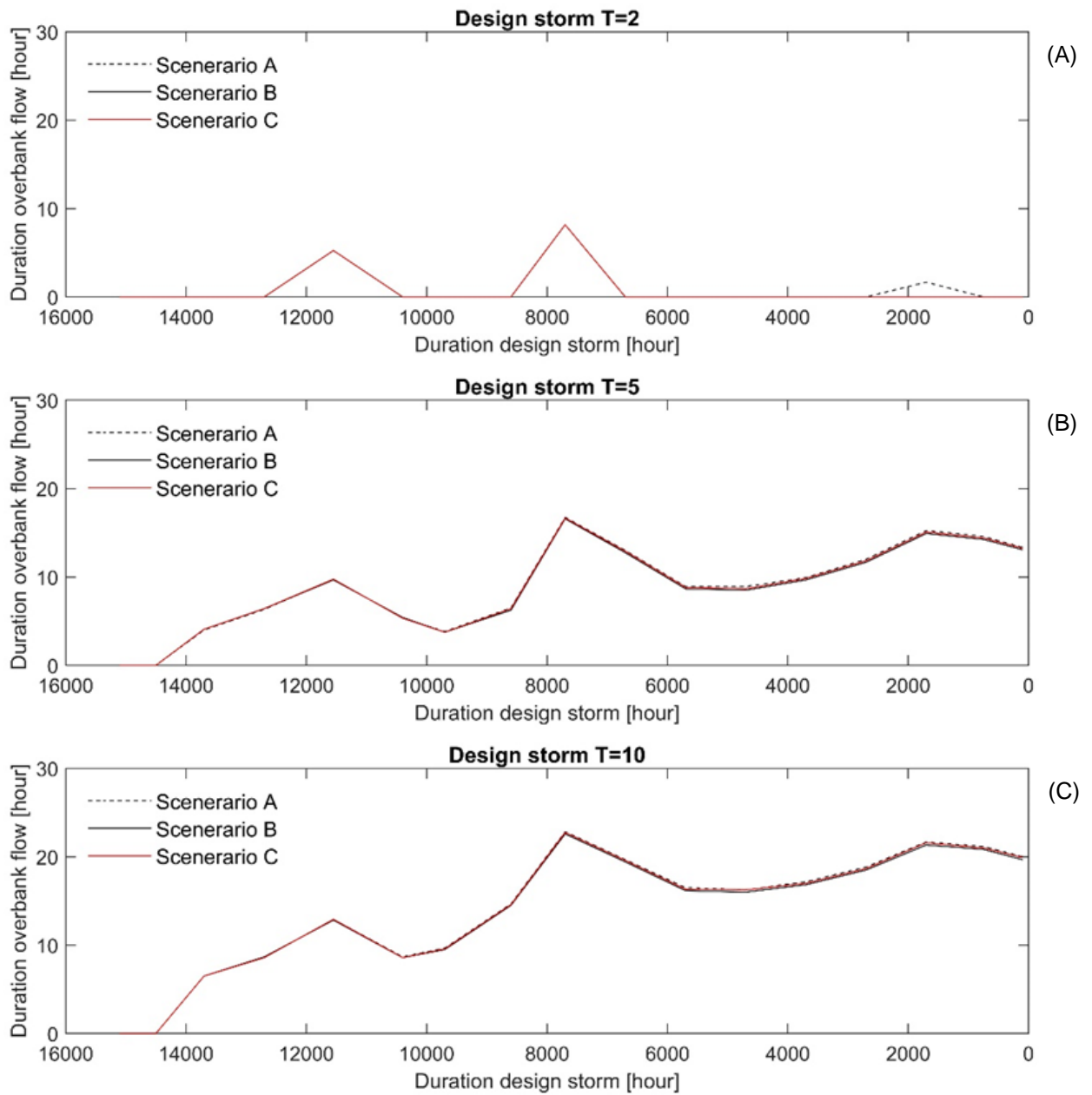


Figure 64: Duration of overbank flow along the longitudinal profile of Tub Ma.

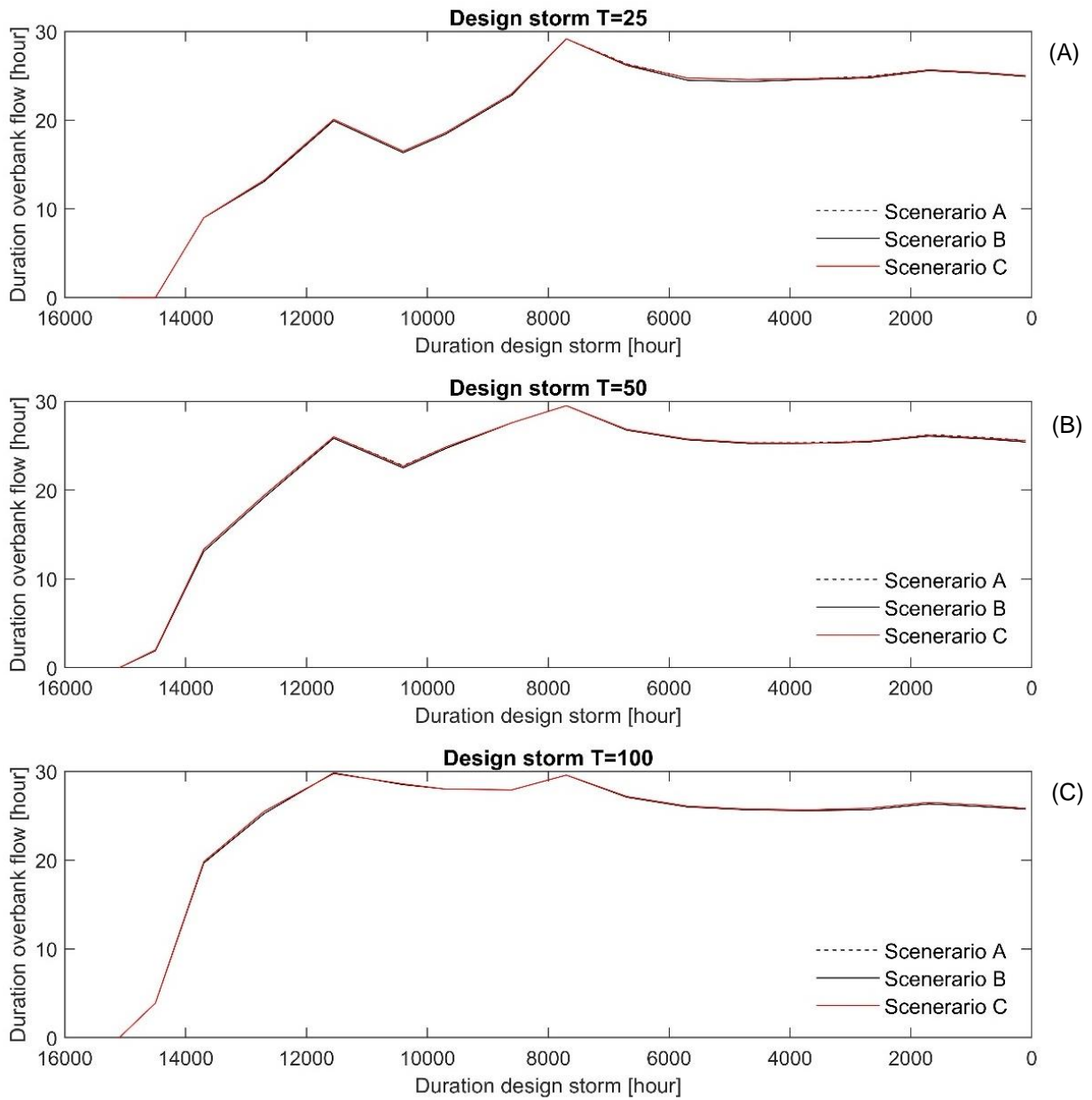


Figure 65: Duration of overbank flow along the longitudinal profile of Tub Ma.

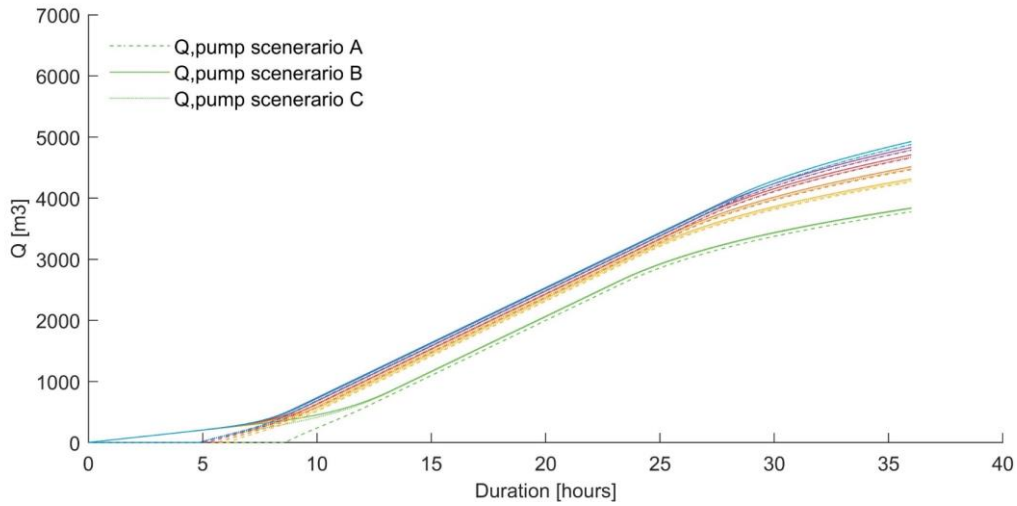


Figure 66: Cumulative pump discharge at the outlet for all scenarios and design storms based on a maximum pump capacity of  $15 \text{ m}^3/\text{s}$  (sensitivity analysis). Each design storm belongs to a separate color (see Figure 37).

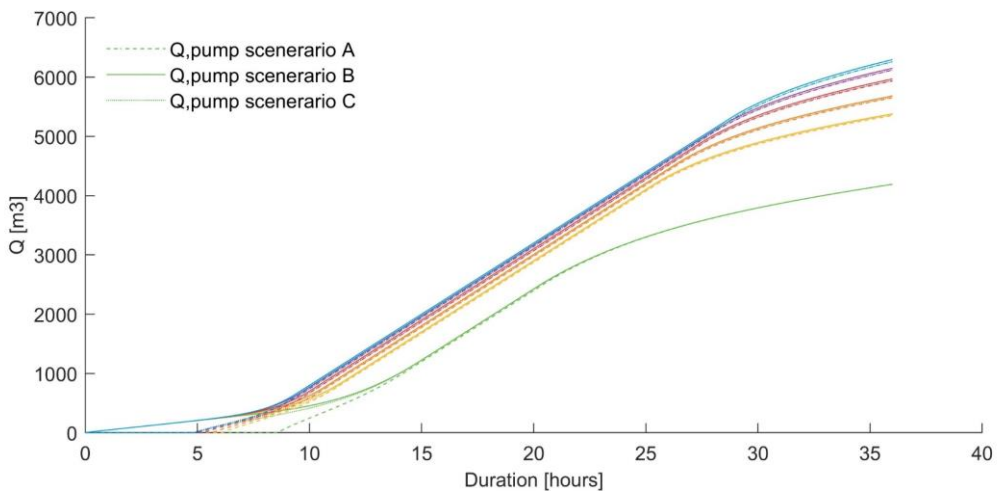


Figure 67: Cumulative pump discharge at the outlet for all scenarios and design storms based on 0.5 m increased floodwall level (sensitivity analysis). Each design storm belongs to a separate color (see Figure 37).

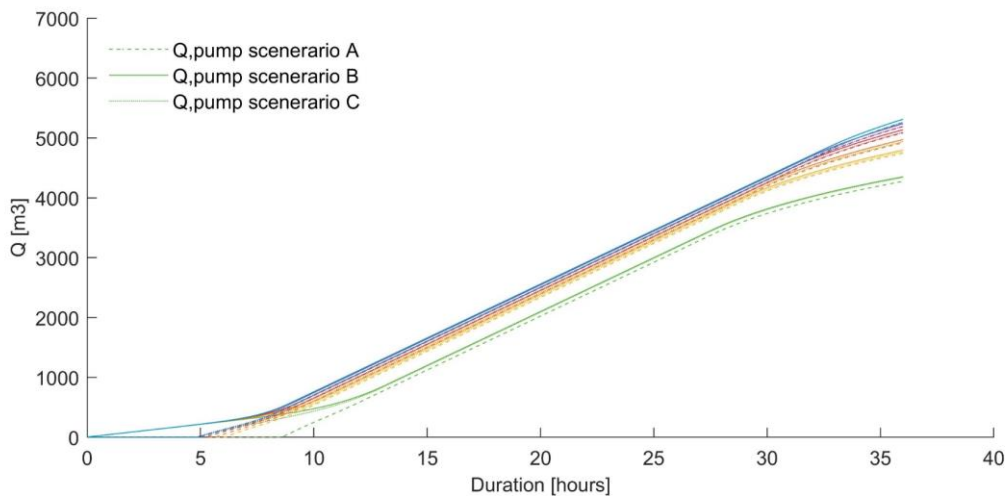


Figure 68: Cumulative pump discharge at the outlet for all scenarios and design storms based 5 hours shift forward in time of the fractional lateral inflow (sensitivity analysis). Each design storm belongs to a separate color (see Figure 37).

# Appendix G. Suggestions for flood mitigation

In this appendix, structural measures are shortly discussed for decreasing flood hazard in Tub Ma.

## Storage facility

Flood volume can be decreased by the temporary storage of water that cannot be discharged. From the flood volumes of the design storms (see section 5.4.3) the required storage area was calculated. Those required surface areas, see Table 11, are realistic to bring into practice. However, for effective flood mitigation, the storage facility needs to reduce the peak discharge. Hence, the storage facility needs to fill when the peak of the flood wave passes by, and a large storage inflow capacity (30-50 m<sup>3</sup>/s) is required. Inflow to a storage facility can be gravitational using weirs parallel to the Tub ma channel. Given the large required inflow capacity, a pumping station would be costly.

Table 11: Storage requirements for the flood volume resulting from the design storms.

Design storm:	T = 2	T = 5	T = 10	T=25	T=50	T=100
Flood volume:	98 000 m <sup>3</sup>	400 000 m <sup>3</sup>	630 000 m <sup>3</sup>	940 000 m <sup>3</sup>	1200 000 m <sup>3</sup>	1400 000 m <sup>3</sup>
Storage area: (0.5 m inundation depth)	0.20 km <sup>2</sup>	0.8 km <sup>2</sup>	1.3 km <sup>2</sup>	1.8 km <sup>2</sup>	2.4 km <sup>2</sup>	2.8 km <sup>2</sup>

## Flood diversion channel

Diversion channels, often referred to as bypasses, are mostly artificial channels designed to divert the excess amount of water to prevent flooding. A bypass rather reduces than prevents flooding since the peak of a flood wave is maximumly lowered by the discharge capacity of the diversion channel.

In a dense urban catchment, it is hard to find space for a new pipe or channel. Using the path of a road can be a cost-saving solution; an example of a diversion channel was designed, following Nakornrayong 3 Rd. This highway connects Tub Ma river with the Gulf of Thailand (see Figure 69). For this example, the flood volume reduction was calculated for a (pumping) discharge of 10 m<sup>3</sup>/s (see Table 12). Logically, the relative reduction of flood volume decreased by increasing return period.

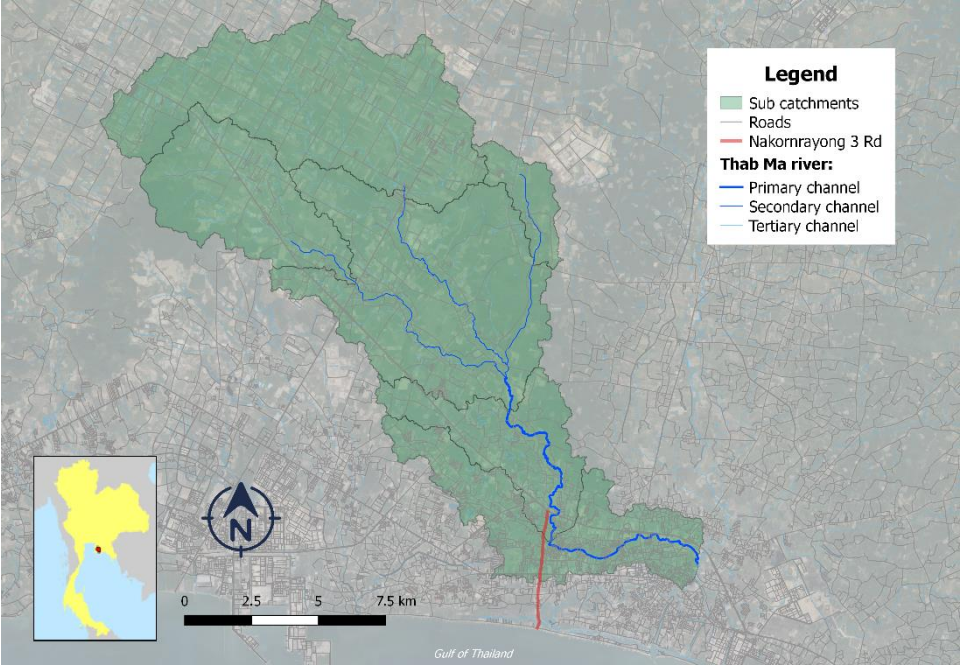


Figure 69: Location of Nakornrayong 3 Rd, connecting the Tub Ma channel with the Gulf of Thailand.

Table 12: Flood volume reduction after schematizing a diversion channel via Nakornrayong 3 Rd.

Design storm:	T = 2	T = 5	T = 10	T=25	T=50	T=100
Flood volume original:	98 000 m <sup>3</sup>	400 000 m <sup>3</sup>	630 000 m <sup>3</sup>	940 000 m <sup>3</sup>	1200 000 m <sup>3</sup>	1400 000 m <sup>3</sup>
Flood volume with bypass channel (10 m <sup>3</sup> /s capacity)	0 m <sup>3</sup>	110 000 m <sup>3</sup>	280 000 m <sup>3</sup>	540 000 m <sup>3</sup>	750 000 m <sup>3</sup>	970 000 m <sup>3</sup>
Decrease:	100 %	73 %	56 %	43 %	38 %	31 %

### Rising channel capacity

The discharge capacity of the Tub Ma channel can be increased by changing the channel geometry. Increasing the width or increasing the dike height results in a larger discharge capacity of the channel. However, given the dense urbanization in the catchment, increasing the width of Tub Ma requires the removal of building directly adjacent to the river. Meanwhile, increasing dike height has the drawback that the water level in Tub Ma can rise higher, but as a consequence, the natural gradient for the sewer systems lower. Pluvial flooding due to failure of the sewer system was already a problem in Rayong and is likely to increase if the water level gradient decreases.

The results from section 5.4.2 showed that the channel capacity approximately equaled the pumping station capacity. Hence, increasing the channel capacity of Tub Ma only reduces fluvial flooding when the floodgate at the outlet can be opened.

### Controlling Stormwater Runoff

Reversing the effects of urbanization on the hydrological cycle (increased run-off ratio and decreased time of concentration, see section 1.1) would result in flatter flood waves. Flattening the discharge curve in Tub Ma (Figure 70) results in less excess water and a reduced flood volume.

Measures that decrease direct run-off can be street-scale investments in green infrastructure and storage, such as rain gardens and rain barrels (Jarden et al., 2016). Also, placing structures in all small tributaries upstream of the Tub Ma channel would increase the catchments time of concentration.

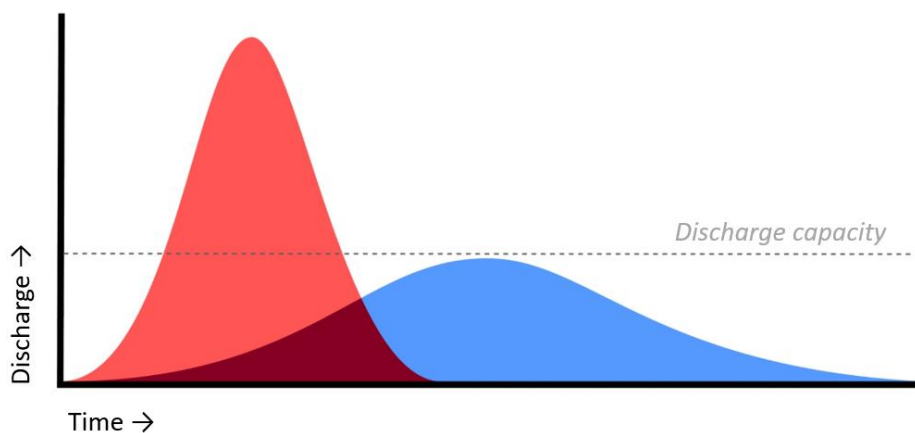


Figure 70: Visualization of a discharge curve causing floods (red) and a flattened discharge curve (blue) which does not exceed the discharge capacity of the channel/outlet.

# Appendix H. Supporting pictures



Picture 5: Cross-section at gauging station Z.38 (picture made during high flow).



Picture 6: Cross-section at gauging station Khlong Kio (picture made during low flow).



Picture 7: Water level survey at gauging station Z.38 with Mobile Water Management (blue staff gauge), Diver (inside blue PVC monitoring tube), and the original staff gauge from the RID (yellow staff gauge).



Picture 8: Diver (Van Essen Instruments B.V. ©).



Picture 9: Monitoring tube for Diver.



Picture 10: Bathymetry survey, picture was taken while the wet part of the cross-section was surveyed by measuring depth every 1 m over the y-axis of the cross-section.



Picture 11: Bathymetry survey, picture was taken while the dry part of the cross-section was surveyed by measuring the width (y-axis) of the cross-section at every meter above water level.